# Seasonal distribution of methane in the surface water and the water column of selected areas of the Baltic Sea

Dissertation

zur

Erlangung des akademischen Grades
doctor rerum naturalium (Dr. rer. nat.)
der Mathematisch-Naturwissenschaftlichen Fakultät
der Universität Rostock

vorgelegt von

Wanda Gülzow

geb. 19.01.1983, Dresden

Rostock, 26.06.2012

urn:nbn:de:gbv:28-diss2013-0005-9

Doctoral Committee:

1. Referee
   Prof. Dr. rer. nat. Gregor Rehder
   Leibniz Institute for Baltic Research Warnemünde
   Department: Marine Chemistry

2. Referee
   Prof. Dr. rer. nat. habil Ralf Zimmermann
   Mathematics and Natural Sciences University Rostock
   Department: Analytical Chemistry

Day of submission: 26.06.2012

Day of defense: 06.11.2012

# TABLE OF CONTENTS

# LIST OF FIGURES

# LIST OF TABLES

# ABBREVIATIONS

AB      Arkona Basin

AMO      Anaerobic Methane Oxidation

BB      Bornholm Basin

BSH      Bundesamt fur Seeschifffahrt und Hydrographie

DWD      Deutscher Wetter Dienst

EoG      East of Gotland

FID      Flame Ionization Detector

GC      Gas Chromatography

GB      Gotland Basin

GoF      Gulf of Finland

GWP      Global Warming Potential

ICOS      Integrated Cavity Output Spectroscopy

IPCC      Intergovernmental Panel on Climate Change

IR      Infrared Radiation

LM86      Model after Liss and Merlivat 1986

LME      Lokal Modell Europa, vom DWD

MBI      Major Baltic Inflows

NDIR      Non-Dispersive Infrared Spectrometry

NOAA      National Oceanic and Atmospheric Administration

nm      Nautical Miles

OMP      Oceanic Methane Paradox

ppbv      Parts Per Billion Volume

ppmv      Parts Per Million Volume

PTM      Purge&Trap Method

PDD      Pulsed Discharge Detector

| | |
|---|---|
| RF | Radiative Forcing Capacity |
| Sc | Schmidt Number |
| SMI | Sulfate Methane Interface |
| SMTZ | Sulfate Methane Transition Zone |
| SMHI | Sweden's Meteorological and Hydrological Institute |
| TCD | temperature conductivity detector |
| VDM | Vacuum Degassing Method |
| VUS | Vacuum Ultrasound Method |
| W92 | Model after Wanninkhof 1992 |
| W09 | Model after Wanninkhof 2009 |
| WS-CRDS | Wavelength Scanned Cavity Ring Down Spectroscopy |
| WMS | Wavelength Modulation Spectroscopy |
| WoG | West of Gotland |

# ABSTRACT

Methane is after carbon dioxide and water vapour the third most important greenhouse gas in the atmosphere, which influences the earth's climate. Especially the distribution and growth rate of methane in the earth's atmosphere received increasing awareness over the past decades. To observe long time changes of atmospheric methane concentrations, great efforts are made to determine methane sources and sinks for the calculation of a global atmospheric methane budget. Particularly estimations over the source strength of marine environments encounter large uncertainties, due to the lack of sufficient amounts of data and adequate measuring facilities, and remain a central subject and problem over the past decades.

In this thesis a new system is presented that allows the continuous and autonomous measurement of methane and carbon dioxide concentrations in surface waters using ships of opportunity. The analytical setup consists of a Methane/Carbon dioxide-Analyzer (MCA, Los Gatos Research), based on off-axis Integrated Cavity Output Spectroscopy (ICOS) joined to an established equilibrator setup. It allows the detection of methane and carbon dioxide in an equilibrated gas phase with high precision and frequency. The system was installed on the cargo ship *Finnmaid* (Finnlines) in November 2009, which commutes regularly in the Baltic Sea between Travemünde (Germany), Gdynia (Poland) and Helsinki (Finland). The instrument gives a new insight into seasonal and regional changes especially in surface methane concentrations with remarkable spatio-temporal resolution. The first year of continuous measurement for example showed surface methane saturations with general minimum values during spring and maximum values during August till September. The system allows the observation of small concentration changes and enables the identification of parameters and processes which influence surface water methane concentrations significantly. Parameters like temperature, wind, mixing depth and processes like upwelling, mix-

ing of the water column and sedimentary methane emissions were investigated and their impact on methane oversaturations and emissions to the atmosphere. Thus, upwelling was found to influence methane surface concentrations in the area of Gotland significantly during the summer period. Further, an event of elevated methane concentrations in the surface water and water column of the Arkona Basin (February 2010) was observed, which can be related to a longer period of strong wind resulting in a potential abrupt methane release at a pockmark.

Based on the surface water measurements, methane fluxes were calculated showing that the Baltic Sea is a source of methane to the atmosphere throughout the year, with highest values during the winter season and significantly regional differences. Stratification was found to intensify the formation of a methane reservoir in deeper regions like the Gulf of Finland, which leads to long lasting elevated methane concentrations and enhanced methane fluxes, when mixed to the surface during its breakdown in autumn and winter.

Additional to observations at the surface water, established discrete measuring techniques were applied to observe the vertical methane distribution in the Arkona Basin and Bornholm Basin. Using temperature and salinity as indicator, a comparative approach with model-derived data were performed to observe dynamics within the water body, which influence the methane distribution. Processes like the seasonal change of the mixing depth, stratification as well as occasional inflow events were observed, effecting vertical methane concentrations significantly. The results imply for example that inflow events might lead to a prominent displacement of methane enriched water masses and to a methane transport from the Arkona Basin into the Bornholm Basin.

# ZUSAMMENFASSUNG

Methan ist neben Kohlenstoffdioxid und Wasserdampf das dritt wichtigste Treibhausgas, welches das Klima auf der Erde beeinflusst. Mit wachsender Aufmerksamkeit wird dabei besonders die Verteilung und Anstiegsrate von atmosphärischem Methan über die letzten Jahrzehnte beobachtet. Mit besonderer Anstrengung wird die Erfassung von Methanquellen und -senken vorgenommen, um ein globales Methanbudget zu erstellen für eine bessere Kontrolle von Langzeitveränderungen der atmosphärischen Methankonzentration. Die Berechnung der Quellstärke von marinen Umgebungen stellt dabei ein spezielles Problem dar, da hier zuverlässige Datenmengen oder genaue Messanlagen fehlen. Die Entwicklung von entsprechenden Messmethoden ist daher ein zentrales Problem und Mittelpunkt vieler Studien der letzten Jahrzehnte.

In der vorliegenden Arbeit wird ein neues Messsystem vorgestellt, welches das kontinuierliche und autonome Erfassen von Methan- und Kohlenstoffdioxidkonzentrationen im Oberflächenwasser ermöglicht. Durch die Installation der Anlage auf z.B. Fähren kann das System entlang von regulären Schiffs- und Transportrouten eingesetzt werden. Das Messsystem besteht aus einem Methan- und Kohlenstoffdioxid-Sensor (MCA, Los Gatos Research), welcher auf dem Prinzip der s.g. off-axis Integrated Cavity Output Spectroscopy (ICOS) basiert, und einem Equilibrator. Der Aufbau ermöglicht die kontinuierliche Erfassung von Methan und Kohlenstoffdioxid in der Gasphase des Equilibrators, welche im Gleichgewicht mit der Wasserphase steht. Im November 2009 wurde das System auf der Fähre *Finnmaid* (Finnlines) installiert, welche regelmäßig auf den Routen zwischen den Häfen Travemünde (Deutschland), Gdynia (Polen) und Helsinki (Finnland) die Ostsee überquert. Die Messmethode ermöglicht neue Einblicke in saisonale und regionale Veränderungen der Oberflächenmethan- und kohlenstoffdioxidkonzentration, mit einer beispiellosen zeit-

lich-räumlichen Auflösung. Bereits geringe Konzentrationsschwankungen können mit dem System erfasst werden, wodurch wiederum eine Vielzahl von Parametern und Prozessen identifiziert werden können, die die Oberflächenmethankonzentration beeinflussen. Parameter, wie die Oberflächentemperatur, Wind und Mischungstiefe sowie die Prozesse Upwelling, Durchmischung der Wassersäule und sedimentäre Emission von Methan, wurden untersucht und deren Einfluss auf Methanübersättigung und Methanfluß zur Atmosphäre. Upwelling, zum Beispiel beeinflusst Oberflächenmethankonzentrationen besonders im Gebiet um Gotland während des Sommers. Weiterhin wurden im Februar 2010 erhöhte Methankonzentrationen im Oberflächenwasser und der Wassersäule der Arkonasee gemessen. Die Daten konnten mit einem mehrere Tage andauernden Sturmereignis in Zusammenhang gebracht werden, welches im Verdacht steht, einen plötzlichen Methanaustoß an einer s.g. Pockmark ausgelöst zu haben.

Mithilfe der Wasseroberflächenmessungen wurden Methanflüsse berechnet, welche zeigen, dass die Ostsee das ganze Jahr über eine Quelle für atmosphärisches Methan ist, mit starken regionalen Unterschieden. Besonders hohe Flüsse wurden dabei während der Winterphase beobachtet. In diesem Zusammenhang konnte gezeigt werden, dass eine sommerliche Wasserschichtung (Stratifikation) den Aufbau eines Methanreservoirs in tiefen Regionen wie dem Golf von Finnland bewirkt. Dies führt wiederum zu erhöhten Methankonzentrationen und -flüssen, wenn das Tiefenwasser, in Folge der Auflösung der Stratifikation im Herbst und Winter, an die Oberfläche gemischt wird.

Zusätzlich zu den Untersuchungen an der Wasseroberfläche wurden diskrete Messmethoden angewandt, um die vertikale Methanverteilung in der Wassersäule des Arkona- und Bornholmbeckens zu erfassen. Die Daten wurden mit Modelldaten verglichen, um natürliche Dynamiken des Wasserkörpers zu bestimmen, die wiederum die Verteilung von Methan in der Wassersäule beeinflussen. Als vergleichende Größen wurden dabei die Temperatur und der Salzgehalt des Wassers entlang ausgewählter Schnitte des Arkona- und Bornholmbeckens modelliert. Die Methanverteilung in der Wassersäule wird demnach entscheidend von Prozessen wie der saisonal schwankenden

Mischungstiefe, Stratifikation und gelegentlichen Salzwassereinströmen aus der Nordsee geprägt. Zum Beispiel deuten erste Ergebnisse darauf hin, dass Salzwassereinströme zu einem Transport von methanreichen Wassermassen aus dem Arkonabecken in das Bornholmbecken führt.

# PREFACE

This thesis contains three main objectives. The first central part of the thesis comprises the development of a new continuous and autonomous measuring system for methane and carbon dioxide in surface waters of aquatic environments. After successful performance tests, the system was deployed on a ship of opportunity (ferry line) travelling the Baltic Sea, which forms the ideal natural laboratory to observe and adjust the performance of the measuring system. The second part of this thesis comprises the discussion of the results of one year of successfully measured surface methane concentrations. Lastly, additional to the intensive observation of methane in the surface water, vertical methane profiles at selected stations of the Baltic Sea were taken. Established measuring methods were applied to gain an overall picture of the seasonal changing methane distribution within the Baltic Sea.

This thesis is subdivided into five chapters. **Chapter 1** gives a brief introduction into key aspects, which are relevant for the general and better understanding of the presented work. **Chapter 2** (*Gülzow et al., 2011*) outlines the new method for autonomous and continuous methane and carbon dioxide measurements in the surface water. General performance tests are highlighted and first successful field measurements are presented. Chapter 2 has been published already at the peer-reviewed international scientific journal Limnology and Oceanography: Methods.

**Chapter 3** (*Gülzow et al., acc. for BGS:D)* focuses on the first year time series of measured surface water methane concentrations in the Baltic Sea. The study gives an insight in parameters and processes, which influence the general methane distribution in the surface water of the Baltic Sea and subsequently methane emissions towards the atmosphere. Chapter 3 contains a manuscript, which has been submitted to

Biogeoscience and is currently under discussion.

**Chapter 4** (*Gülzow et al., in prep.*) objects the methane distribution within the water column of the Arkona Basin and the Bornholm Basin, along two time series and several transects in connection with seasonal dynamics and vertical mixing processes. Methane concentrations were observed in accordance to the seasonal changing oxygen distribution as well as model-derived data, showing principle dynamics within the water column of selected areas. Chapter 4 contains a manuscript, which is planned to be submitted to the Journal of Marine Systems.

The main findings and a general conclusion as well as a future perspective is given in **Chapter 5**

W. Gülzow is co-author of the publication *Schmale et al., 2010*, which is shown in the **Appendix**. This chapter gives an additional insight and overview of the general methane distribution in the water column across the Baltic Sea.

The references of all chapters were compiled to one reference list at the end of this thesis. Due to the manuscript structure, repetitions of text parts were ineluctable.

# General Introduction

## 1.1 Methane

Methane ($CH_4$) is one of the most abundant organic compounds on earth. The tetrahedral molecule consists of one carbon (C) - atom with four equivalent hydrogen (H) - bonds. Methane is the simplest molecule of the family of the alkanes and the most reduced form of carbon.
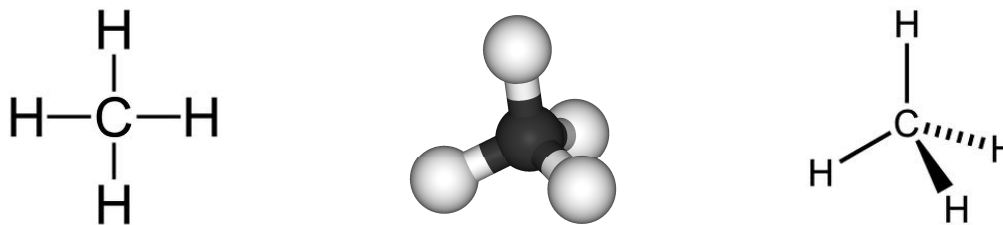


**Figure 1.1** – Illustrations of the molecule structure of methane.

Methane is a colorless and scentless gas at room temperature and standard pressure conditions, with a boiling point of -161° C. The solubility of methane in water is very low due to the non-polar molecule structure and depends on temperature, salinity and hydrostatic pressure. A basic introduction of the solubility of gases in sea water is given below and in chapter II.

### 1.1.1 Methane Effects on the Atmosphere

The current global average methane concentration is 1.81 ppmv (parts per million volume, personal communication with Dlugokencky, NOAA). Due to the unequal landmass distribution, more natural and anthropogenic methane sources exist in the northern hemisphere leading to higher methane concentrations up to 1.89 ppmv and only 1.70 ppmv in the southern hemisphere (Fig. 1.2; *Lelieveld*, 2006; NOAA).
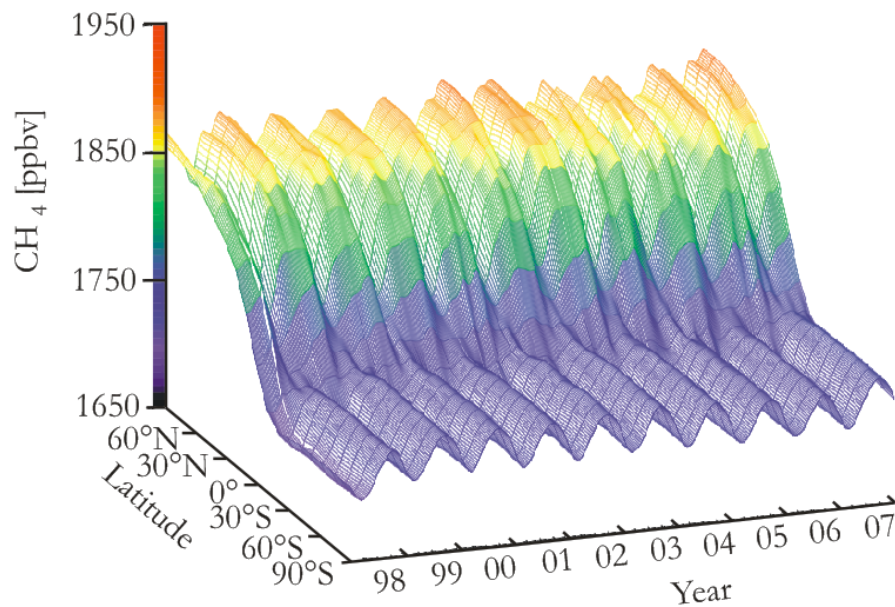
**Figure 1.2** – Atmospheric methane development in the northern and southern hemisphere from 1998 - 2007. (NOAA, www.esrl.noaa.gov)

Methane concentrations in the troposphere remain constant up to 12 km height and start to decrease only in the stratosphere (concentration in 35 km height with 0.50 ppm; *Heyer et al.*, 1990).

Several studies subject the reconstruction of the earth climate and the atmospheric history until 420,000 years before present using trapped gas of ice cores from Greenland and the Antarctica (*Petit et al.*, 1999; *Spahni et al.*, 2005). Records of the atmospheric parameters temperature, carbon dioxide and methane of the Vostok ice core confirm the strong correlation between atmospheric greenhouse gas concentrations and Arctic temperatures (*Chappellaz et al.*, 1990, 1993; *Petit et al.*, 1999; *Wuebbles and Hayhoe*, 2002; *Spahni et al.*, 2005). The time series shows that the main trend of the methane concentration follows the glacial-interglacial transitions rising from 320 - 350 ppbv (glacial) up to 650 - 780 ppbv (interglacial; *Petit et al.*, 1999).

Methane concentrations at present day have almost tripled with increasing tendency. The correlation of methane and temperature raised the question, if methane emissions initiate climate change or if elevated methane concentrations are a response to rising atmospheric temperatures (*Wuebbles and Hayhoe*, 2002). Various studies

support the theory that with climate change methane emissions of wetlands increase, leading to elevated atmospheric methane concentrations (*Chappellaz et al.*, 1990, 1993; *Thompson et al.*, 1993; *Blunier et al.*, 1995; *Brook et al.*, 1996; *Velichko et al.*, 1998; *Dällenbach et al.*, 2000). *Brook et al.* (2000) showed that the methane increase lagged the warming and ruled out methane as reason for glacial-interglacial climate change.

Continuous monitoring of methane on several remote sampling stations verified the continuous increase of methane in the atmosphere of more than 1 % during the past decades (Fig. 1.3; *IPCC* 2007).
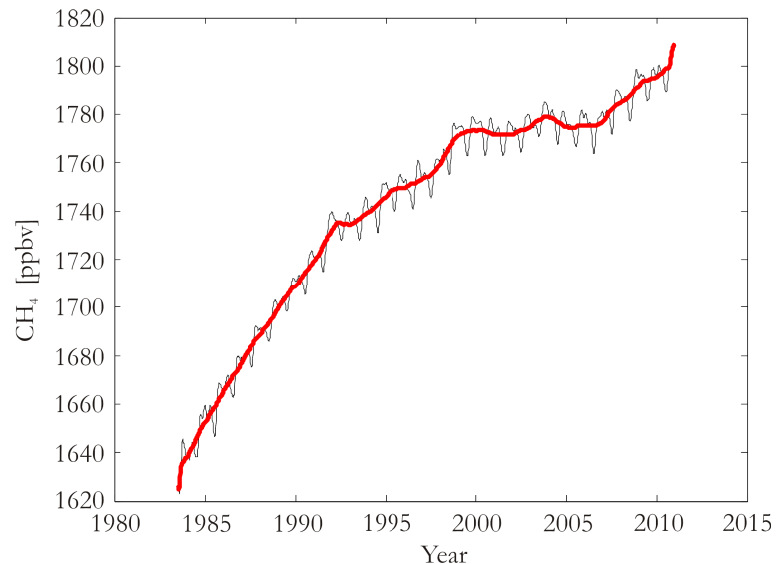


**Figure 1.3** – Global atmospheric methane development from 1982 - 2011. (NOAA, www.esrl.noaa.gov)

Several studies confirmed the correlation of increasing atmospheric methane concentrations with increasing population, agricultural emissions and increasing use of fossil fuels (*Etheridge et al.*, 1992; *Dlugokencky et al.*, 1994; *Etheridge et al.*, 1998; *Khalil and Shearer*, 2006; *IPCC*, 2007). The highest growth rate during the past 200 years was calculated by *Blake and Rowland* (1988) showing an increase of methane throughout the 1970s of approximately 20 ppbv per year. During 1979 until 1996 the increasing rate diminishes with an average growth rate of 8.9 ppbv per year (Fig. 1.2; *Khalil and Rasmussen*, 1993, 1994a,b; *Dlugokencky et al.*, 1994, 1998). *Chen and Prinn* (2006) and *Morimoto et al.* (2006) suggested that spreading of wetlands and

rice regions followed by boreal biomass burning sources caused the measured anomaly of the high methane growth rate during the exceptional warm year 1998.

The global atmospheric methane concentration remained almost constant during the period from 1999 to 2006 with an average increase of only 0.4 ppbv per year (Fig. 1.2; *Dlugokencky et al.* 2009). Since 2007, the global averaged atmospheric methane concentration begun to increase again. *Dlugokencky et al.* (2009) suggest warm temperatures in the Arctic during 2007 and increased precipitation in the tropics in 2007 and 2008 as causes for the recent growth rate. The reason for the long term slowing of the growth rate of methane is still under debate, but might be caused by either an increase in methane removal or declining methane emissions (see also section 1.1.2; *Prather et al.*, 2001; *Wuebbles and Hayhoe*, 2002; *Keppler et al.*, 2006). Though, several studies constitute no changes in atmospheric hydroxyl (OH) concentrations over the past decades, since the reaction with OH forms a major sink for atmospheric methane (section 1.1.2; *Prinn et al.*, 1995; *Dlugokencky et al.*, 1997; *Bekki and Law*, 1997; *Etheridge et al.*, 1998). Further, *Dlugokencky et al.* (2009) point out the challenge of quantifying changes of anthropogenic methane emissions especially for wetlands and biomass burning over large areas. *Lelieveld* (2006) and *Bousquet et al.* (2006) discuss the importance of reassessing isotopic carbon signatures of atmospheric methane, showing that a drying of wetlands and the diminishing of biogenic methane emissions might mask increasing anthropogenic emissions like burning fossil fuels in emerging nations.

The balance of the climate system is influenced by the abundance of greenhouse gases and aerosols. After carbon dioxide and water vapour, methane is the most abundant greenhouse gas in the atmosphere followed by nitrous oxide. Methane absorbs the infrared radiation (IR, long-wave or terrestrial radiation; from 3.3 - 3.6 $\mu$m and 7.1 - 8.3 $\mu$m; *van Loon and Duffy*, 2005) emitted by the earth surface.

To estimate the potential future impacts of different gas emissions upon the climate system, several relative indexes were invented. The radiative forcing capacity (RF) is the amount of energy which is absorbed by a greenhouse gas per unit area and

time. For methane a radiative forcing of 0.48 W m$^{-2}$ was calculated in 2005 relative to pre-industrial conditions (*Forster et al.*, 2007). Despite the low abundance of 0.5 % compared to carbon dioxide, the direct radiative effect of the methane to the total change in radiative forcing from the mid 1700s was calculated with 19 % (*Wuebbles and Hayhoe*, 2002; *IPCC*, 2007; *Boucher et al.*, 2009). Including the indirect effects of the decomposition process of methane in the atmosphere (formation of water vapour, ozone, carbon monoxide, carbon dioxide etc.; see below), this percentage increases significantly as discussed in *Boucher et al.* (2009).

The Global warming potential (GWP) is a relative measure of the amount of heat a certain mass of greenhouse gas can trap in the atmosphere in comparison to the amount of heat, which can be trapped by the same mass of carbon dioxide. The GWP is calculated referring to a specific time horizon of 20, 100 or 500 years. Especially the time interval of 100 is commonly used for relative comparing of greenhouse gases in climate policies like the International Panel of Climate Change or the Kyoto Protocol (*Forster et al.*, 2007; *Plattner et al.*, 2009; *Boucher et al.*, 2009). The GWP includes the absorption of the amount and the spectral location of infra-red radiation by a certain greenhouse gas as well as its life time in the atmosphere. In particular for methane, the GWP also includes the indirect climate effects. Atmospheric methane effects the atmospheric concentrations of ozone and water vapour (see below) giving a positive feedback and enhancing the direct and lifetime effects of methane (*Boucher et al.*, 2009). *Forster et al.* (2007) calculated the GWP of methane with 25 (100 years), which means that for the same amount of methane and carbon dioxide, emitted to the atmosphere, methane will trap 25 times more heat than carbon dioxide over a time horizon of 100 years. *Boucher et al.* (2009) recommend a larger value for the GWP with 28, including methane coming from fossil fuel sources.

The principle removal process of methane is oxidation via hydroxyl radicals ($\cdot$OH) in the troposphere and accounts for more than 88 % for the removal of methane from the atmosphere (*van Loon and Duffy*, 2005; *Boucher et al.*, 2009). Minor methane sinks (Table 1.1) are the reaction with chlorine (*Platt et al.*, 2004; *Allan et al.*, 2005),

the transport into the stratosphere (7 %; *Boucher et al.* 2009) and dry soil oxidation (5 %; *Born et al.*, 1990; *IPCC*, 2007; *Boucher et al.*, 2009).

**Table 1.1** – Compilation of methane sinks based on several publications listed in IPCC 2007.

| Sinks | Uptake [Tg $CH_4$/year] |
|---|---|
| Tropospheric OH | 428 - 507 |
| Loss to Stratosphere | 30 - 35 |
| Soil uptake | 26 - 43 |
| Total | 492 - 577 |

The majority of OH-radicals (75 %) react with carbon monoxide (CO), forming carbon dioxide ($CO_2$) in the atmosphere (Eq. 1.2).

$$CH_4 + \cdot OH \rightarrow \cdot CH_3 + H_2O \tag{1.1}$$
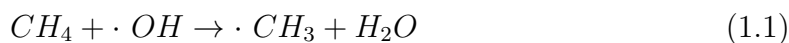
Almost 25 % of the remaining OH-radicals react with methane (*Thompson*, 1992).

$$CO + \cdot OH \rightarrow \cdot H + CO_2 \tag{1.2}$$

The oxidation rate of methane in the atmosphere depends on the availability of atmospheric hydroxyl radicals and is slow (12 years) compared to other hydrocarbons (*Wahlen*, 1993; *van Loon and Duffy*, 2005). The decomposition of methane undergoes a continuous slow sequence of oxidation reactions and is linked to a variety of other trace gas reaction cycles (e.g. CO, $CO_2$; *Crutzen*, 1991; *van Loon and Duffy*, 2005).

The atmospheric methane decomposition is closely linked to the availability of nitrogen oxide ($NO_x$; Fig. 1.4) as catalysts and is shown in detail e.g. in *Thompson et al.* (1989), *Crutzen* (1991), *Lelieveld et al.* (1998) and *Plattner et al.* (2009).

The formation of methylperoxyl-radicals ($CH_3COO\cdot$), carbon monoxide and carbon dioxide are independent from nitrogen oxide levels in the atmosphere. Environments of high nitrogen oxide levels support the formation of ozone and formaldehyde ($CH_2O$; Fig 1.4). Low nitrogen oxide levels on the contrary support the decrease in atmospheric ozone and formaldehyde ($CH_2O$) by involving the reaction of $CH_3COO\cdot$

with hydroperoxyl ($HO_2$) and methyl peroxide ($CH_3O_2H$; Fig 1.4; *Crutzen*, 1988; *Wuebbles and Hayhoe*, 2002).

$NO_x$- rich environment          $NO_x$- depleted environment
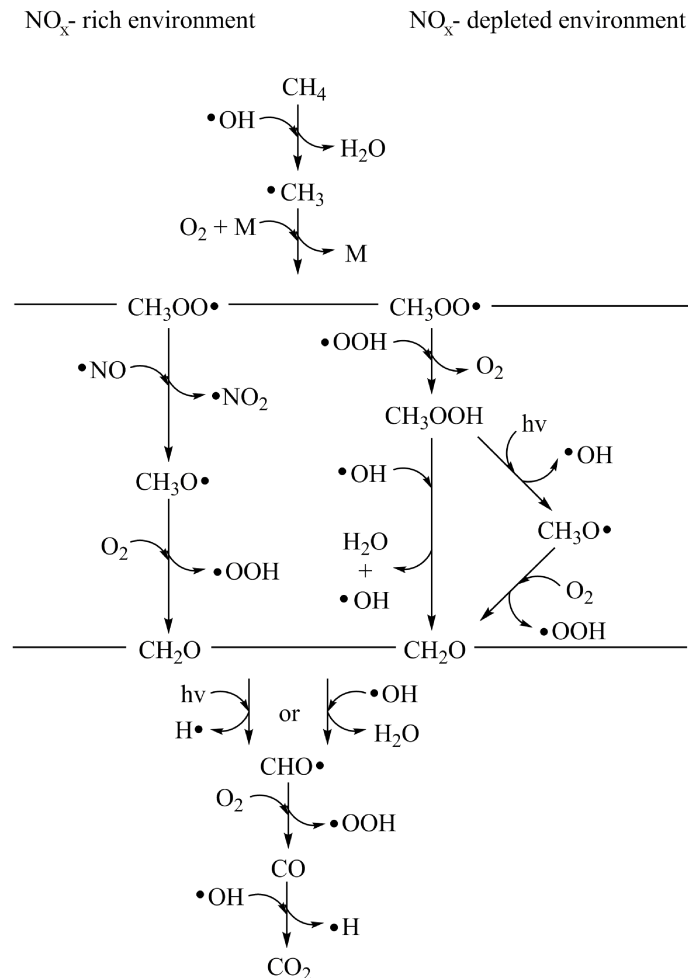


**Figure 1.4** – Decomposition of methane in the troposphere under rich and low $NO_x$ - concentration levels. M illustrates a coalition partner (after (*Thomas*, 2011)).

During the atmospheric decomposition of methane secondary products like water vapor, formaldehyde, carbon monoxide and carbon dioxide (*Lelieveld and Crutzen*, 1992; *van Loon and Duffy*, 2005; *IPCC*, 2007) are formed, leading to additional radiative forcing. Complex chain reactions with trace gases like methane and carbon monoxide lead to formation of OH-radicals, keeping the total amount of OH-radicals in balance. However, the increase of methane in the atmosphere will lead to a substantial decrease of OH-radicals giving a positive feedback to further increase of methane concentrations in the atmosphere and further radiative forcing (*Crutzen*,

1991; *Thompson et al.*, 1989; *IPCC*, 2007).

### 1.1.2 Methane Sources

Global atmospheric methane sources and sinks are relatively well known. Methane sources have been investigated by experimental measurements of methane emissions in various environments and ecosystems by comparing the isotopic composition, bio-statistical analyses or model approaches (*Wahlen*, 1993; *IPCC*, 2007). Atmospheric methane sources can be grouped depending on the formation processes in biogenic and non-biogenic or depending on the contribution to the global budget in natural or anthropogenic and are shown in table 1.2 .

**Table 1.2** – Compilation of methane sources based on several publications listed in IPCC 2007.

| Sources | Emissions to the atmosphere [Tg $CH_4$/year] |
|---|---|
| Wetlands | 100 - 231 |
| Termites | 20 - 29 |
| Oceans | 4 - 15 |
| Ruminants | 76 - 92 |
| Rice cultivation | 31 - 112 |
| Biomass burning | 14 - 88 |
| Landfills | 35 - 69 |
| Natural gas | 30 |
| Geological sources | 4 - 14 |
| Hydrates | 4 - 5 |
| Fossil Fuels | 74 - 106 |
| Total | 503 - 610 |

Emissions from fossil fuel mining and burning (natural gas, petroleum, and coal), biomass burning, waste treatment or geological sources like mud volcanoes and fossil methane seepage in marine environments belong to non-biogenic methane sources. Biogenic sources account for more than 70 % of the total global methane budget and include wetlands, rice agriculture, livestock, landfills, forests, and termites (*Wuebbles and Hayhoe*, 2002; *Forster et al.*, 2007).

The estimation of a total global methane budget is still under debate (*Forster et al.*, 2007) and undergoes continuous adjustments. *Bergamaschi et al.* (2005) considers that the national inventories based on *bottom-up* studies (field measurements) underestimate methane emissions and *top-down* based assessments (model-derived) of reported emissions will be required for verification (*IPCC*, 2007). Anthropogenic methane sources contribute more than 60 % to the global methane budget (*IPCC*, 2007).

**Fossil fuels**   Methane from fossil fuels is released to the atmosphere during extrapolation of natural gas, coal and oil and via leaks during transport and processing (*Wuebbles and Hayhoe*, 2002). The loss rate has been estimated with 1 - 15 % depending on the quality of pipelines, extrapolation process or leakage control (*Mitchell*, 1993; *Beck et al.*, 1993; *Wuebbles and Hayhoe*, 2002). The quantification of methane emissions related to fossil fuels is difficult and contain large uncertainties (*Lelieveld*, 2006). Recent studies subject the development of improving gas leakage controls or trapping of emitted methane and carbon dioxide to reduced climate effects (*Chakma*, 1997; *Rao and Rubin*, 2002; *IPCC*, 2007).

**Landfills, Biomass burning**   Incomplete combustion and biomass burning forms a substantial source for atmospheric methane (*Crutzen and Andreae*, 1990; *Levine et al.*, 2000). The amount of methane emitted from landfills depends on a variety of parameters like temperature, soil moisture or organic composition (*Wuebbles and Hayhoe*, 2002). There are sufficient technologies to trap methane from waste water or landfills to reduce emissions or to use it as energy source (*Borjesson and Svensson*, 1997; *Wuebbles and Hayhoe*, 2002).

**Geological sources**   The determination of the source strength and investigation of geological methane emissions like mud volcanoes, terrestrial as well as marine seeps, geothermal and volcanic emissions is still under debate and may be underestimated (*Milkov et al.*, 2003; *Kopf*, 2003; *Etiope et al.*, 2008).

**Wetlands, Rice fields** Inundated environments like marshes, ponds and swamps as well as flooded rice fields provide anaerobic conditions for bacterial methane production (methanogenesis) in the soil beneath the water surface and is similar to the methane formation in marine environments (see also section 1.1.3; *Cicerone and Shetter* 1981; *Sass et al.* 1990; *Wahlen* 1993). Methanogenesis in fresh water environments benefits from the absence of sulfate. The high amount of sulfate in marine environments causes competing conditions for the decomposition of organic matter between sulfate-reducing bacteria and methanogens (see also section 1.1.3; *Jørgensen and Kasten*, 2006). The decomposition of organic material in water sediments and the formation of methane can reach methane oversaturation levels, right below the sediment surface, which leads to the formation of gas bubbles and the release of methane to the atmosphere ( Fig. 1.5).

Methane production from wetlands represent the strongest natural source and contribute approximately 40 % of the global methane emissions with increasing tendency of 1 % annually due to increasing rice cultivation (*Dlugokencky et al.*, 1994; *Cao et al.*, 1998; *IPCC*, 2007). Methane emission rates of wetlands and the influencing parameters like availability of organic matter, vegetation type and cover and seasonality have been investigated by a variety of studies (*Cao et al.*, 1998; *Middelburg and Nieuwenhuize*, 2000; *Khalil and Shearer*, 2000). Investigations on methane emissions from rice field showed variations of fluxes depending on the growing stadium of the crops, temperature and agricultural practices like fertilization (*Wahlen*, 1993; *Boone*, 2000; *van Bodegom and Scholten*, 2001; *Xu et al.*, 2007). Big efforts were made to diminish such agricultural-depended methane emissions (*Khalil and Shearer*, 2006). Based on model simulations of future temperature rises due to global warming, methane emissions from wetlands are expected to increase (*Boone*, 2000; *Wuebbles and Hayhoe*, 2002), considering expected sub-arctic permafrost melting (see e.g. (*Christensen et al.*, 2004), (*Walter et al.*, 2006)), or either to decrease due to drying of current wetland areas (*Boon et al.*, 1997).

**Forests, Savannas** *Keppler et al.* (2006) showed, that methane is readily formed

in situ in terrestrial plants under oxic conditions by a hitherto unrecognized process. The potentially large methane source of 10 to 30 % of the global total, was only recently discovered by *Keppler et al.* (2006), reflecting the high uncertainty of the global methane budget calculation and the need for a new estimation of the source strength of living plants as well as for plant litter. Subsequent studies confirmed the need of an elevation of the global allotment of tropical rainforests and savannas (*Houweling et al.*, 1999; *Keppler et al.*, 2006; *Crutzen et al.*, 2006; *Miller et al.*, 2007).

**Livestock, Termites**   Methane is formed by bacterial fermentation in stomachs of ruminants (*Crutzen et al.*, 1986; *Wahlen*, 1993; *Moss et al.*, 2000; *Lassey*, 2007). Due to the global population growths, methane emissions by domestic ruminants increased over the last decades (*Crutzen et al.*, 1986) and a variety of studies subject methods for reducing methane production in the stomachs of ruminants (*Kreuzer and Hindrichsen*, 2006; *Buddle et al.*, 2010).

**Marine environments**   The main source of methane in marine environments is the anoxic microbial fermentation of organic matter (methanogenesis) in marine sediments and anoxic marine basins (see also section 1.1.3; *Cicerone and Oremland* 1988; *Heyer et al.* 1990; *Hovland* 1992). Further sources are seepage of gas or fluid flow and geological sources like mud volcanoes (*Judd*, 2003, 2004). Emissions of methane from marine sediments into the water column are controlled by the *anaerobic oxidation of methane* (AOM), which converts the majority of the methane produced in marine sediments, before it enters the hydrosphere (see also section 1.1.3; *Treude et al.*, 2003; *Jørgensen and Kasten*, 2006). Methane concentrations within the hydrosphere are additionally depleted by aerobic oxidation of methane (see also section 1.1.3). Therefore, methane emissions from marine environments play only a modest but yet uncertain role in the global atmospheric methane budget with approximately 2 % (*Bange et al.*, 1994) to 10 % (*Grunwald et al.*, 2009). The large uncertainties reflect the lack of sufficient data especially of estuaries and coastal areas, which contribute the majority (up to 75 %) of marine methane emissions (*Bange*, 2006). The limi-

tations of discrete data measurements alluded in several studies (e.g. *Bange et al.* 1994; *Bange* 2006) could be addressed with the developing of a autonomous system for continuous measurements of surface methane concentrations (*Gülzow et al.* 2011; see also chapter II).

### 1.1.3  Methane Formation in Marine Environments

The formation of methane during the degradation of organic matter is part of the carbon cycle and is to a great extend linked to microbiological processes. Organic particles in the water column of the oceans are derived from plankton production in the photic surface layer and sink as continuous, so called *marine snow* to the sea floor. The degradation of organic material starts already in the water column by respiration of micro-organisms and zooplankton. Additional organic material enters the oceans by river runoff or airborne dust. The amount of organic material reaching the sea floor decreases with increasing water depth and distance form the coast. Only 20 - 50 % of the phytoplankton productivity in the overlaying water reaches the shallow continental shelves (*Jørgensen*, 1982). *Jahnke* (1996) reports of only 1 - 2 % in the deep regions of the ocean. The organic matter segments and gradually mineralizes at the sediment surface due to mechanical stress (macro fauna, bioturbation) and biochemical degradation.

Depending on the concentration and the energy gain of the mineralization process, dominant oxidants change with sediment depth and marine sediments can be distinguished in biochemical zonations with aerobic and anaerobic conditions (Figure 1.5). Oxygen ($O_2$) is the most favoured oxidant and electron acceptor for microorganisms. The thickness of the surface oxic sediment layer is influenced by the overlaying water column, bioturbation at the sediment surface and productivity of organic matter mineralization. When oxygen is consumed the sediment turns anoxic and microorganisms start to use alternative electron acceptors for the mineralization of organic matter (Figure 1.5). Depending on the thermodynamic energy gain dominant oxidants are nitrate ($NO_3^-$), manganese oxide (Mn(IV)), iron oxide (Fe(III)) and sulfate
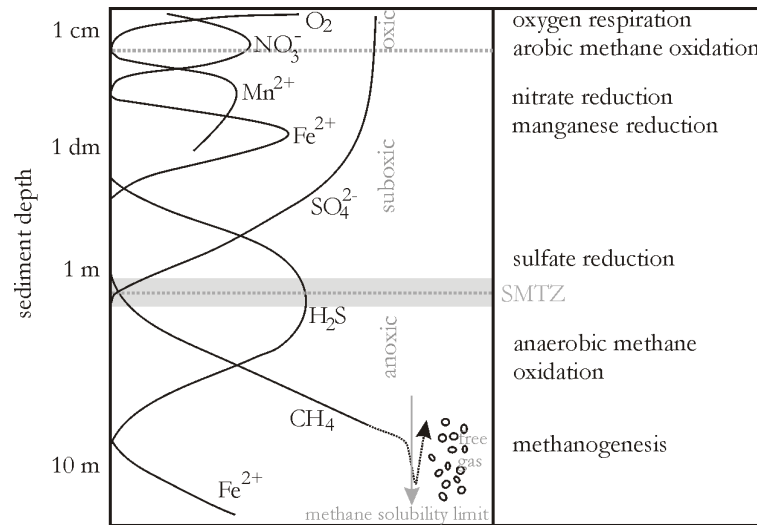
**Figure 1.5** – Biochemical zonations in marine sediments after *Whiticar* (1996) and *Jørgensen and Kasten* (2006).

($SO_4^{2-}$). Subsequent zonations can be formed in the sediment as illustrated in Fig. 1.5 (*Heyer et al.*, 1990; *Jørgensen and Kasten*, 2006).

Below the sulfate zone organic carbon is degraded to methane and carbon dioxide. Methanogenesis describes the final thermodynamic step of decomposition of organic matter in the absence of oxygen (*Heyer et al.*, 1990; *Jørgensen and Kasten*, 2006).

Depending on the substrate used for the formation of methane methanogenic bacteria retrieve different amounts of energy. The majority of bacteria is using carbon dioxide and hydrogen for carbonate respiration (*Heyer et al.*, 1990; *Fritsche*, 1999; *Ferry and Lessner*, 2008).

$$CO_2 + 4H_2 \rightarrow CH_4 + 2H_2O \qquad (1.3)$$
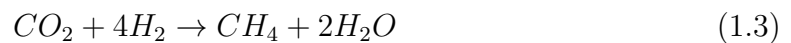
The second major pathway for the formation of methane in marine sediments is acetate fermentation:

$$CH_3COO^- + H^+ \rightarrow CH_4 + CO_2 \qquad (1.4)$$
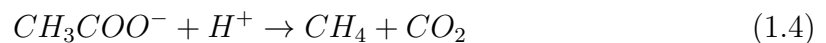
Other methanogenic bacteria are able to use acetic acid, methanol, methylamine or carbon monoxide as source of energy (*Heyer et al.*, 1990; *Fritsche*, 1999; *Jørgensen*

*and Kasten*, 2006). The formation rate of methane in the sediment depends on a variety of parameters like sedimentation rate of readily biodegradable organic matter, water circulation and movement in the sediment and seasonal temperature changes (*Heyer et al.*, 1990; *Schmaljohann*, 1996; *Fritsche*, 1999).

A competitive process for methanogenesis is sulfate reduction (*Schmaljohann*, 1996; *Jørgensen and Kasten*, 2006). Sulfate reducing bacteria use the same substrates (acetate, hydrogen and carbon dioxide) as source for energy like methanogenic bacteria.

$$4H_2 + SO_4^{2-} + 2H^+ \rightarrow H_2S + 4H_2O \qquad (1.5)$$

$$SO_4^{2-} + CH_3COO^- + 3H^+ \rightarrow H_2S + 2H_2O + 2CO_2 \qquad (1.6)$$
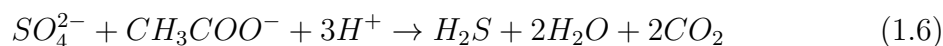
Since sulfate reduction is thermodynamically more efficient, sulfate reducing bacteria suppress methanogenic bacteria at the presence of sulfate. The thin horizon, where both bacterial communities coexist, leading to low methane and sulfate concentrations, is called the *sulfate methane transition zone* (SMTZ) or *sulfate methane interface* (SMI) and has been extensively studied (e.g. *Iversen and Jørgensen* 1985; *Schmaljohann* 1996; *Whiticar* 1996; *Treude et al.* 2005; *Parkes et al.* 2007).

Methane accumulates in deep sediments and diffuses either upwards (major part) into the sulfate zone where it is again oxidized to carbon dioxide, or it diffuses deeper into the sediment (minor part), where it gradually becomes buried. After thousands or millions of years and diagenetic processes, the remaining methane contributes to a fossil methane source in marine sediments (*Jørgensen and Kasten*, 2006).

If there are sufficient amounts of metabolizable carbon within methanogenic sediments, methane concentrations increase to oversaturation levels, forming free gas bubbles (Fig. 1.5; e.g. *Albert et al.* 1998; *Thießen et al.* 2006; *Laier and Jensen* 2007). Free gas can be detected as acoustic turbidity during seismo-acoustic surveys of the sediment, which inhibits further penetration of the acoustic signal below the gassy zone leading to a blanking of deeper sediment layers (e.g. *Albert et al.* 1998;

*Anderson et al.* 1998; *Moros et al.* 2002; *Thießen et al.* 2006; *Laier and Jensen* 2007; *Jensen and Bennike* 2009). The position of the boundary between free gas and oversaturated but dissolved methane in pore water depends on the sediment temperature and the total pressure of the overlaying water column. Short-term pressure or temperature shifts can lead to a sudden shift of this boundary layer, leading to an instability of the sediment, which again may cause bubble ebullition to the water column (see also chapter III; *Jackson et al.* 1998; *Wever et al.* 2006).

The re-oxidation of methane during its diffusion towards the sediment surface and into the SMTZ is a key process in marine sediments and is called *anaerobic methane oxidation* (AMO). AMO is subject of a variety of studies involving reaction-transport modelling, and isotopic measurements (*Iversen and Jørgensen*, 1985; *Whiticar et al.*, 1986; *Jørgensen and Kasten*, 2006; *Mogollon et al.*, 2011). Methane oxidation and sulfate reduction rates were calculated in this zone by *Jørgensen and Kasten* (2006), showing that methane oxidation accounts for 89 % of the sulfate reduction at this depth. Significant amounts of energy are transferred within the SMTZ, and the reducing power during the mineralization of organic carbon (formation of $CO_2$ and $CH_4$) encounters the efficient electron acceptor sulfate (*Jørgensen and Kasten*, 2006). Assuming a one-to-one stoichiometry between $CH_4$ and $SO_4^{2-}$, a coupled reaction has been proposed (*Jørgensen and Kasten*, 2006):

$$CH_4 + SO_4^{2-} \rightarrow HCO_3^- + HS^- + H_2O \tag{1.7}$$
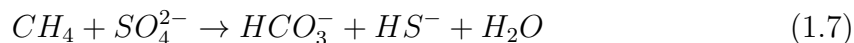
Microorganisms for aerobic and anaerobic oxidation of methane (see below) are well known and subject of several studies (e.g. *Bowman*, 2006 and *Hinrichs et al.*, 1999; *Nauhaus et al.*, 2005; *Jørgensen and Kasten*, 2006).

Methane concentrations substantially diminish during diffusion towards the sediment water interface (*Whiticar*, 1978; *Jørgensen and Kasten*, 2006). After entering into the oxic layers of the sediment, methane is oxidized by aerobic bacteria using oxygen (*Heyer et al.*, 1990; *Jørgensen and Kasten*, 2006).

$$CH_4 + 2O_2 \rightarrow CO_2 + 2H_2O \qquad\qquad (1.8)$$

The majority of the methane is consumed within the sediment before it enters the water column as described above. The intensity of methane oxidation thereby varies, depending on the transport of methane via diffusion or via release from methane hydrated or gassy sediments as well as bacterial communities within the sediment (*Heyer et al.*, 1990; *Reeburgh et al.*, 1993; *Valentine et al.*, 2001; *Treude et al.*, 2003; *Jørgensen and Kasten*, 2006).
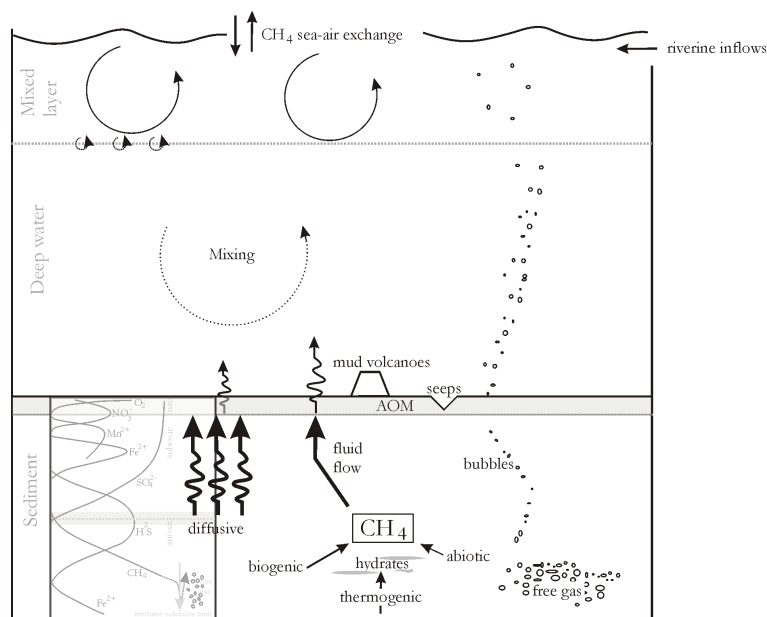


**Figure 1.6** – Diagram of methane pathways at the marine system, after *Schneider von Deimling* (2009).

Methane enters the water column either by diffusion, dissolved in fluids (pore water or ground water) or as free gas in form of bubbles (cold or thermal gas seeps, gassy sediments, mud volcanoes; *Jensen et al.* 1992; *Bussmann and Süss* 1998; *Judd et al.* 2002; *Kopf* 2003; *Schmale et al.* 2005; *Jørgensen and Kasten* 2006; *Sauter et al.* 2006; *Schneider von Deimling et al.* 2011). Within the oxic layers of the water column, dissolved methane is significantly extenuated via aerobic microbial oxidation as described above and is slowly mixed from deeper water layers towards the sea

surface, where it eventually enters the atmosphere (see also chapter IV).

The methane distribution in the water column of the deep oceans and shallow regions differ significantly. Oceanic water column methane profiles were found to be undersaturated in methane with respect to the atmosphere due to efficient aerobic methane oxidation and smaller methane concentrations in the atmosphere in the past (*Tilbrook and Karl*, 1995; *Rehder et al.*, 1999; *McGinnis et al.*, 2006; *Karl et al.*, 2008). Elevated methane concentrations within the water column were found for example in the Gulf of Mexico (*Solomon et al.*, 2009) or in coastal areas of the North Sea and the North Atlantic (*Bange*, 2006). The brackish systems of the Black Sea and the Baltic Sea, with permanent or temporal anoxic conditions in deeper water layers, show particular differing methane water column profiles with bottom layer methane concentrations up to 1 $\mu$mol (see also chapter IV; *Amouroux et al.* 2002; *Schmale et al.* 2010b).

During the transport of methane through the water column, a gradient develops of higher methane concentrations in the deeper water layers and low concentrations in the surface water (e.g. of the Baltic Sea; *Schmale et al.* 2010b; see also section 1.2.1 and chapter IV). The diffusive and mixing transport of methane from deeper layers is strongly linked to the stratification of the water column (for the Baltic Sea see section 1.2.1; chapter III and chapter IV), resulting in almost inhibited methane transport towards the sea surface during strong stratification of the water column (*Schmale et al.*, 2010b). Inhibited mixing of deeper layers during summer stratification and the depletion of oxygen may further lead to anoxic conditions in the water column (see also section 1.2) and the surface sediment layers, resulting in additional methanogenesis and higher methane concentrations in the deeper water column (*Heyer et al.*, 1990).

Bubble-mediated methane transport is not restricted by water column stratification (*Schneider von Deimling*, 2009) and can sometimes form huge methane plumes (flares) extending into the water column (e.g. *Schmale et al.* 2005; *Sauter et al.* 2006; *Schneider von Deimling* 2009). During the ascent of gas bubbles, methane is partially dissolved in sea water forming layers of elevated methane concentrations around

a methane plume (*McGinnis et al.*, 2006; *Sauter et al.*, 2006; *Schneider von Deimling*, 2009). *Schneider von Deimling* (2009) uses the dependency of the bubble size released from the sediment and its dissolution rate, showing that the initial bubble size also effects the transport of methane in certain depths of the water column. Observations of methane releases from the Tommelliten field situated in the North Sea show, that bubbles with 5 - 6 mm initial diameter are expected to reach the sea surface and the atmosphere (*Schneider von Deimling et al.*, 2011).

Elevated methane concentrations in the oxygenated upper water column were found during several studies (e.g. *Tilbrook and Karl*, 1995; *Karl et al.*, 2008). The upper water column of the oceans contain high amounts of oxygen, which suspends methanogenesis as strictly anaerobic formation pathway of methane. The phenomenon of elevated methane concentrations in the upper water column was therefore named *oceanic methane paradox* (OMP, *Karl et al.*, 2008). One explanation for OMP is the formation of methane in anaerobic microniches like digestive tracts and faecal pellets of zooplankton, presented in a variety of studies (*DeAngelis and Lee*, 1994; *Karl and Tilbrook*, 1994). *Karl et al.* (2008) hypothesizes methane formation during bacterial production and decomposition of methylphosphonate in phosphate stressed waters as potential pathway for the aerobic formation of methane in the upper water column. Yet, the confirmation of the theory by field observations is still missing.

Further explanations of increased methane concentrations in the upper water column are lateral inflows of rivers (e.g. *Rehder et al.*, 1999; *Valentine et al.*, 2001) or upwelling of deeper water masses to the surface (e.g. *Rehder et al.*, 2002; see also chapter III).

## 1.2   Study Area Baltic Sea

The Baltic Sea is situated in the northern part of Europe (10 - 30° N and 54 - 66° S) and forms one of the largest brackish water reservoirs on earth.

Born as a melt water lake (Baltic Ice Lake) at the end of the last ice age 13,000 - 14,000 years ago, the Baltic Sea belongs to the youngest seas on earth. The continental ice started to melt 11,000 years before present, leading to a rapid sea level rise and the connection of the Baltic Ice Lake with the Atlantic. The brackish Yoldia Sea was formed. The connection with the Atlantic through the central of Sweden was drying due to postglacial crustal uplift (10,000 BP). The new Ancylus Lake was turning once again into a fresh water reservoir. Due to a newly developed passage through the present day Skagerrak, Kattegat and Danish Strait the Littorina Sea was formed at 9,000 BP. Further small uplifts of the European Crust and sea level rises during the past 6,000-7,000 years formed the present day shape of the Baltic Sea, which is still changing. It is assumed that the Gulf of Bothnia will be cut of the Baltic Sea due to ongoing crustal uplift within the next 3,000 years (*Voipio*, 1981; *Björck*, 1995; *Rheinheimer*, 1995).

With an average depth of 52 m, the Baltic Sea is a rather shallow marginal sea. A variety of submarine sills divide the Baltic Sea in several sub basins, which can be distinguished and characterized by different geochemical and hydrographical gradients. Main basins are

- Arkona Basin (maximum depth, 45 m)

- Bornholm Basin (100 m)

- Baltic Proper with Eastern Gotland Basin (with Gotland Deep, 250 m) and Western Gotland Basin (with Landsort Deep, 460 m)

- Gulf of Finland (120 m)

- Gulf of Bothnia with Bothnian Sea (120m) and Bothnian Bay (80 m)
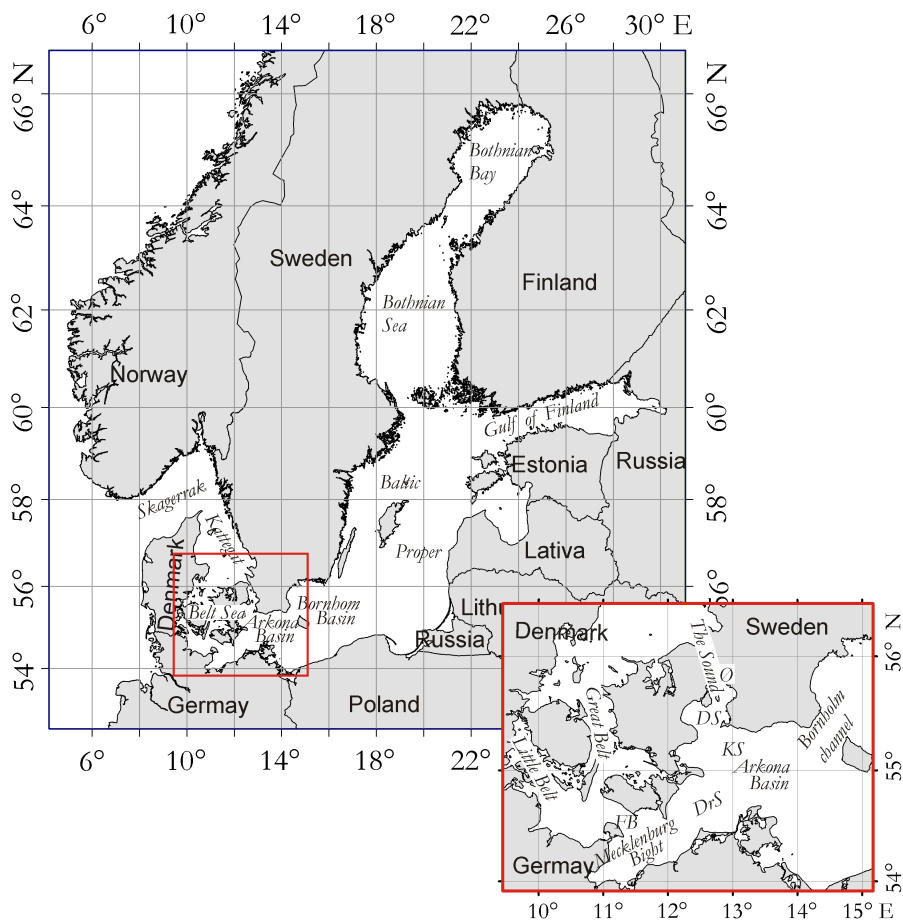
**Figure 1.7** – Overview of the Basins of the Baltic Sea with the detailed south western Belt Sea and the Arkona Basin. The Sound can be divided in the Øresund (Ø) and Drogden Sill (DS) which is connected with the Arkona Basin via the Kriegers Shoal (KS). The Belt Sea can be divided into the Little Belt and the Great Belt Sea and is connected with the Mecklenburg Bight via the Fehmarn Belt (FB). The Darss Sill (DrS) separates the Mecklenburg Bight and the Arkona Basin.

Today, the Skagerrak and Kattegat remain the only connections with the North Sea and the open ocean. Especially the *transition zone* formed by the shallow Belt Sea (Fig. 1.7) in the south western part of the Baltic Sea, including the Danish Straits, the Darss Sill and the Drogden Sill limit the water exchange with the North Sea. The Baltic Sea is governed by an estuarine circulation and a positive freshwater balance supplied by river runoff from its large drainage area in conjunction with the humid climate (*Reissmann et al.*, 2009).

The Baltic Sea stretches over several degrees of latitude. As a consequence the general humid climate of the Baltic Sea is affected by rather temperate climate in

the southern part (e.g. Arkona Basin) and by the boreal-continental climate in the northern parts (e.g. Bothnian Sea, Bothnian Bay; *Voipio*, 1981; *Rheinheimer*, 1995; *Feistel et al.*, 2008).

### 1.2.1   Hydrography of the Baltic Sea

The methane distribution in the water column of the Baltic Sea is influenced by its hydrographic regime. Important parameters are the strong density gradient, influenced by temperature and salinity, the oxygen concentration and the turbulence regime of the water column of the Baltic Sea, which will be introduced in the following sections. The interplay of the parameters determine the hydrographic and ecological properties of the Baltic Sea like deep water formation, ventilation, nutrient balance or stratification (*Feistel et al.*, 2008).

**Salinity**   The surface salinity gradient in the Baltic Sea reaches from 30 psu in the Skagerrak over 10 psu in the central Belt Sea to 2 psu in the north east (Bothnian Bay). The salinity balance of the Baltic Sea is controlled by episodic saline inflow events and a surplus of an annual freshwater input (river runoff and precipitation exceeds evaporation), which leads to a positive water balance. A general flow pattern can be described with a less saline or brackish out-flowing surface layer (so called Baltic Current, see also section 1.2.2) and a more saline in-flowing bottom layer, which are separated by a strong halocline. A principle profile of the vertical salinity gradient for the Baltic Sea is given in figure 1.8. Together with the vertical temperature change (see below), the vertical salinity gradient forms a strong density stratification within the water column, which remains permanent in some parts of the Baltic Sea (Baltic Proper, Fig. 1.8). The permanent halocline in the Gotland Deep leads to the development of a permanent redoxcline (oxic to sub- or anoxic conditions, see also section 1.2.1), and the formation of biogeochemical zonations (*Nausch et al.*, 2008).
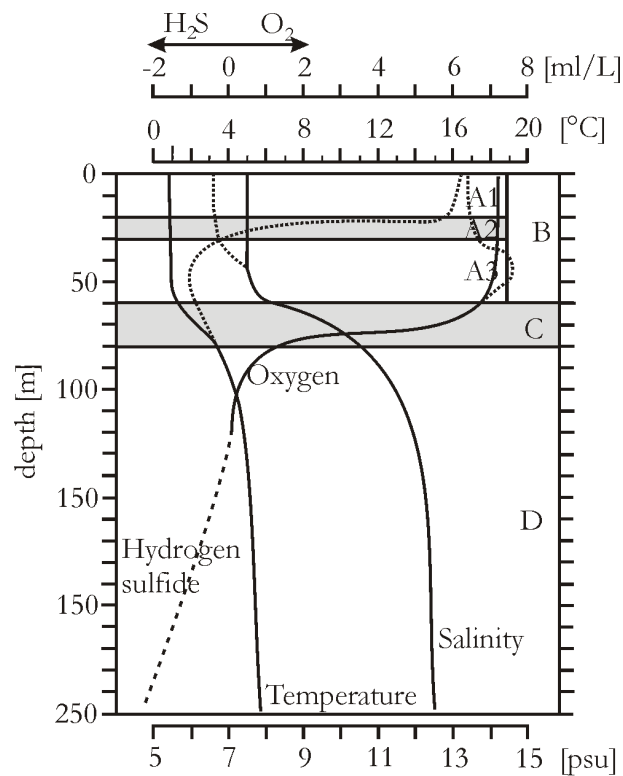
**Figure 1.8** – Principle temperature, salinity and oxygen/hydrogen sulfide water column profiles of the central Baltic Sea during winter (solid line) and summer (dotted line). During summer stratification a warm surface layer (A1) is separated by the thermocline (A2) from the cold intermediate winter layer (A3). B shows the well mixed cold winter surface layer; C the permanent halocline and D the deep layer (after *Feistel et al.* (2008)).

**Temperature**    The water column temperature of the Baltic sea shows large seasonal variations. The sea surface temperature increases significantly during the warming period in spring and summer (Fig. 1.8). The transport of heat into deeper layers is significantly slower than the rapid warming of the surface layer (A1, Fig. 1.8). Therefore a colder intermediate water layer between 30 to 60 m depth can be found in the Baltic Sea during summer (A3, Fig. 1.8). The warm and less dense surface layer and the colder, slightly denser intermediate water layer are separated by a thermocline, which is indicated by a sharp temperature gradient (A2, Fig. 1.8). The thermocline develops at approximately 20 - 30 m depth and inhibits vertical mixing with deeper water layers (*Feistel et al.*, 2008). Enhanced vertical mixing and decreasing atmospheric temperatures during autumn and winter lead to the erosion of the thermocline

and the upper water column reaches homothermal conditions. In some parts of the Baltic Sea, low surface temperatures (below the freezing point) lead to the formation of a thin winter thermocline.

Temperatures of deeper water layers are less affected by seasonal changes and remain almost isolated. Highest annual temperature changes can be observed in the south western parts of the Baltic Sea with fluctuation from 2 to 14° $C$ in deep water layers. The temperature in the Gotland Deep varies comparable little ranging form from 4 to 6° C (*Feistel et al.*, 2008).

Ice conditions are very variable in the Baltic Sea ranging from completely covered from January to April (Bothnian Bay) to a probability of ice occurrence of less than 25 % (*Voipio*, 1981; *Rheinheimer*, 1995; *Feistel et al.*, 2008). The daily ice distribution of the Baltic Sea is monitored by the Swedish Meteorological and Hydrological Institute, SMHI (www.smhi.de/oceanografi/iceservice/). The occurrence of ice constrains the emission from the water to the atmosphere (e.g. for methane see chapter III).


**Oxygen**   A principle vertical oxygen profile of the central Baltic Sea is given in Fig. 1.8. Oxygen is generally in equilibrium with the atmosphere within the upper water layer until the thermocline. Below the thermocline till the halocline oxygen concentrations decrease during summer time (*Feistel et al.*, 2008). Oxygen values below the permanent halocline are generally low with temporal hypoxic or anoxic conditions (Fig. 1.8).

Hypoxic conditions or hypoxia are defined by $O_2$ concentrations below 90 $\mu$mol $L^{-1}$ or 2 ml $L^{-1}$. Anoxic conditions or anoxia are defined by the absence of oxygen (0 $\mu$mol $L^{-1}$ or 0 ml $L^{-1}$ $O_2$) and the occurrence of dissolved hydrogen sulfide ($H_2S$). Hypoxic or anoxic conditions are likely to occur in stratified marine systems during longer water residence times, low water exchange and ventilation and high carbon production or export to the bottom layer (*Rabalais et al.*, 2010).

The Baltic Sea is an eutrophic brackish sea with two considerable algae blooms in spring and summer (cyano bacterial bloom; *Feistel et al.* 2008). During the sinking of the organic matter produced in the surface water of the Baltic Sea, large amounts

of organic carbon sink towards the sediment. Its mineralization lowers the oxygen content of the water column, particularly in the permanent stratified basins. During longer stagnation periods (see also section 1.2.2), oxygen can be completely consumed in the water column below the halocline (anoxia) and hydrogen sulfide is formed leading to toxic conditions in the bottom water (*Feistel et al.*, 2008; *Reissmann et al.*, 2009). Further, the formation of hydrogen sulfide influences the marine ecosystem and its biochemical composition like the nutrient distribution in deeper regions of the Gotland Deep, leading to e.g. enhanced liberation of phosphate and Fe(II)-ions (*Diaz and Rosenberg*, 2008; *Naqvi et al.*, 2009; *Reissmann et al.*, 2009; *Conley et al.*, 2009, 2011).

Several studies subject increasing eutrophication as main reason for expansion of hypoxia in coastal areas over the past decades (*Diaz and Rosenberg*, 2008; *Naqvi et al.*, 2009; *Rabalais et al.*, 2010; *Conley et al.*, 2011). Eutrophication describes the increase of primary production and the accumulation of organic carbon, which leads to increasing demands of respiratory oxygen (*Rabalais et al.*, 2010). Eutrophication is fueled by increasing nutrient load of riverine runoff due to fertilizers, waste water, urbanization and population growth, agriculture and resource intensification (*Diaz and Rosenberg*, 2008; *Conley et al.*, 2009, 2011; *Rabalais et al.*, 2010). *Conley et al.* (2009, 2011) describes climate change and its influence of the physical processes (e.g. eutrophication) as important driver for hypoxia in the Baltic Sea. Since anthropogenic impacts and climate change occur on the same time scale, a clear separation between enhanced human activities and natural ecosystem changes are difficult and need further investigation (*Conley et al.*, 2009, 2011).

Regarding to the strictly anaerobic microbial formation process of methane, the worldwide increasing number of areas with hypoxic and anoxic conditions in the lower water column and the sediment gives reasons of concern (*Diaz and Rosenberg*, 2008; *Bange et al.*, 2010; *Rabalais et al.*, 2010; *Conley et al.*, 2009, 2011). Only few studies subject hypoxia as source of methane in the deeper water column (*Bange*, 2006; *Naqvi et al.*, 2009; *Bange et al.*, 2010; *Schmale et al.*, 2010b). Future predictions raise the question if methane concentrations in the deeper water column will increase due to the

expansion of hypoxia and if this will lead to enhanced methane emissions to the atmosphere (*Bange*, 2006; *Bange et al.*, 2010; *Naqvi et al.*, 2009). Bange and co-workers confirm enhanced methane emissions to the atmosphere in late summer/autumn after increased accumulation of methane in hypoxic areas during the summer stratification (*Bange et al.*, 2010). The correlation of hypoxic conditions and elevated methane concentrations on the contrary could not yet be observed (*Bange et al.*, 2010). Instead, a bimodal seasonality of methane concentrations in the bottom layer of Boknis Eck (Eckernförder Bight, Baltic Sea) was observed, which could be triggered by enhanced sedimentary organic material after phytoplankton blooms (*Bange et al.*, 2010).

Therefore, frequent inflows and ventilation of the deeper regions are of particular importance for the ecological regime of the Baltic Sea. A time line of changing oxic to anoxic conditions between 1960 and 2003 of the Gotland Deep can be found in *Feistel et al.* (2008).

### 1.2.2   Dynamics in the Water Column

The water exchange between the North Sea and the Baltic Sea via the transition zone (see section 1.2) encounters effective mixing and is controlled by barotropic and baroclinic pressure gradients (see below), local winds, bathymetry and stratification (*Schmidt et al.*, 1998; *Feistel et al.*, 2008; *Reissmann et al.*, 2009). Mesoscale mixing of the water column in the transition zone within timescales of half a day to a few days significantly influence the salt and oxygen signature of the brackish Baltic water and the re-entering of out-flowing brackish waters after mixing with saline deep waters (*Schmidt et al.*, 1998). The long time water exchange between the Baltic Sea and the North Sea can be described by the classical approach of Knudsen (*Voipio*, 1981). The comparable substantial variations of the hydrography within the transition zone stands in contrast to the limited variations in the deeper regions of the Baltic Sea, which is particularly important for their chemical and biological condition (*Feistel et al.*, 2008).

Episodic inflow events occur irregularly (every year to several decades) and can

be distinguished in barotropic and baroclinic inflows.

**Baroctropic Inflows**    Barotropic bottom inflows are driven by substantial sea level differences between the Kattegat and the Arkona Basin, formed by persistent westerly winds usually during the autumn, winter and spring season. The formation of a barotropic inflow starts with strong easterly winds, lasting several weeks, resulting in a sea level drop of several decimeters. The change towards strong winds from westerly directions (longer than 5 days) pushes saline water through the Belt Sea into the Baltic Sea (*Reissmann et al.*, 2009). They are characterized by low temperatures, high salinity and oxygen values and a water import of typically 200 km$^3$ (*Reissmann et al.*, 2009). Recent major events could be observed in 1983, 1993, and 2003 (*Burchard et al.*, 2009). Such *Major Baltic Inflows* (MBI) are described in many studies (*Wyrtki*, 1954; *Matthäus and Franck*, 1992; *Lass and Matthus*, 1996; *Schmidt et al.*, 1998; *Feistel et al.*, 2008; *Reissmann et al.*, 2009) and usually enter the Baltic through the Belt Sea and Darß Sill, changing the hydrography in the deep waters of the Central Baltic Sea significantly. According to *Matthäus and Franck* (1992) MBI's last more than 30 days, accompanied by a significant rise of the sea level. The period between two MBIs is defined as stagnation period. Depending on the duration of the stagnation period significant changes in salinity and oxygen as well as subsequent nutrient changes have been observed *Matthäus and Franck* (1992); *Feistel et al.* (2008); *Reissmann et al.* (2009).

**Baroclinic Inflows**    Intermitted baroclinic inflows are driven by a horizontal density gradient between the Kattegat and the Baltic Sea, formed by persistently calm wind conditions, occurring typically during late summer. They are characterized by warm temperatures, significant amounts of saline waters and low oxygen concentrations. Still, the oxygen-deficient water masses are important to ventilate the deep anoxic Baltic basins via entrainment. They occur several times a year and typically

enter the Baltic Sea via the Øresund and the Drogden Sill and embed in the intermediate layers of the Bornholm Basin (*Feistel et al.*, 2008; *Reissmann et al.*, 2009). Such small inflow events gain only recently more awareness (*Mohrholz et al.*, 2006; *Burchard and Rennau*, 2008). Significant events were observed in summer 2002 and 2003 (*Burchard and Rennau*, 2008).

The strength and classification of an inflow event is estimated by its related total mass of imported salt (*Matthäus and Lass*, 1995; *Reissmann et al.*, 2009):

> 3 Gt = very strong inflow

2 - 3 Gt = strong

1 - 2 Gt = moderate

The amount of dense water arriving in the central Baltic Sea depends of the amount of water passing the Belt Sea and its mixing with ambient brackish water along its pathway (*Reissmann et al.*, 2009).

**Mixing Processes**   The dynamics within the water column of the Baltic Sea are very complex and differ from the regime of the open ocean. There are several mechanisms of vertical mixing which are not yet fully understood. In the following section general mechanisms of vertical mixing and the dynamics of general wave types important for the Baltic Sea are introduced. Detailed descriptions using common basic mathematical approaches go beyond the scope of this introduction and therefore continuative literature (e.g. *Kundu and Cohen*, 2008; *Tomczak and Godfrey*, 1994) is recommended.

The most important convection process of the Baltic Sea is the *estuarine circulation*, which again is governed by a variety of additional mixing processes. The pycnocline defines the strongest salinity gradient within the water column. During the summer period, a thermocline develops above the pycnocline leading to the formation of a less dominant salinity gradient (*Feistel et al.*, 2008). The thermocline
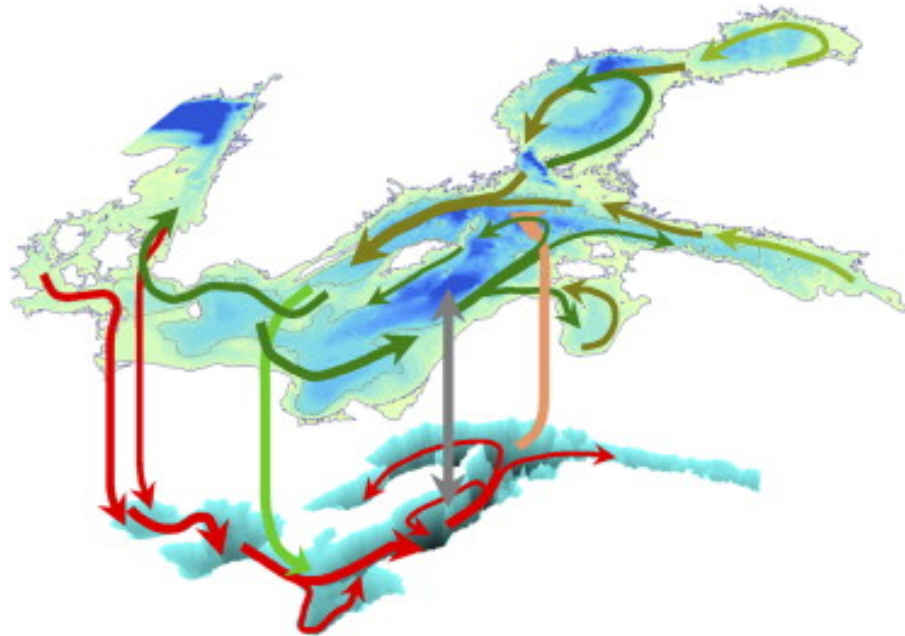
**Figure 1.9** – Diagram of the large-scale circulation in the Baltic Sea (*Elken and Matthäus*, 2008). Green (brackish surface water) and red (saline bottom water) arrows show the surface and bottom layer circulation, respectively. The light green and beige arrows denote entrainment. The gray arrow indicates diffusion.

disappears during autumn and winter, leading to a well mixed surface layer. Episodic inflow events underlay the ambient bottom water and lift the current pycnocline (e.g. Arkona Basin up to 80 cm; Fig. 1.9, red arrows *Reissmann et al.*, 2009;). Thus, intense mixing of the water column during winter-time leads to an erosion of the pycnocline (lowering) and mixing of elevated saline water into the mixed surface water. The so called *Baltic Current* transports the brackish surface water via the Kattegat into the North Sea (Fig. 1.9).

The principle, wind driven vertical energy transport into the water column was first described by Walfried Ekman in 1905 (*Ekman transport*, see also *Feistel et al.*, 2008; *Kundu and Cohen*, 2008). The wind induced current profile below the sea surface can be described by the Ekman spiral, showing decreasing current speed with clockwise changing direction. The Ekman transport in the Baltic Sea together with the consistent west wind belt inhibits the formation of a permanent geostrophic current or specific up- or downwelling areas like in the open oceans (*Feistel et al.*, 2008).
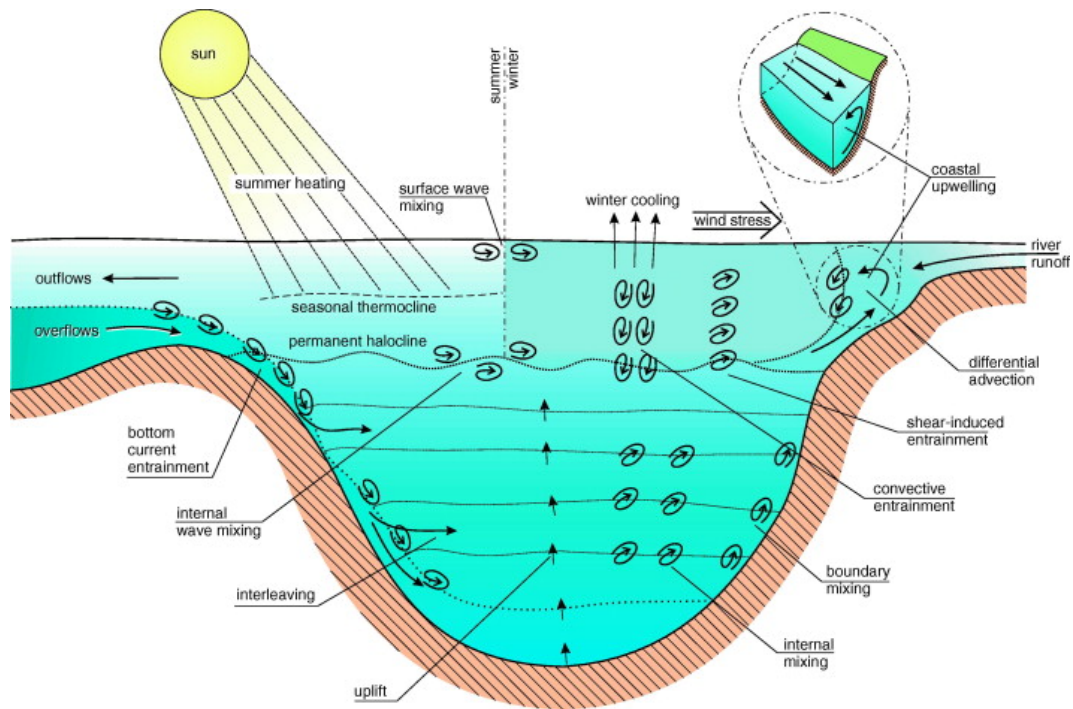
**Figure 1.10** – Schematic view of mixing processes in the Baltic Sea (*Reissmann et al.*, 2009).

Still, *up- and downwelling* phenomenons are typical for the Baltic Sea and well documented (Fig. 1.10; *Alenius et al.*, 1998; *Vahtera et al.*, 2005; *Lehmann and Myrberg*, 2008; *Lips et al.*, 2009). The process is characterized by winds blowing predominantly parallel to the coast, for longer than a initial period. One initial period reflects the response time of an upwelling event to the initial start of a wind event (*Feistel et al.*, 2008). The surface water is directed perpendicular (Coriolis effect) to the direction of the blowing wind from the coast towards the open water. The displacement of the surface water leads to the upwelling of deeper water at the coast. Depending on the strength and period of the wind forces, upwelling can range from a small scale coastal event to a large scale open sea influencing phenomenon. Upwelling occurs throughout the year and can be easily observed via satellite imaging of the surface temperature during summer (Fig. 1.11; e.g. *Siegel*, 2000; *Siegel and Gerth*, 2000; *Siegel et al.*, 1994). During an upwelling event dense, cooler (interstitial winter water) and usually nutrient-rich water is shifted towards the sea surface, whereas warmer and nutrient-depleted summer surface water is replaced. The displacement

and mixing during upwelling events involves great effects for the nutrient supply and the biochemistry and ecological regime of the surface water (*Alenius et al.*, 1998; *Vahtera et al.*, 2005; *Feistel et al.*, 2008; *Lehmann and Myrberg*, 2008).
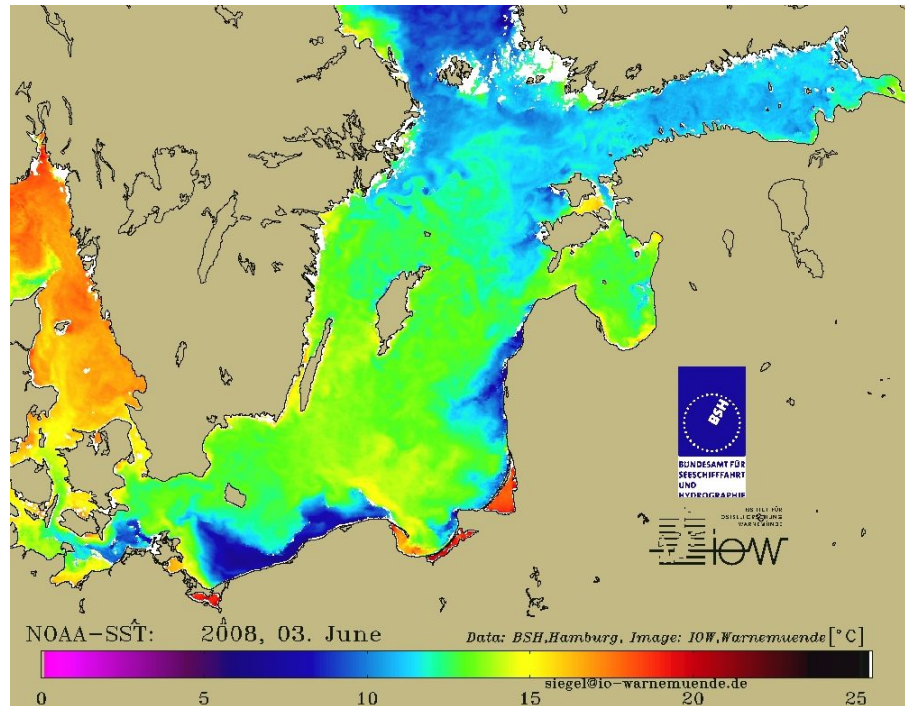


**Figure 1.11** – Satellite image of the central Baltic Sea on June $3^{rd}$ 2008. Sea surface temperatures show a displacement of the warm surface water (yellow) towards the Swedish coast and cold upwelling water (blue) along the Polish and Latvian coastline during easterly blowing wind conditions. (Data by BSH, processing by H. Siegel, IOW).

*Coastal jets* are formed during persistent up- or downwelling events, which lead to local lowering or rising of the sea level and the development of a horizontal pressure gradient. Together with the Coriolis forces, this pressure gradient accelerates coastal currents and transports water masses at times over large distances along the coast (*Feistel et al.*, 2008).

The surface water of the Baltic Sea is influenced by a variety of waves and wave induced mixing like surface gravity waves, seiches, Kelvin waves, topographic waves or eddies. *Surface gravity waves* describe the distortion of a flat surface and the transport of energy without significant movement of material. A short overview and the mathematical approach is given in *Feistel et al.* (2008) and *Kundu and Cohen* (2008). Turbulences of the sea surface are particular important for the sea-air gas transfer and

have been discussed e.g. in *Liss and Merlivat* (1986), *Wanninkhof* (1992), *Wanninkhof et al.* (2009) and *Lass et al.* (2010).

Turbulent mixing at the sea surface also effects the water column and several mechanisms have been described, which resulting in vertical mixing. Still, the relevance of each wave type for the Baltic Sea and particularly for the vertical and horizontal methane distribution is not fully understood yet.

*Internal gravity waves* occur at interfaces between two layers of different densities (Fig. 1.10; *Garrett and Munk*, 1979; *Munk*, 1981). Internal waves are considered as main reason for sporadic instabilities, turbulences and mixing between layers of the water column. Turbulences between water layers cause vertical displacement and an uplift of phytoplankton into the sunlit layer, which leads to enhanced productivity implying an ecological relevance (*Kamykowski*, 1974; *Konovalov et al.*, 2003; *Reissmann et al.*, 2009).

Van der Lee and Umlauf (2011) showed that near-inertial waves can be associated with shear-bands of enhanced dissipation rates and mixing within (and slightly above) the permanent halocline. Investigations at the sediment surface showed strong bottom stress and bands of elevated shear and dissipation rates especially during the winter season, creating a well mixed bottom layer of up to 4 m thickness (*van der Lee and Umlauf*, 2011).

The shear stress between water layers of different densities as well as between the bottom layer and the sediment surface are assumed to contribute significantly to internal mixing of the water column and is subject of several studies (Fig. 1.10; e.g. *Munk*, 2001; *Lass and Mohrholz*, 2003; *Umlauf and Arneborg*, 2009; *van der Lee and Umlauf*, 2011).

Dense bottom water inflows or *bottom gravity waves* enter the Arkona Basin via the transition zone and basically spiral cyclonically (Kelvin-wave type) along the rims of the Basin, influenced by the Coriolis force and the pressure gradient (*Mohrholz et al.*, 2006; *Umlauf et al.*, 2007; *Burchard and Rennau*, 2008; *Feistel et al.*, 2008; *Reissmann et al.*, 2009). The residence time of inflowing water in the Arkona Basin range up to 3 month (*Lass et al.*, 2005).

*Lass and Mohrholz* (2003) identified several dynamics and mixing mechanisms along inflowing bottom saltwater plumes in the Arkona Basin: (i) Wind-induced mixing is particularly effective at shallow depths. At deeper regions, bottom waters are rather protected from mixing by stratification. (ii) During differential advection, heavier salt water from the back of a plume is shifted to the front and above lighter ambient water, resulting in an unstable vertical stratification and strong mixing by vertical convection. (iii) Between inflowing dense bottom water (Ekman bottom friction layer, *Kundu and Cohen*, 2008) and ambient water masses sheer stress occurs, leading to increased mixing between the layers.

*Vertical mixing* within the water column of the Baltic Sea can be described using three approaches. Inflowing sea water characterized by horizontal advection below the halocline, upwelling dominating at the rims of the basins and vertical diffusion accounting for the transport through the halocline (*Feistel et al.*, 2008; *Reissmann et al.*, 2009). Additional parameters influencing a turbulent model assumption are breaking of internal waves, shear stress between water layers of stratified systems or the sediment surface and Langmuir circulations. The energy transfer from primary internal waves, turbulent mixing, shear stress and breaking of internal waves and subsequent generation of boundary mixing is subject of several studies (e.g. *Umlauf et al.*, 2007; *Burchard et al.*, 2009; *van der Lee and Umlauf*, 2011).

Dynamics within the water column of the Baltic Sea are very complex and influence the transport and mixing of water masses with different salinity and temperature as well as dissolved nutrients. The impact of vertical and horizontal mixing on the water column methane distribution within the Baltic Sea is not yet understood, but first observations are presented in chapter IV.

### 1.2.3   Methane in the Baltic Sea

The general methane distribution within the water column of the Baltic Sea is shown in *Schmale et al.* (2010b) (see also appendix Fig. A.1). Figure A.1 shows

generally low methane concentrations within the surface water of the Baltic Sea with values of approximately 4 nM. Elevated methane concentrations in the deeper and bottom layers of the basins (e.g. Western and Eastern Gotland Basin) on the contrary reach up to 1086 nM (*Schmale et al.*, 2010b). The sharp methane gradient follows the redoxline showing high methane concentrations in the anoxic, lower water body, which can be observed e.g. in the Eastern Gotland Basin (Fig. A.1, b and c). The coherence of elevated methane concentrations in anoxic waters within the southern and central Baltic Sea are also shown in studies from *Geodekyan et al.* (1991), *Dzyuban et al.* (1999) and *Bange et al.* (1994). Methane concentrations in anoxic waters of shallow regions like the Kiel Harbour (Germany; *Schmaljohann*, 1996) or the Mariangers Fjord (Denmark; *Fenchel et al.*, 1995) reach 3,000 and 30,000 nM, respectively.

Strong seasonal variations within the surface water methane concentrations and methane saturation values could be observed in selected areas of the Baltic Sea (*Bange et al.*, 1994, 1998; *Schmaljohann*, 1996; *Heyer and Berger*, 2000; *Abril and Iversen*, 2002; *Gülzow et al.*, acc. for BGS:D). *Bange et al.* (1994) quote mean area-weighted methane surface saturation values of 113 % and 398 % in February and July/August for the southern and central Basin of the Baltic Sea, respectively. Even larger fluctuations could be observed in shallow coastal areas like Fjords (e.g. Randers Fjord - Denmark or Eckernförde Bay - Germany) or lagoons (Oder River estuary area - Germany; *Bange et al.*, 1998; *Bussmann and Süss*, 1998; *Heyer and Berger*, 2000; *Abril and Iversen*, 2002).

The main source of methane within the water column of the Baltic Sea is the diffusional transport from the sediment (section 1.1.3; (*Fenchel et al.*, 1995; *Schmaljohann*, 1996; *Bussmann and Süss*, 1998; *Heyer and Berger*, 2000; *Bange et al.*, 2010). The emission rate of methane depends on the availability of organic matter (*Heyer et al.*, 2002; *Bange et al.*, 2010). Still, the sedimentary anaerobic and aerobic oxidation of methane effectively reduces methane emissions to the water column (*Jørgensen et al.*, 1990; *Schmaljohann*, 1996; *Piker et al.*, 1998; *Dzyuban et al.*, 1999; *Dahlke et al.*, 2000; *Abril and Iversen*, 2002; *Whiticar*, 2002). Especially the dependency of sulfate reduction and methane production was observed in the Gotland Deep (section 1.1.3;

*Piker et al.*, 1998) and the Baltic Sea - North Sea transition area (*Jørgensen et al.*, 1990). The aerobic oxidation of methane within the water column of the Baltic Sea was observed e.g. by *Fenchel et al.* (1995) and *Schmaljohann* (1996).

Other methane sources are natural seepage, gassy sediments or riverine input. Seepage and pockmark areas were observed e.g. in the Eckernförde Bay (*Bussmann and Süss*, 1998; *Whiticar*, 2002; *Schlüter et al.*, 2004) and the Gdansk Basin (*Pimenov et al.*, 2010). Bubble-mediated release of methane from (gassy) sediments were reported by *Laier et al.* (1992) and *Dando et al.* (1994) for the Kattegat, by *Söderberg and Flodén* (1992) for the Stockholm Archipelago and by *Jackson et al.* (1998) for the Eckernförde Bay. Significant amounts of methane are transported into the Baltic Sea via riverine input (*Bange et al.*, 1998), but most of it is oxidized and released to the atmosphere within the upper estuarine area (*Abril and Iversen*, 2002).

Estimates about methane fluxes from selected areas of the Baltic Sea towards the atmosphere vary significantly. First approximations for the southern and central Baltic Sea are presented in *Bange et al.* (1994) ranging from 9.5 to 14.6 $\mu$mol m$^{-2}$ d$^{-1}$ during winter and from 101.1 to 1200.1 $\mu$mol m$^{-2}$ d$^{-1}$ during summer (based on discrete data measurements). Opposing flux estimations with low methane emission rates during summer and high emissions during winter are presented and discussed in chapter III. Attempting the generation of a total emission rate for the Baltic Sea, *Bange et al.* (1994) postulated an under-estimation of methane fluxes from shallow areas due to the lack of data. Methane fluxes for the Randers Fjord (Denmark) were estimated ranging from 40 to 355 $\mu$mol m$^{-2}$ d$^{-1}$ (*Abril and Iversen*, 2002). Several parameters influencing methane emissions of the Baltic Sea towards the atmosphere like seasonal variations of temperature or wind speed were observed and identified during several studies (see chapter III; *Bange et al.*, 1998, 2010; *Heyer and Berger*, 2000; *Abril and Iversen*, 2002).

## 1.3   Sea - Air Exchange

The exchange of a slightly soluble non-reactive gas between a water body and the atmosphere depends on the concentration difference of the gas in both phases and the gas transfer velocity $k$ [m s$^{-1}$]. The gas flux $F$ [mol m$^{-2}$ s$^{-1}$] can be defined with

$$F = k \ (C_w - C_o) \tag{1.9}$$

where $C_o$ is the concentration at the water surface [mol m$^{-3}$] and $C_w$ is the gas concentration in the well-mixed water body [mol m$^{-3}$]. $k$ can be defined as the kinetic forcing function, whereas the concentration difference can be described by the thermodynamic driving potential. $C_o$ can also be expressed as the concentration of the gas in the atmosphere $C_a$ and the dimensionless Henry coefficient $\alpha$ (Equation 1.10). The Henry coefficient defines the ratio of a gas concentration in air and its concentration dissolved in water, at equilibrium.

$$F = k \ (C_w - \alpha * C_a) \tag{1.10}$$

A negative flux in equation 1.10 describes the gas transfer from the atmosphere towards the water body. Using the thermodynamic driving force in terms of the partial pressure of a gas in the atmosphere and the water body, equation 1.10 can be written in case of methane:

$$F = k * s \ (p_{CH4w} - p_{CH4a}) \tag{1.11}$$

where $s$ [mol L$^{-1}$ atm$^{-1}$] is the solubility of methane in water, $p_{CH4a}$ is the partial pressure of methane in the atmosphere and $p_{CH4w}$ is the partial pressure of methane in the water body.

Several conceptual models for air-sea gas exchange show, that $k$ is controlled by aqueous phase hydrodynamics at the air-sea water interface (*Wanninkhof et al.*, 2009). The simplest model is the *stagnant-film model*, based on the two layered model approach after *Liss and Slater* (1974). The model describes the gas transfer in terms

of molecular diffusion through a thin layer of water with a steady thickness at the air-sea interface. Based on Fick's first law of diffusion it can be written:

$$k = \frac{D}{\delta} \tag{1.12}$$

with the molecular diffusivity $D$ [m$^2$ s$^{-1}$] divided by the thickness of the stagnant film $\delta$ [m]. Equation 1.12 shows, that a decrease of $\delta$ results in an increase of $k$ and that $k$ is directly proportional to the diffusivity $D$. Several studies subject $k = D^n/\delta$ with $n$ between one half and two thirds, depending on the turbulence at the air-sea interface (*Jähne et al.*, 1987; *Nightingale et al.*, 2000; *Wanninkhof et al.*, 2009)

An improved model approach is the *surface renewal model* introduced by *Liss and Merlivat* (1986). The model describes the boundary layer as a periodically renewing layer from the bulk. The film replacement rate is than the limiting step in the gas transfer (*Liss and Merlivat*, 1986). $k$ is proportional to $D^{0.5}$. The surface renewal model is physically more realistic than the stagnant film model, but is only little applied during environmental investigations due to the difficulty of specifying the film replacement rate (*Liss and Merlivat*, 1986).

A third approach is the *boundary layer model* after *Jähne et al.* (1987), which describes gas flow similar to mass and momentum transfer using the Schmidt number $Sc$. $Sc$ is defined by the ratio of the kinematic viscosity $\nu$ and diffusivity $D$:

$$Sc = \frac{\nu}{D} \tag{1.13}$$

The model approach assumes a smooth sea surface and *Jähne et al.* (1987) confirms the dependency of the transfer velocity on the Schmidt number in wind channel experiments with $k$ being proportional to $Sc^{-2/3}$ and $D^{2/3}$ respectively. Assuming a rough surface, $k$ can be described using $Sc^{-1/2}$. The third step is the breaking wave regime with bubble entrainment, which implies an even higher gas exchange (*Liss and Merlivat*, 1986). Additional, *Jähne et al.* (1987) subject the strong temperature dependency of the Schmidt number and the diffusivity coefficient in fresh and saline waters respectively.

The introduced conceptional model approaches can be improved by involving meteorological parameters like wind and wave formation for the determination of the transfer velocity $k$. The model of *Liss and Merlivat* (1986) (LM86) determines the transfer velocity based on tracer experiments with $SF_6$ and wind channel experiments. *Liss and Merlivat* (1986) define three linear regimes for carbon dioxide in fresh water (Sc = 600) depending on the wind velocity $u_{10}$ measured in 10 m hight:

$$u_{10} \leq 3.6 ms^{-1} \qquad\qquad\qquad k = 0.17 * u_{10} \qquad\qquad (1.14)$$

$$3.6 < u_{10} \leq 13 ms^{-1} \qquad k = (2.85 * u_{10} - 9.65) \qquad\qquad (1.15)$$

$$u_{10} > 13 ms^{-1} \qquad\qquad k = (5.9 * u_{10} - 49.3) \qquad\qquad (1.16)$$

A second approach, introduced by *Wanninkhof* (1992) (W92), uses global bomb ^{14}C data and wind-wave tank results. *Wanninkhof* (1992) determines the uptake of ^{14}C in sea water regarding to meteorological aspects and a water temperature of 20° C. *Wanninkhof* (1992) suggested a quadratic dependency of the wind velocity with $u_{10}^2$ and that the gas transfer scales with the wind stress $\tau$. Using the Schmidt number 660, it can be written:

$$k_{660} = 0.39 * u_{10}^2 \qquad\qquad (1.17)$$

The coefficient 0.39 can be taken for long-term applications. For shorter time scales it becomes necessary to consider the wind variability and a coefficient of 0.31. The relationship introduced by *Liss and Merlivat* (1986) yields approximately 50 % lower global fluxes that the relationship of *Wanninkhof* (1992).

Other parametrizations of $k$ are given by *Nightingale et al.* (2000) for fetch limited environments like coastal seas. *Sweeney et al.* (2007) performed inverse modelling to deduce the gas transfer and wind velocity relationship. This approach underestimates the relationship by 33 % compared to *Wanninkhof* (1992). All approaches are quadratic with zero intercept and are applicable to all sparingly soluble gases

*Wanninkhof et al.* (2009) by correction of the Schmidt number. A revised relationship for wind velocities $u_{10} < 15 \ m \ s^{-1}$, applicable for a global constrain is given by *Wanninkhof et al.* (2009) (W09) with

$$k_{660} = 0.24 * u_{10}^2. \tag{1.18}$$

The relationships after *Liss and Merlivat* (1986) and *Wanninkhof* (1992) are commonly used for flux estimations of gases towards the atmosphere, in which LM86 can be considered as lower boundary of the estimation and W92 as upper boundary. W09 integrates between both estimations. For flux calculations performed within the framework of this thesis, the approach after *Wanninkhof et al.* (2009) with the equation 1.18 was used.

## 1.4 Methane Measurements

First measuring techniques for dissolved gases based on physiological fluid measurements using manometric and microgasometric techniques (*Reeburgh*, 2007). Today, methane is determined within the gaseous phase using gas chromatography (GC). The measuring principle of gas chromatography is the separation of chemical compounds due to different polarizations of its functional groups. The volatile compounds of a sample are separated between a mobile and a stationary phase, based on absorption and desorption. The sample is injected into a mobile phase, an inert carrier gas such as helium or nitrogen. The mobile phase flows over a stationary phase packed in a column. Important for the separation process, is the length $l$, the internal diameter $id$ and the packing material of the column.

Two types of columns can be distinguished: packed and capillary columns. Packed columns (l:1.5 - 10 m, id: 2 - 4 mm) are usually made of stainless steel or quartz glass, containing fine divided, inert, solid support material (e.g. diatomaceous earth). Capillary columns are formed by a microscopic layer of liquid or polymer inside a quartz glass or metal tubing. Depending on the characteristics of the microscopic liquid and

the gas sample, gaseous compounds will be adsorbed with a different strength at the liquid. The buffer stage or plate number $N$ determines thereby the amount of equilibrations adjusted by the columns of a substance between the stationary and mobile phase in the column. The higher $N$ is, the more equilibriums of compounds of the substance can be accomplished along a column, which results in a better separation quality of the column. During the flow of the mobile phase through the column, the gaseous compounds are separated and leave the column at different times. The so called *retention time* is characteristic for each chemical compound and depends on its interaction with the stationary phase. A long retention time indicates strong interactions with the stationary phase. The retention time is used for the identification of each chemical compound and constitutes the principle determination parameter of gas chromatography.

Methane can be determined using a *flame ionization detector* (FID), a *temperature conductivity detector* (TCD) or a *pulsed discharge detector* (PDD). In this thesis a FID was used, which is the most utilized detector for ionisable substances in gas chromatography due to his high selectivity (1 ng), robustness and his linearity over a wide concentration range. Organic compounds are burned in a hydrogen flame and are thus partially ionised. During the ionization, electrons are released and captured at the circular collector electrode, placed around the flame. The caption of the electrons gives a signal, which is recorded as peak. More informations about the principle measuring technique and applications using gas chromatography and FID is given in *Hübschmann* (2009).

For the application of gas chromatography on measurements at marine environments, several methods were developed to extract the gaseous phase from the liquid phase.

**Headspace method**   The headspace technique is a static method, based on the development of an equilibrium of a compound between the gaseous phase and a liquid phase. The water sample is transferred into a sealed headspace vial and overlaid with a inert gas (e.g. nitrogen, helium). After a period of thoughtfully shaking (*Rehder*

*et al.*, 1999) or resting, an equilibrium of the partial pressure of the volatile within the gaseous phase and the liquid phase develops. With a gas tight syringe, a subsample from the gaseous phase of the headspace vial can be taken and injected into the gas chromatograph for determination. The amount of substance $n$ [mol] dissolved in the liquid phase distributes between the liquid phase ($n_{aq}$) [mol] and the gaseous phase ($n_g$) [mol] during the development of the equilibrium. The concentration of methane within the liquid phase $C_{CH4}$ [mol L$^{-1}$] can be calculated with

$$C_{CH4} = \frac{n_g + n_{aq}}{V_{aq}}. \tag{1.19}$$

Therein $V_{aq}$ [L] implies the volume of the liquid phase. The distribution of methane between the liquid and the gaseous phase depends on the ideal gas law

$$n_g = \frac{p_{CH4} * V_g}{R * T} \tag{1.20}$$

with the partial pressure of methane $p_{CH4}$ [atm] in equilibrium with the liquid phase, the volume of the gas phase $V_g$, the universal gas constant $R = 8.314$ [J mol$^{-1}$ K$^{-1}$] and the absolute temperature $T$ [K]. The solubility of methane $c_i$ in the liquid phase in particular is defined by Henry's law:

$$c_i = s * p_{CH4} \tag{1.21}$$

The solubility coefficient $s$ [mol L$^{-1}$ atm$^{-1}$] for methane is calculated after *Wiesenburg and Guinasso* (1979). The mole fraction of methane in the liquid phase of the headspace vial is then given by:

$$n_{aq} = V_{aq} * c_i = V_{aq} * s * p_{CH4} \tag{1.22}$$

With equation 1.20 and 1.22 it can be formed:

$$C_{CH4} = \frac{p_{CH4} * V_g}{R * T * V_{aq}} + s * p_{CH4} \tag{1.23}$$

The equilibrium time and the enrichment of methane in the headspace can be influenced by a variety of parameters. *Lammers and Süss* (1994) observed that a large relation between the gaseous and the liquid volume results in a better methane yield after equilibration. Depending on the salinity and temperature of the water sample, the measured compound and the shaking frequency, the period until equilibrium is reached varies additionally (*Hübschmann*, 2009).

**Purge & Trap method**   With the introduction of the sample conditioning method presented by *Swinnerton et al.* (1962) bigger sample volumes can be measured and significant higher sensitivities can be achieved. The purge and trap method (PTM) is a dynamic head space technique (*Hübschmann*, 2009). Methane (and other volatiles) is continuously extracted from a matrix (water sample) during the purge phase and concentrated in an adsorption trap during the trapping phase. During the purge phase, methane is driven out of the water sample by a purge gas (e.g. helium or nitrogen), which passes through a special frit in the base of the purge vessel (Fig. 1.12). The generation of small gas bubbles allows a maximised surface area between the purge gas and the liquid phase. After the extraction, the purge gas transports all dissolved gases from the sample to the trap. The cold trap inhibits the passage of water vapour to protect the following traps and trap materials (Fig. 1.12). Methane is trapped and concentrated using a cooled, packed column as adsorbent (*Swinnerton and Linnenbom*, 1967). During the following heating process of the column, methane is released from the adsorbent and transported by a carrier gas to the gas chromatograph for detection (Fig. 1.12). The amount of volume, which is purged from the sample depends on the purge time and flow rate (*Hübschmann*, 2009).

During this thesis, a Purge&Trap setup based on *Michaelis et al.* (1990) was used. The setup consists of three main units: the extraction or purge vessel, the adsorption or trapping unit and the gas chromatograph for detection and analysis and is described in more detail in *Thomas* (2011).

*Weiss* (1981) introduced an automated gas chromatographic system for the measurement of carbon dioxide, methane and nitrous oxide in combination with the strip-
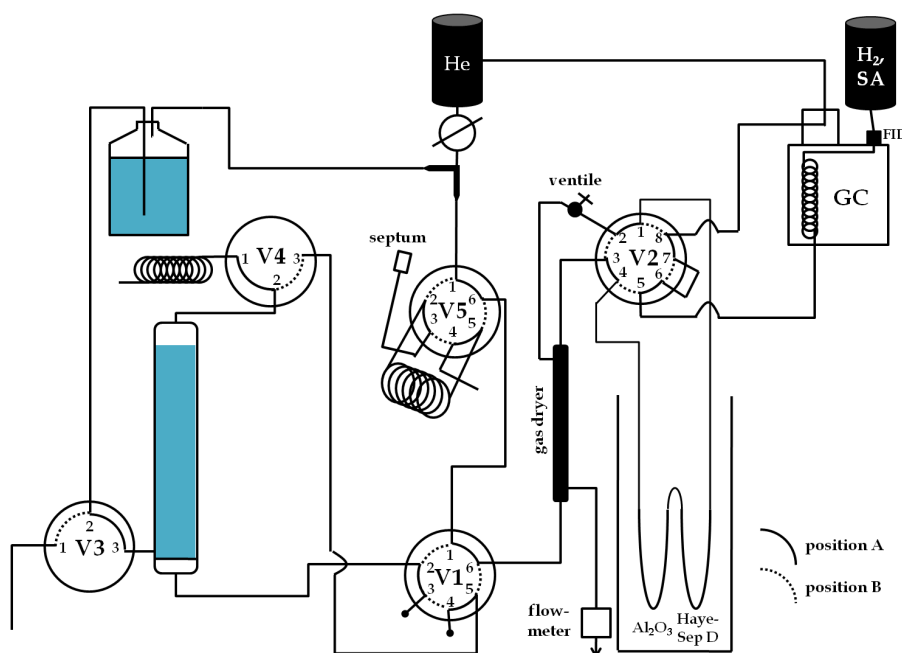
**Figure 1.12** – Schematic of the Purge&Trap setup with the valves V1-V5. Depending on the analyst, different trapping materials can be used e.g. $Al_2O_3$ for the volatile organic compounds $C_2$-$C_5$, or HayeSep D for methane (*Thomas*, 2011).

ping Purge&Trap method. Advantageous for this method is, that quantitative extraction of dissolved gases are also possible for small concentration ranges. The sampling and storing (after poisoning) procedure is comparatively easy. Unfavourable are the instrumental and time consuming expenses as well as the on board performance of the PTM.

**Vacuum degassing method** The discrete sampling method was introduced by *Schmitt et al.* (1991). Schmitt and coworkers developed a method to extract dissolved gases from a water sample using ultrasound and vacuum (VUS). *Lammers and Süss* (1994) showed, that the quantitative yield of methane from the water sample using VUS is only at $62 \pm 3.8$ %. The improved vacuum degassing method (VDM, without ultrasound; *Rehder et al.*, 1999) used during this thesis additionally offers an isotope sample. With this method, a methane yield of $87.4 \pm 11.2$ % could be achieved (*Thomas*, 2011).

The sample flasks need to be evacuated before the sampling. With a special
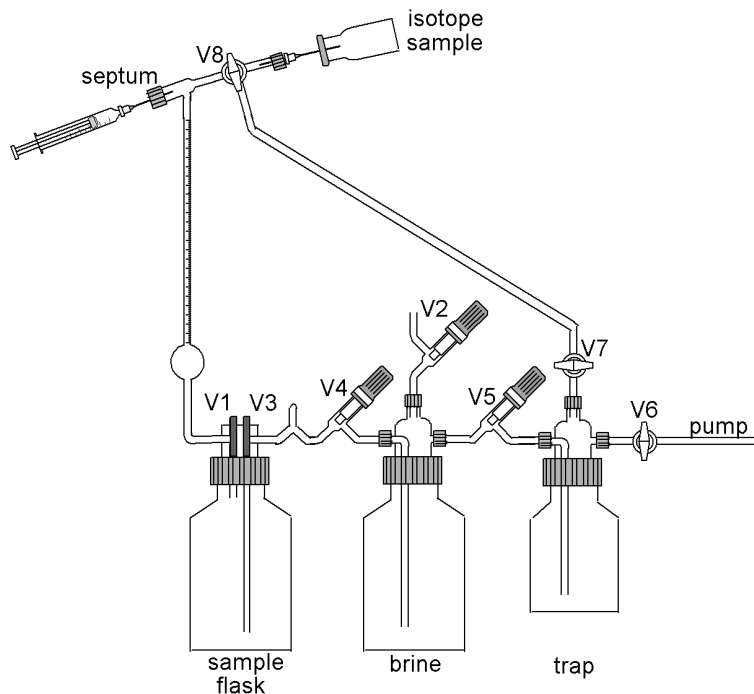
**Figure 1.13** – Schematic of the vacuum degassing method with the valves V1-V8 (*Thomas*, 2011).

designed cap, the water sample can be transferred from a Niskin bottle into the pre-evacuated flasks without contamination of the water sample with ambient air. The flask is filled with 2/3 of sample, closed and agitated to support the development of an equilibrium between the gaseous and the liquid phase. Subsequently, the flask is mounted into the measuring setup. The hole measuring setup is now evacuated, including the vial for isotopic measurements. With the closing of valve V5 and the opening of valve V2, the pressure compensation leads to the transfer of the high saline, degassed brine into the sampling flask. According to the higher density, the brine underlays the sample water within the sample flask. With the closing of valve V8 and the opening of valve V1, the headspace of the sample flask is pressed into the burette. The volume of the gaseous phase can be determined. After taking a subsample for injection into the gas chromatograph for determination, valve V8 can be opened to transfer the remaining gaseous phase into the isotope vial. The methane concentration within the subsample can be calculated using equation 1.24.

$$C_{CH4} = \frac{x_{CH4} * V_g}{V_{mol} * V_{aq}} \tag{1.24}$$

with the mole volume for ideal gases $V_{mol}$ = 22.41 L mol$^{-1}$. Since the extraction coefficient varies, consistent operational conditions need to be provided to obtain high reproducibility. Therefore, methane can also be calculated using the approach based on the theoretical total gas composition, solved in one litre water sample. Nitrogen, argon and oxygen constitute 99 % of the main dissolved components in water.

$$c_{total} = c_{N2} + c_{Ar} + c_{O2} \tag{1.25}$$

The equilibrium concentration for argon and nitrogen can be calculated after *Weiss* (1970). The oxygen concentrations were determined using Winkler titration (*Grasshoff et al.*, 1999). Equation 1.24 and 1.25 result in:

$$C_{CH4} = \frac{x_{CH4} * c_{total}}{V_{mol}} \tag{1.26}$$

The determination of the methane concentration of a sample using the approach of the total gas composition can not be applied for anoxic water samples, due to the significant change of the nitrogen content via denitrification and other reactions (*Murray et al.*, 2003, 2005)

The vacuum degassing method allows on-board measurements. Very low concentrations can be detected and an additional samples for isotopic measurements can be provided. Unfavourable are the extensive preparations before sampling as well as the time consuming and complex handling of the set up. Samples can not be stored longer than a few hours, due to the degradation of the vacuum within the sample bottle.

PTM and VDM are discrete measuring systems and in general characterized by time consuming handling and sampling as well as high man power expenses. Therefore lots of efforts were made to generate automated, autonomous and continuous

measuring systems during the past decades. The first step for improved measuring of methane was the replacement of the discrete sampling technique via an equilibration system. *Butler et al.* (1989) developed the first equilibration system in combination with gas chromatography. The equilibrators used in this thesis are characterized by a glass (or acryl glass) flask with a continuous flow-through of the sampling water and the counter current flow of carrier gas through the water. During the passage of the carrier gas through the water phase via small bubbles, the gaseous phase equilibrates with the liquid phase. The gaseous phase can than be diverted and transported towards the GC. A detailed description about the performance of an equilibrator system is given in chapter II. *Bange et al.* (1994) and *Rehder* (1996) describe successful measurements of methane using equilibrator systems. Disadvantages of this methods using gas chromatography are the consumption of sample during the measuring process and that for each measuring sequence the equilibrium becomes disrupted.

Since 1980s *infrared absorption spectrometry* (IR-spectroscopy) has been used for measurements of trace gases in the lab. The gas molecules absorb specific frequencies of the infrared spectrum of the non visible light (0.8 - 1000 $\mu$m), depending on the characteristic of their structure (*Skoog*, 1996; *Atkins and de Paula*, 2006). During the measuring procedure, a beam of infrared light passes through the sample. The emitted energy is absorbed, when its frequency matches the vibrational frequency of a bond. By analysing the frequency range after the passing through the sample and a reference sample, details about the molecular structure of the sample can be achieved. Only molecules with changing dipole structure can be considered for IR-spectroscopy. Methane for example is characterized by four bonds (Fig. 1.1).

The application of IR-spectroscopy for various field techniques implies serious problems in drift and low sensitivity (*Zahniser et al.*, 1995). It can be distinguished between open-path and closed-path techniques. An open-path methane analyser (e.g. *McDermitt et al.*, 2011; LICOR Bioscience, www.licor.com) can be used for eddy flux covariance measurements above marshes, tundras or agricultural field. Methane concentrations are measured using *wavelength modulation spectroscopy* (WMS) at near 1.65 $\mu$m.

Closed-path analysers employ advanced technologies such as *wavelength scanned cavity ring down spectroscopy* (WS-CRDS) or *integrated cavity output spectroscopy* (ICOS).

WS-CRDS is a measuring technique used for example at PICARRO analyzers (*Rella*, 2010; www.picarro.com). During the measuring process, a tunable single-frequency laser diode enters a cavity defined by two or more high reflectivity mirrors (reflectivity of 99.999 %). The cavity fills with the circulating laser light and a detector senses the small amount of light passing through the mirrors, producing a signal that is directly proportional to the intensity in the cavity. After reaching a threshold level at the detector (in a few tens of microseconds), the laser is abruptly turned off. The light intensity inside the cavity decays exponentially to zero, which is called the 'ring down' or 'ring down time'. A sample within the cavity accelerates the ring down time compared to a cavity without a sample. Tuning the laser to different wavelengths, the "cavity only" ring down time can be determined for several compounds.

A competing method is presented by *Baer et al.* (2002) using ICOS with a highly specific narrowband laser (e.g. www.losgatos.com). Whereas at WS-CRDS, the sample flow stops during the measuring sequence, the absorption of the band laser using ICOS is measured under continuous sample flow. In this thesis a LOS GATOS sensor using ICOS in combination with an equilibrator system for continuously methane and carbon dioxide measurements was used.

The CAPSUM technology GmbH (since 1999; www.capsum.de) provides a semi conductive sensor for continuous measurement of methane in aquatic systems. CON-TROS (www.contros.eu) uses non-dispersive infrared spectrometry (NDIR). Both sensors base upon the diffusion of methane through a silicon membrane into a measuring cell. Problems occur with the alteration of the membrane, the long response time and the low sensitivity, which makes these sensors less applicable for measurements in marine science.

# A new method for continuous measurement of methane and carbon dioxide in surface waters using off-axis integrated cavity output spectroscopy (ICOS): An example from the Baltic Sea.

Gülzow. W.[1*], Rehder, G.[1], Schneider, B.[1], Schneider v. Deimling, J.[1],

Sadkowiak, B.[1]

[1] Leibniz Institute for Baltic Sea Research, Seestraße 15, D-18119 Warnemünde, Germany

[*] Corresponding author: wanda.guelzow@io-warnemuende.de

## 2.1 Introduction

Methane is an atmospheric trace gas that directly and indirectly influences the climate on Earth to a significant degree. It is the most important greenhouse gas after water vapor and carbon dioxide. As a natural source for atmospheric methane, oceans play only a modest role in the global methane budget, but a great part of that (up to 75 %) is emitted from estuaries and coastal areas (*Bange*, 2006). The main source of methane in these environments is the anoxic microbial fermentation of organic matter (methanogenesis) in marine sediments and anoxic marine basins (*Cicerone and Oremland*, 1988; *Hovland*, 1992). Minor sources are seepage of gas (*Bussmann and Süss*, 1998; *Laier et al.*, 1992) or methane-rich advective porewater flow and riverine input. Also various mechanisms in the oxygenated water column

like formation of methane in microniches (fecal pellets, zooplankton guts; *Karl and Tilbrook*, 1994) have been discussed. Whereas a considerable number of studies describe methane distributions in coastal and shallow waters and estuaries (e.g. *Bange et al.*, 1994, 1998; *Rehder et al.*, 1998; *Schmale et al.*, 2005). *Bange* (2006) recently concluded that coastal methane emissions to the atmosphere may be underestimated due to the lack of data, and *Schneider von Deimling et al.* (2011) points out a seasonal bias through predominant sampling during summer season for trace gas flux measurements. Continuous measurements can remedy this lack of data and help to better understand the methane distribution in surface waters and the spatio-temporal variability of air-sea fluxes from these regions. *Schmale et al.* (2010b) show that strong stratification in large parts of the Baltic affect the distribution of dissolved methane in the water column. In deep and anoxic waters, methane concentrations exceed 400 nM, whereas the transfer to the upper mixed and surface layers is inhibited. In other regions, stratification is less dominant and processes like wind-induced mixed layer deepening or local upwelling can mix methane- enriched deeper water masses to the surface. *Schmale et al.* (2010b) show that both vertical methane distribution and surface water concentrations are highly variable in the Baltic Sea, making this semi-enclosed sea an ideal area to study the variability of methane air-sea fluxes in a coastal environment. Methane is measured in the gaseous phase, and until the introduction of gas chromatography (GC) in the early 1950s, dissolved gas measurements were conducted using manometric and microgasometric techniques (*Reeburgh*, 2007). Higher sensitivity was achieved by the sample conditioning method (purge&trap) presented in *Swinnerton et al.* (1962). *Weiss* (1981) introduces an automated gas chromatographic system for the measurement of $CO_2$, $CH_4$, and $N_2O$ in combination with the purge&trap-method (PTM). *Schmitt et al.* (1991) introduced another discrete sampling technique using vacuum to extract the amount of dissolved methane from a water sample. Further improved methods (*Lammers and Süss*, 1994; *Rehder*, 1996; *Keir et al.*, 2005) offer additional subsamples for stable isotope analysis. *Butler et al.* (1989) were the first to design an equilibration system (equilibrator developed by R.F. Weiss) in combination with gas chromatography to determine the surface con-

centrations for methane and a variety of other trace gases by discrete sampling of an air volume continuously equilibrated with a flow of water. Successful measurements of methane using various equilibrator systems have been performed since that time (e.g. *Bange et al.*, 1994; *Rehder and Süß*, 2001). However, disadvantages of using gas chromatography are the discrete sampling and the consumption of sample during the measurement process, which leads to the disruption of the equilibrium during each measurement sequence. Since the 1980s, infrared absorption spectrometry has become popular for measurements of trace gases in the lab. The development of various field techniques has revealed serious problems with drift and low sensitivity (*Zahniser et al.*, 1995). Today, the commonly implemented usage for $CO_2$ continuous measurements is the nondispersal infrared spectroscopy (LICOR $CO_2$ detector; *Schneider et al.*, 1992, 2006), which was a major breakthrough for unmaintained detection of $CO_2$ partial pressures from surface waters. These observations have made it possible to assess the seasonal patterns of global oceanic $CO_2$ fluxes (*Takahashi et al.*, 2009). However, until recently, the combination of continuous water-air equilibration coupled to spectroscopy was limited to $CO_2$, because the concentrations of other climatically relevant trace gases are too small for the approach. A new method presented by *Baer et al.* (2002) is the off-axis integrated cavity output spectroscopy (ICOS) technique, using a highly specific narrowband laser for measuring methane and carbon dioxide at atmospheric levels with high precision and accuracy. In this article, we present a new method using ICOS in combination with an equilibrator system for continuous, nonconsuming $CH_4$ and $CO_2$ measurements. Laboratory experiments and first encouraging initial field results are presented presented. The system was installed on the cargo ship *Finnmaid* (Ferry Company Finnlines) in November 2009 as a complement to an existing system (*Schneider et al.*, 1992, 2006). The ferry line commutes regularly between Travemünde (Germany), Rostock (Germany), Gdynia (Poland), and Helsinki (Finland) and continuously measures parameters such as carbon dioxide, oxygen, temperature, salinity, chlorophyll a, fluorescence, and now methane in the surface water of the Baltic Sea.

## 2.2  Materials and procedures

The schematic setup of the analytical system is shown in figure 2.1.
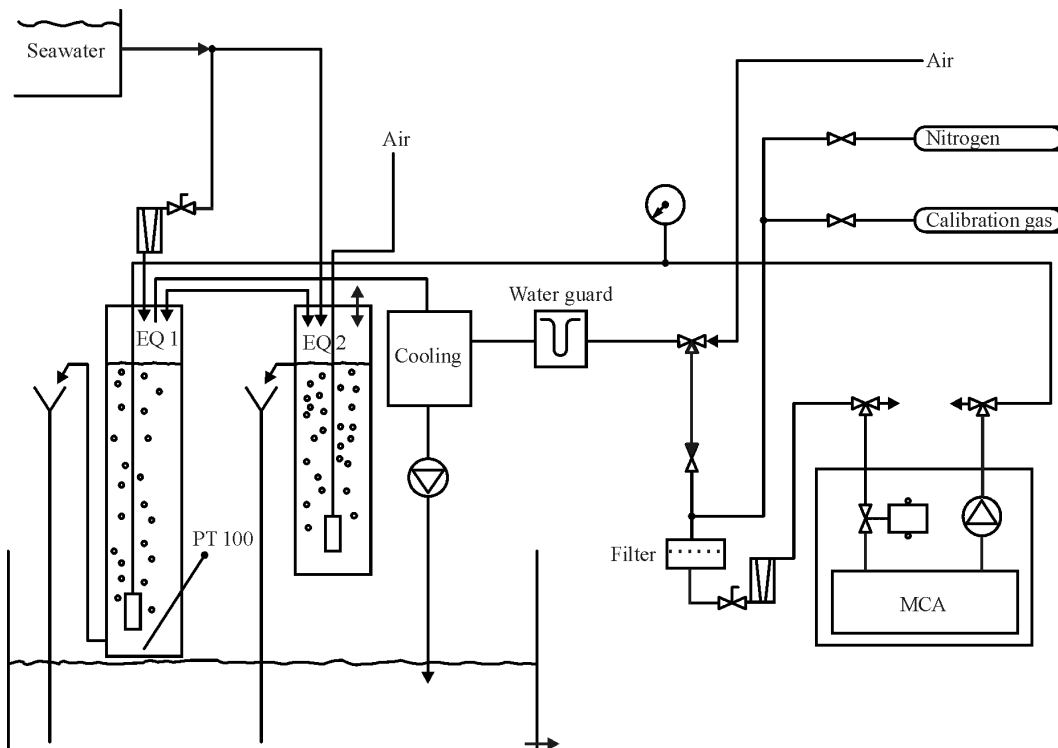


**Figure 2.1** – Schematic drawing of the system setup. Seawater enters the two equilibrators (EQ1, EQ2) with a flow rate of 500 mL min$^{-1}$. A constant volume of air is circulating through the water column in EQ1 and equilibrates with the water phase. The air is dried, transported to the MCA and measured via ICOS before it equilibrates again with the water column. Alternatively, ambient air, nitrogen, or calibration gas can be measured. Satellite image of the central Baltic Sea June $3^{rd}$ 2008. Sea surface temperatures show a displacement of the warm surface water towards the Swedish coastline and cold upwelling water along the Polish coastline and Latvia coastline.

A bubble-type equilibrator (EQ1, *Schneider et al.*, 1992; *Körtzinger et al.*, 1996) is joined to the methane - carbon dioxide analyzer (MCA; Los Gatos Research). An external pump generates the continuous flow of seawater through the main equilibration cell (EQ1; height: 26 cm, diameter: 5 cm, water volume: 500 mL). The sample flow is diverted from the total water flow of 3.5 L min$^{-1}$ and adjusted to a flow rate of 500 mL min$^{-1}$. The seawater enters the EQ1 at the top and leaves it through a siphon, regulating a constant water volume in the EQ1 by leaving a headspace of approximately 70 mL. The water temperature in the EQ1 is recorded continuously

with a precision of 0.02 °C. The membrane pump of the MCA is used to circulate a total volume of about 250 mL air at a flow rate of 450 mL min$^{-1}$ through the water column in EQ1 and the measuring cell of the sensor. The bubbles in the equilibrator are generated by pressing the air through a glass frit. The bubbles pass through the water column, equilibrate with the water phase and enter the measuring cell in the MCA before the air is lead back to the equilibrator again. To protect the sensor from water inleakage the air flow passes a cooling trap (5 °C) and a water guard, which interrupts the air flow toward the MCA if necessary. The remaining humidity in the air flow is measured before it enters the measuring cell of the sensor. The measuring cell holds an underpressure of 184 hPa to achieve a better measuring signal by limiting peak broadening.
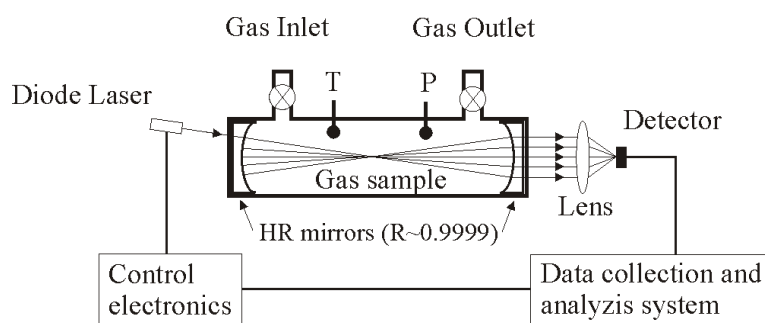


**Figure 2.2** – Schematic diagram of the measuring cell after *Baer et al.* (2002). The stainless steel tube is sealed with a pair of high-reflectivity mirrors (reflectivity 0.9999).

Because the air runs through a closed loop, the connection to a second equilibration chamber (EQ2, height: 20 cm, diameter: 5 cm) allows for compensation of potential air volume changes caused by humidity removal, solubility changes due to warming or cooling of the water, or disequilibrium of one of the main dissolved gases (e.g. oxygen, *Schneider et al.*, 2007). The purpose of the second equilibrator, with similar water flow and air flow provided by an external membrane pump, is to provide pre-equilibrated air for this case to minimize contamination in the main equilibrator.

$CH_4$ and $CO_2$ are determined using off-axis integrated cavity output spectroscopy (ICOS; Fig. 2.2; *Baer et al.*, 2002; *Hendriks et al.*, 2008). First, the gas flows continuously to the measuring cell (volume: $0.55 * 10^{-3}$ m$^3$; length: 0.20 m; Fig. 2.2). The band laser beam (DFB diode laser) is then directed into the measurement cell

at a slight angle. It passes the cell numerous times (1 - 10 * $10^4$ passes) due to reflection at highly reflective mirrors (reflectivity ∼0.9999; *Hendriks et al.*, 2008), creating an absorption path length of 2 - 20 * $10^3$ m. The detector measures fractional absorption of light at the methane resonant wavelength of 1600 nm, which is an absolute measurement of the methane concentration in the cell (*Hendriks et al.*, 2008). The average period over which the laser is being reflected in the measurement cell is called the mirror ring down time (MRT) and is continuously monitored by the MCA; likewise monitored are temperature (T) and pressure (∼184 hPa) in the cell.

The MCA measures methane in the concentration range from 0.1 - 8 ± 0.002 ppmv (operational range: 0.005 - 30 ppmv) and carbon dioxide from 200 - 16,000 ± 2.5 ppmv (operational range: 20 - 64,000 ppmv) with a total uncertainty of <1 %. The sampling frequency can be chosen from 0.01 Hz up to 20 Hz. Data output is provided via RS-232 or Ethernet. Data acquisition is performed by customized software that processes all important parameters and calculations including date, time, position, and salinity provided by the vessel-mounted sensors, in situ temperature of the seawater and atmospheric pressure, which are stored with a 1-min time interval.

The calculation for $CO_2$ is described in detail in *Schneider et al.* (2006) and *Schneider et al.* (2007). The resulting methane concentration in the seawater is calculated based on Henry's Law.

$$C_{CH4} = s * p_{CH4} \qquad (2.1)$$

where $C_{CH4}$ [mol $L^{-1}$] is the concentration of methane in water and $p_{CH4}$ [atm] is the partial pressure of methane in equilibrium with the sea water. The solubility coefficient s [mol $L^{-1}$ $atm^{-1}$] for methane is calculated after *Wiesenburg and Guinasso* (1979). Before the gaseous phase enters the measuring cell, it is cooled down to 5 °C and dried to avoid condensation processes. The cooling does not entirely remove all of the water vapor in the gaseous phase. Therefore the sensor measures the mole fraction of methane, $x$ [ ], not in dry but only almost dry air. The residual amount of water vapor, $x_{H2O}$ [ ], needs to be included in the calculation.

$$p_{CH4\,EQ} = \left(\frac{x}{1 - x_{H2O}}\right) * (P_{atm} - P_{H2O}) \tag{2.2}$$

$p_{CH4\,EQ}$ [atm] describes the partial pressure of methane in the headspace of the equilibrator, where $P_{atm}$ [atm] is the absolute atmospheric pressure and $P_{H2O}$ [atm] the saturation vapor pressure of water in equilibrium with the atmosphere, which is calculated from the following equation after *Weiss and Price* (1980).

$$ln\,(P_{H2O}) = 24.4543 - 67.4509 * \left(\frac{100}{T}\right) - 4.8489\,ln\left(\frac{T}{100}\right) - 0.000544\,S \tag{2.3}$$

where $T$ [K] is the absolute seawater temperature and $S$ [psu] is the seawater salinity. Due to temperature changes of seawater during its way from the intake port to the equilibrator, a temperature correction has to be made. The solubility coefficients ($s_{(TEQ)}$ and $s_{(Tinsitu)}$) [mol L$^{-1}$ atm$^{-1}$] are calculated (*Wiesenburg and Guinasso*, 1979) using the in situ temperature $T_{(insitu)}$ [K] and the temperature measured in the equilibrator $T_{(EQ)}$ [K]:

$$p_{CH4} = \left(\frac{s_{(T\,EQ)}}{s_{(T\,insitu)}}\right) * p_{CH4\,EQ} \tag{2.4}$$

The resulting carbon dioxide partial pressures in the seawater ($p_{CO2}$) are calculated likewise by correcting for the temperature and the partial pressure of water vapor. In general, the influence of temperature and salinity on solubility is higher for carbon dioxide than for methane.

$$p_{CO2} = p_{CO2EQ} * exp(0.0423 * (T_{(insitu)} - T_{(EQ)})) \tag{2.5}$$

where $p_{CO2EQ}$ [atm] is the partial pressure of carbon dioxide in the headspace, corrected by the temperature coefficient 0.0423/°K determined by *Takahashi et al.* (1993) and the partial pressure of water vapor as described above.

To describe the exchange process of methane and carbon dioxide in the equilibrator system and to identify variables that control the equilibration time, the system

needs to be parameterized. The detailed derivation can be retraced in *Schneider et al.* (2007). The time constant $\tau$ describes the time interval in which the gas concentration difference between the gaseous and aqueous phase in the equilibrator declines exponentially to 1/e (36.8 %) with respect to its starting value. $\tau$ can be expressed as:

$$\tau = \left( \frac{1}{A * k * s * RT * \left( \frac{1}{V_a} + \frac{1}{V_w} \right)} \right) \tag{2.6}$$

with

$A$ surface area $[\text{m}^2]$

$k$ transfer coefficient $[\text{m s}^{-1}]$

$R$ universal gas constant $[\text{J mol}^{-1} \text{ K}^{-1}]$

$T$ absolute temperature $[\text{K}]$

$s$ solubility coefficient $[\text{mol L}^{-1} \text{ atm}^{-1}]$

$V_a$ Volume gaseous phase $[\text{L}]$

$V_w$ Volume water phase $[\text{L}]$

and it can be written

$$\Delta pC_{CH4} = \Delta pC_{CH4}{}^0 * exp^{\frac{-t}{\tau}} \tag{2.7}$$

where $\Delta pC_{CH4}$ describes the changing methane concentration difference between the gaseous phase and the water phase from an initial concentration difference $\Delta pC_{CH4}{}^0$. The water in the equilibrator is constantly renewed and therefore $1/V_w$ becomes much smaller than $(s * RT * 1/V_a)$ and thus can be neglected in Eq. 2.7. In this case, it can be written:

$$\tau = \left( \frac{V_a}{A * k * s * RT} \right) \tag{2.8}$$
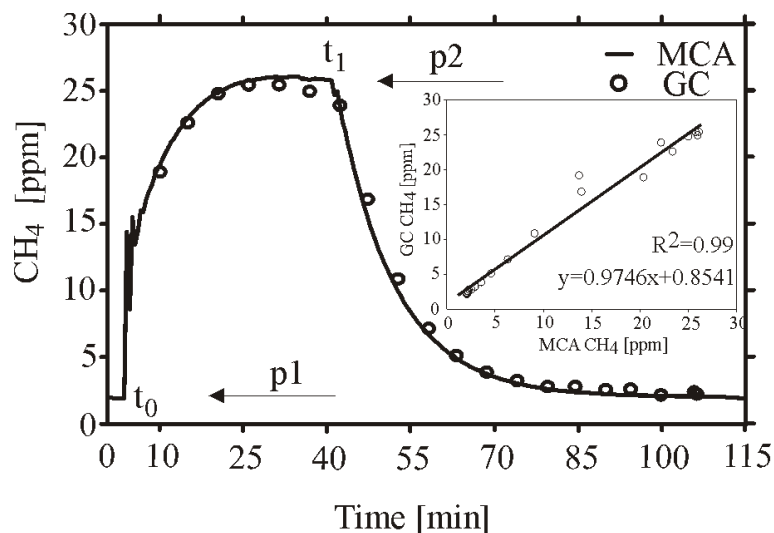
**Figure 2.3** – Step experiment carried out to determine the time constant of the equilibrator using two water reservoirs with different methane concentrations (p1, p2). At $t_0$ and $t_1$, the system is switched between the water reservoirs. The MCA signal (solid line) versus the GC signal (circles) show good agreement ($R^2 = 0.99$, slope 0.975). The fluctuations at the beginning of the experiment result from air contaminations.

The equation shows that for an intended small t the ratio of $(A * k * s * RT)$ needs to be as large as possible. The variables $A$, $k$ and $V_a$ can to some extent be controlled by the setup. Choosing a large exchange surface (e.g., many, small bubbles) in combination with a small air volume the transfer velocity can be enhanced and therefore $\tau$ can be reduced.

## 2.3 Assessment

Several performance tests have been carried out in the laboratory to determine the time constant t, reproducibility, and accuracy for methane and carbon dioxide measurements. The methane data are presented here in detail.

The time constant $\tau$ of the system depends on the velocity of the exchange process of the gaseous phase with the liquid phase and is controlled by the respective volumes and the fluxes of the entire system. To determine the time constant of the system, a step experiment was performed. Two 100 L reservoirs were filled with fresh water. One was left for equilibration with the ambient atmosphere to generate a methane concentration in the water in equilibrium with the atmospheric partial pressure of
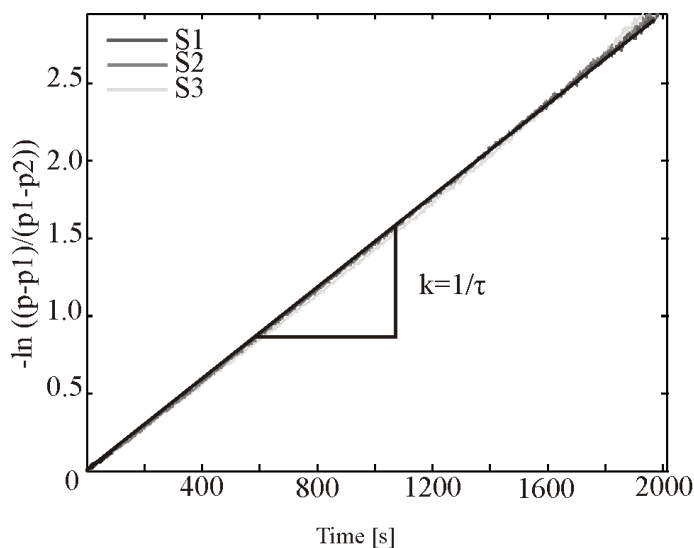
**Figure 2.4** – Linearized change of the methane concentration in the headspace of the equilibrator over time. For the graphical determination of the time constant, $\tau$ the declining legs of the step experiments (S1, S2, S3) are plotted.

p1 = 1.89 ppm. To generate high methane concentrations in the second reservoir, 2 L fresh water were saturated with methane separately by aeration with 100 % methane gas for over 15 min. Twenty millilitres of the saturated methane water were mixed into the second reservoir to generate a methane concentration in the water corresponding to equilibrium with a partial pressure of p2 = 25 ppm. The water was pumped into the equilibrator system. Via a three-way valve, it was possible to switch from one reservoir to the other without any time delay. The water flow was regulated with a calibrated flow controller to 500 mL min$^{-1}$. First, the water reservoir with the low methane concentration was led through the equilibrator until the methane concentration was constant at 1.89 ppm. Then (time = $t_0$, Fig. 2.3) the three way valve was switched to the methane enriched reservoir. The change in methane partial pressure in the equilibrator over time until equilibrium (variation $\sim 0.1$ %) was recorded with the MCA. After reaching equilibrium, the three-way valve was switched a second time ($t_1$) and the decay of the methane concentration in the gas phase was recorded until equilibrium was reached (Fig. 2.3).

Corresponding to equation 2.7, the reduction of the methane difference in the headspace of the equilibrator (pt) should follow first order kinetics:

$$\left(\frac{dpt}{dt}\right) = -k(pt - p2) \tag{2.9}$$

where $\kappa$ is the reciprocal of t in the equilibrator, a measure of how fast the headspace reacts to changes in methane concentrations in the water phase. With the gaseous phase in the equilibrator in equilibrium with the low concentration reservoir (p1) at $t_0$, the integration of equation 2.9 yields:

$$pt = p2 + (p1 - p2) * exp\left(-\frac{t}{\tau}\right) \tag{2.10}$$

Rearranging equation 2.10, $\tau$ can be calculated. The linear relation between $ln\left[(pt - p1)/(p1 - p2)\right]$ and time confirms the kinetic of first order; the slope reveals $\tau = 676$ s for methane (Fig. 2.4, inset). For the determination of t only the declining process of the repeated experiments was used. Because the experiment was performed with reservoirs that were open to the atmosphere, the methane concentration in the methane-enriched reservoir changed over time, due to diffusion processes at the water surface. With a leakage of 1.2 ppm methane over an experimental time interval of 6 h (time for one set of step experiments), the inflowing water changes concentration over time and the system does not strictly fulfil the boundary conditions for first-order kinetic.

For carbon dioxide, a time constant of $\tau = 226$ s was determined. Equation 2.8 shows in this case the dependency of $\tau$ on the solubility constant, which explains the observed discrepancy between the equilibration times for methane and carbon dioxide. For the exchange of gas through a bubble interface, the gas-specific parameters influencing the gas transfer is given by the product of the square root of the gas diffusivity $D$ and its solubility s ($D^{0.5} * s$, *Clift et al.*, 1978; *Rehder et al.*, 2002). Calculating these values using the equations summarized in *Wanninkhof* (1992), a ratio of 5 could be expected.

According to the calculated time constant, equilibrium of methane between the gaseous and the water phase takes longer than 35 min (3 * $\tau$, 95 % $\Delta p$-relaxation). Using the instrument under field conditions on the ferry line, the ship is moving at a

speed of 24 knots, and methane and carbon dioxide water concentrations are changing constantly. Therefore, the resulting signal will not reflect equilibrium concentrations but will be integrating and lagging in time. The accuracy of the MCA was compared with state-of-the art measuring systems. First, $CH_4$ concentrations derived by the MCA were compared with gas chromatographic measurements during the lab experiments. Therefore, a subsample of 1 ml gas was taken with a Hamilton syringe every 5 min during the step experiment described above (Fig. 2.3). The samples were taken just before the air flow entered the MCA and was injected into a Thermo Finnegan Trace GC Ultra gas chromatograph calibrated with the same calibration gas than the MCA. The comparison of the two methods shows excellent agreement ($R^2 = 0.99$, slope 0.975; Fig. 2.3).

The MCA is calibrated manually. Using a calibration gas (2.001 ppm $\pm$ 0.03 % $CH_4$, 381.49 ppm $\pm$ 0.01 % $CO_2$), the sensor takes over 3000 single scans for each gas for calibration. The sensor measures methane with 0.002 ppm and carbon dioxide with 2.5 ppm precision. The MCA cannot be calibrated remotely, therefore nitrogen and a calibration gas is measured at the beginning of each transect of the ferry line. The software starts the measuring progress as soon as the ship leaves the harbour. For a time interval of 10 min each, first nitrogen, a methane and carbon dioxide calibration gas and ambient air is measured before the water measurement starts. Whereas the LICOR-System can be calibrated during this procedure, the ICOS-system only records data separately for later drift assessment of the measurements. The drift for methane and carbon dioxide over a 70 d time period of continuous operation is illustrated in figure 2.5. $CH_4$ and $CO_2$ show a slight increase in sensitivity, recognizable by an increase of the values of $8 * 10^{-5}$ ppm per day and 0.036 ppm, respectively. During this period, a shift in the laser spectrum has been observed as well as a steady reduction in MRT due to lingering staining of the high-reflective mirrors. Subsequently, the drift was adjusted manually by wavelength correction and cleaning of the mirrors to reduce further drift. An additional filter for the air circuit was installed, and the procedure is now repeated regularly during maintenance.

To compare the overall performance of the system the MCA was run in parallel
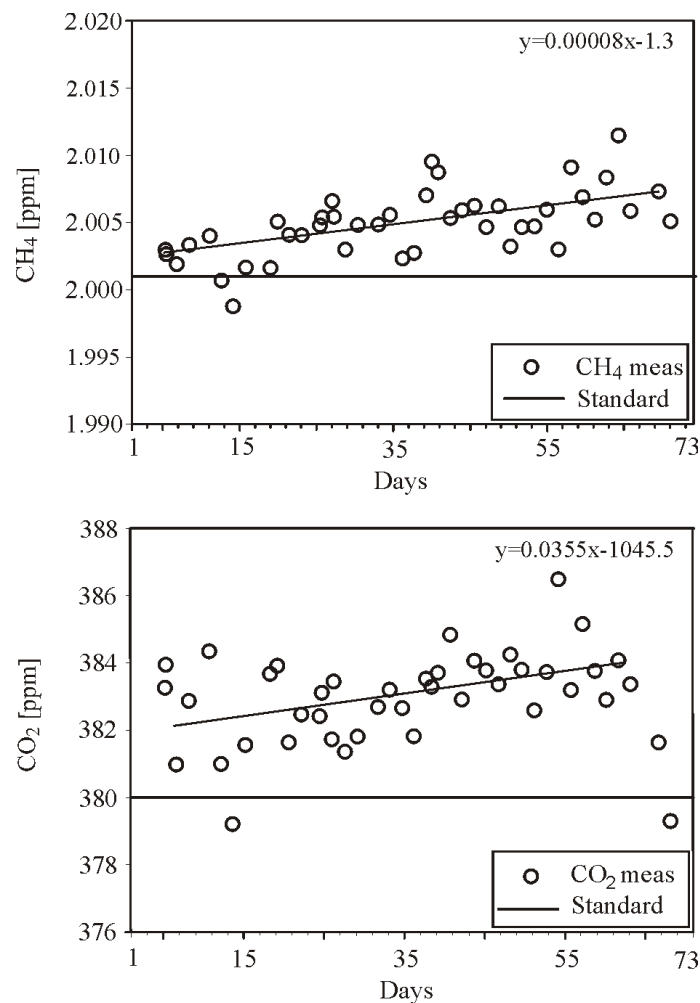
**Figure 2.5** – Time series over 70 d of calibration gas measurements for drift observations of methane and carbon dioxide. A standard gas with 2.001 ppmv $CH_4$ and 380 ppmv $CO_2$ (solid lines) was used. The regression is plotted with the equation, respectively. The axis intercept in the regression functions refer to day 0 of the Julian day record and can be neglected.

with an established $CO_2$ measuring system (*Schneider et al.*, 1992, 2006) at the cargo ship Finnmaid. *Schneider et al.* (1992) is using the same equilibrator type in combination with a LICOR sensor in a completely independent system using the same seawater supply. In figure 2.6, $CO_2$ concentrations measured by the parallel running systems with MCA and LICOR are shown over the transect Travemünde/Helsinki, measured on $6^{th}$ Jan 2010. Data show an excellent consistency ($R^2 = 0.99$, slope 1.01).

During the first measuring period from November 2009 till May 2010, several tran-
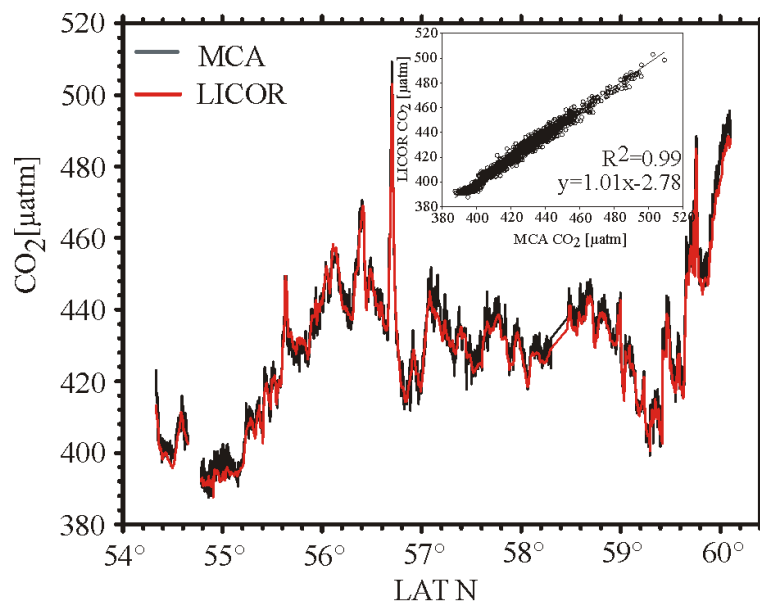
**Figure 2.6** – $CO_2$ concentrations derived from the MCA (black line) versus the one from the LICOR (red line) over a transect starting from Travemünde to Helsinki show excellent agreement ($R^2$=0.99, slope 1.01).

sects crossing the Baltic Sea were regularly observed, which highlight the advantages of the system (Fig. 2.7). Methane concentrations show large regional differences, especially in shallow regions. The concentration in the open water of the Gotland Sea maintain background concentrations of around 3.8 nM methane (close to equilibrium with the atmosphere; Fig. 2.7), whereas concentrations in near shore regions reach up to 16.8 nM (Gulf of Finland, Arkona Basin). The observed methane concentrations in the surface water stand in good agreement with the recent study by *Schmale et al.* (2010b), which gives an overview of the methane distribution along a hydrographic section in the Baltic Sea, based on a well-established analytical technique.

Additionally, spatial coherences can be seen in the methane data according to the distance to the shore line, which demonstrates the reproducibility of the data and that the low noise level makes it possible to reveal even small natural variations. The high temporal resolution allows following very small trends in surface concentrations, which at the lower sampling frequency (20 - 30 min; *Bange et al.*, 1994; *Rehder and Süß*, 2001) of gas chromatographybased systems would be interpreted as noise (Fig. 2.8). Data of several transects (not shown) passing the eastern Gotland Basin along the

shelf line (Western opening of Golf of Riga) show increasing methane concentrations at shallower water depth.
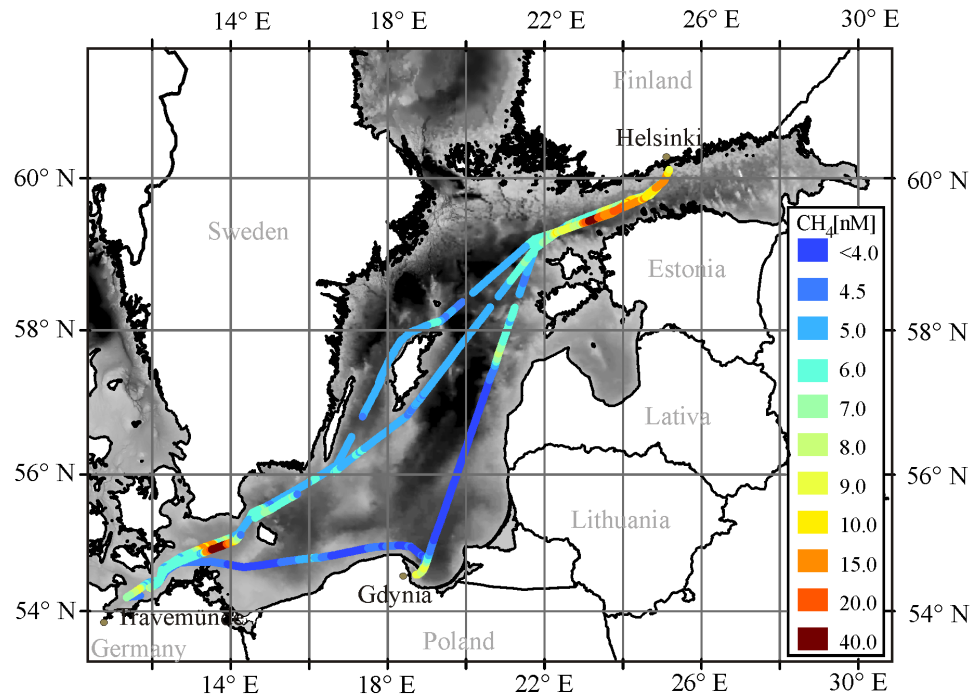


**Figure 2.7** – The map shows methane concentration (color-coded) for three transects gathered with the system installed on Finnmaid. The bathymetry (Seifert, IOW) is plotted grey shaded (light: shallow, dark: deep). The line passing Gdynia was taken in Nov 2009. The other lines are from Feb 2010.

Extraordinary surface concentrations of up to 40 nM (Arkona Basin, Fig. 2.7) have been observed as a short-time phenomenon. Further data (not shown) document depletion in surface water methane concentration within the following 4 d to 12 nM. Knowing that large areas of the Arkona Basin contain free shallow gas within an organic-rich Holocene mud (*Thießen et al.*, 2006; *Laier and Jensen*, 2007), this phenomenon can be related to a strong wind event (wind speeds $> 11$ m s$^{-1}$, data not shown) allowing a deeper mixing of the water column and enhanced transport of methane to the water surface. In contrast, elevated methane concentrations with up to 20 nM methane in surface waters (data not shown) in the entrance of the Gulf of Finland could be observed to be a phenomenon lasting several weeks.
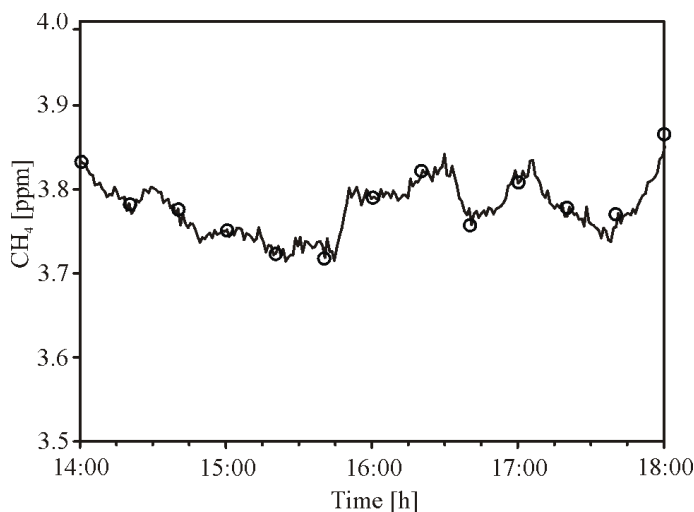
**Figure 2.8** – Methane concentrations over a time interval of 4 h gathered with the system (solid line) at $16^{th}$ Dec 2009 at a transect crossing the Gotland Sea to demonstrate the noise level at minute average collection rate. Using a lower sampling frequency (20 min, circles) by gas chromatography based systems, small signal changes would be interpreted as noise.

The listed examples of highly dynamic surface methane concentration patterns show that only by continuous and almost maintenance-free operation on ships of opportunity these high-resolution and long-term time series allow a comprehensive interpretation of the methane distribution and its governing processes. Especially the high frequency of data allow the interpretation of day-to-day changes in methane and carbon dioxide concentrations and offer the possibility to distinguish between short-term, long-term, periodic, and episodic phenomena.

## 2.4 Discussion

Since the installation of the system in November 2009, successful measurements of methane and carbon dioxide in surface waters could be continuously achieved through some maintenance was required due to a malfunction of the instrumentation in spring. The results demonstrate that the presented system can be used at a diversity of marine settings for monitoring methane and carbon dioxide concentration ranges with adequate accuracy and reproducibility. Using ships of opportunity allows high temporal and spatial coverage and permits a detailed recording of seasonal features in

contrast to observations just performed on regular research vessels. Therefore, future targets will be the detailed correlation of surface methane concentrations with water temperature, weather conditions, upwelling, and algal bloom events. In combination with vertical profiling methane measurements of the water column, the method presented here provides an important tool for a better understanding of the methane cycle in marine systems. The biogeochemical interpretation of the first year of data gathered from the instrument is beyond the scope of this paper. The extension of ferry line systems to monitor greenhouse gas fluxes other than $CO_2$ appears to be an important future development within the marine activities of the European ICOS (Integrated Carbon Observation Systems) initiative, in particular in coastal zones.

## 2.5   Comments and recommendations

Whereas the developed system allows surface water measurements in a hitherto unrivalled frequency and precision, there is potential for technical improvement. The newest version of the Los Gatos Research greenhouse gas analyzer using two laser systems provides a better S/N ratio in particular for $CO_2$, has a considerably reduced baseline drift, and allows direct detection of the water vapor in the system, which is favourable for the measurement of partly dried air as realized in our system. The system described here has recently been upgraded with this sensor system. With the Picarro G2301 sensor based on wavelength-scanned cavity ringdown spectroscopy, an alternative competing technology exists for the sensor unit, with reported similar accuracy, precision, and stability. The time constant for the system set up for methane was determined to be 676 s, which limits the spatial resolution. By reducing the headspace volume, enhancing the exchange area via reducing the bubble size or enhancing the path length of the gas through the water and the gas flow, the time constant can effectively be reduced. Here, the Picarro G2301 is advantageous because of its considerably smaller inner volume. Contact of water and air phase via a gas permeable membrane can considerably shorten the equilibration time (*Saito et al.*, 1995; *Groszko and Moore*, 1998) and we scrutinize this option for a mobile system to be

used on research vessels. However, for the continuously and almost maintenance-free application on ships of opportunity, we cannot recommend this option unambiguously due to the risk of surface alteration, in particular for a high production area such as the Baltic Sea.

# One year of continuous measurements constraining methane emissions from the Baltic Sea to the atmosphere using a ship of opportunity.

Gülzow, W.[1*], Rehder, G.[1], Schneider v. Deimling, J.[2], Seifert, T.[1], Tóth, Zs.[3]

[1] Leibniz Institute for Baltic Sea Research, Seestraße 15, D-18119 Warnemünde, Germany

[2] Helmholtz Centre for Ocean Research Kiel (GEOMAR), Wischhofstraße 1-3, D-24148 Kiel, Germany

[3] University of Bremen, Klagenfurter Straße, D-28359 Bremen, Germany

[*] Corresponding author: wanda.guelzow@io-warnemuende.de

## 3.1   Introduction

To constrain the biogeochemical cycle of the greenhouse gas methane ($CH_4$) and to estimate its future role in climate on earth, processes which influence the strength of its various sources and sinks need to be determined accurately. Various studies over the last decades subject single methane sources with the aim to quantify its contribution to the global methane budget. Emission estimates of the world's ocean range from 2 % (*Bange et al.*, 1994) to 10 % (*Grunwald et al.*, 2009) of the total global methane source strength to the atmosphere. *Bange et al.* (1994) and *Bange* (2006) comments the underestimation of shallow marine areas due to the lack of data and the uncertainty of the role of estuaries, shelf and coastal areas, which may contribute 75 % of the total marine methane emissions to the atmosphere. In fact, many studies face the limitations of discrete data measurements to observe influencing methane production parameters or processes like seasonality, weather conditions or

anthropogenic impact. Therefore, the marine methane budget and estimations of the resulting fluxes to the atmosphere still contain large uncertainties.

### 3.1.1 Baltic Sea as shallow marginal sea

The Baltic Sea is located in the northern part of Europe and forms one of the largest brackish water reservoirs on earth with an average water depth of 52 m. Today, the Skagerrak and the Kattegat remain the only connection with the North Sea and the open ocean. A series of submarine sills divide the Baltic Sea in several sub basins, which can be distinguished and characterized by different geochemical and hydrographical gradients. The positive freshwater balance and episodic saline inflow events from the North Sea lead to the formation of a less saline surface layer and a more saline deep and bottom water layer separated by a halocline. The surface salinity gradient reaches from 17 in the west (Belt Sea) to 3 in the north east (Bothnian Bay). The vertical salinity gradient is leading to a strong density stratification, hampering vertical mixing. Especially in the central deep regions of the Baltic Sea this stratification persists throughout the year. The limited ventilation together with high productivity leads to the development of a permanent redoxcline, marking the transition from oxic to sub- or anoxic conditions in the deeper stratified basins.

Geographically, the Baltic Sea stretches over several lines of latitude and is affected by warm temperate climate in the southern part (e. g. Arkona Basin, AB) and the boreal climate in the northern parts (e. g. Bothnian Sea, Bothnian Bay). For a comprehensive treatise of climate and weather in the Baltic Sea region see *Feistel et al.* (2008).

### 3.1.2 Methane in the Baltic Sea

Glacial and postglacial sedimentary deposits of the Baltic Sea are characterized by fine-grained, organic rich clay and mud layers (Holocene sediments; *Thießen et al.*, 2006; *Laier and Jensen*, 2007; *Feistel et al.*, 2008). Methanogenesis of the organic matter in the organic-rich surface sediments is the major methane source in the Baltic Sea (*Whiticar et al.*, 1986; *Butler et al.*, 1988; *Thießen et al.*, 2006). This process

leads to the occurrence of shallow gas in the sediment, especially in the Arkona and Bornholm Basin (BB; *Thießen et al.*, 2006; *Laier and Jensen*, 2007).
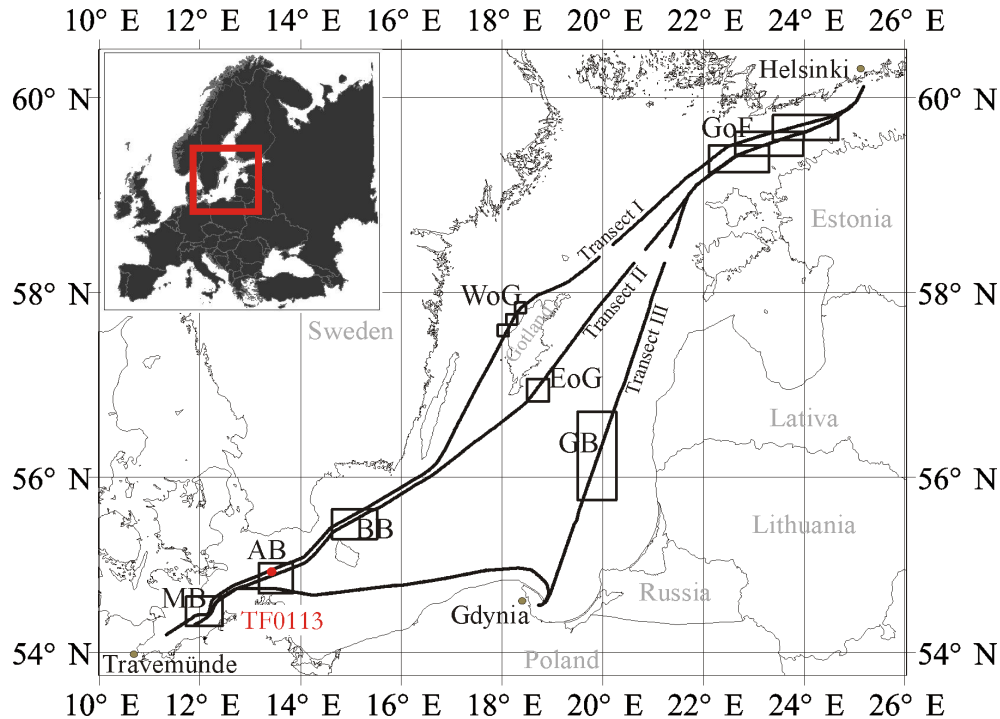


**Figure 3.1** – Cruise tracks of the ship of opportunity *Finnmaid*. The ferry line crosses the Baltic Sea via three transects and connects Travemünde (Germany) with Helsinki (Finland) and Gdynia (Poland) in an interval of 2 to 3 days. Transect I passes the Mecklenburg Bight (MB), Arkona Basin (AB), Bornholm Basin (BB), West of Gotland (WoG) and the Gulf of Finland (GoF). Transect II records the same route but East of Gotland (EoG). Transect III passes Gdynia and the Gotland Basin (GB). Boxes indicate selected areas for detailed investigations (see also table 1). Station TF0113 is part of a regular monitoring program of the Leibniz Institute for Baltic Sea Research Warnemünde.

Methane concentrations in anoxic surface sediments are not only controlled by the production but also by the degradation of methane via bacterial oxidation (*Boetius*, 2000; *Thießen et al.*, 2006), whereby 87 - 99 % of the produced methane is estimated to be oxidized within the sediment (*Berger and Heyer*, 1990). Pockmark structures and seep areas are potential sources for methane emissions towards the water column, but only few positions are known in the Baltic Sea (*Dando et al.*, 1994; *Bussmann and Süss*, 1998; *Thießen et al.*, 2006; *Pimenov et al.*, 2010). Additional methane sources which might affect sea surface methane concentrations are riverine input, ground-

water discharge, and formation in the upper water column, including production in anaerobic microniches like digestive tracts of zooplankton (*DeAngelis and Lee*, 1994), fecal pellets and sinking organic particles (*Karl and Tilbrook*, 1994) or the use of methylated compounds under oxic conditions (*Karl et al.*, 2008).

Methane generated in the sediment transfers into the water column via diffusion, fluid flow or bubble transport. As a consequence, a methane gradient towards the water surface is usually observed in the Baltic, with high concentrations in the deeper layers and low concentrations at the sea surface (*Schmale et al.*, 2010b). During the transport through the water column towards the sea surface, methane is substantially reduced by methane oxidation especially in the oxic/anoxic transition layer, as has been shown for the Black Sea (*Schmale et al.*, 2011). Besides oxidation, methane emission towards the atmosphere constitutes another major sink of methane in the Baltic Sea.

There are only few assessments of methane concentrations and fluxes to the atmosphere from the Baltic Sea. *Bange et al.* (1994) determined atmospheric and dissolved methane using an automated gas chromatographic system and describe the Southern Belt Sea and the central Baltic Sea as source for atmospheric methane. Bange and coworkers show strong seasonal variations in surface methane saturations with high values during the summer (e.g. 168 % Arkona Sea, 157 % Bornholm Sea) and lower values during the winter (e.g. 117 % Arkona Sea, 107 % Bornholm Sea). They highlight the importance of shallow shelf regions for global methane flux estimations. *Bange et al.* (1998) describe the seasonal distribution of methane and nitrous oxide in the Bodden Sea, using an equilibrator combined with a gas chromatograph, postulating that methane emissions of this area account for 17 % of the total Baltic Sea methane emissions. Based on six measuring campaigns (1995, 1996) in the shallow coastal area between the Island of Rügen and Hiddensee (Southern Baltic Sea) using floating measuring chambers with continuously and automatic sampling equipment, *Heyer and Berger* (2000) found a strong correlation of the amount of organic matter in the sediment and interannual as well as seasonal variations of methane emissions. *Abril and Iversen* (2002) describe methane emissions to the atmosphere along the

salinity gradient in the estuarine zone of Randers Fjord (Denmark) from February to December 2000. They observed that the shallow estuarine morphology increases the influence of the sediment on methane dynamics (production and consumption of methane) compared to deeper regions and amplifies rapid changes in methane concentrations and fluxes due to short and episodic weather events (stormy winds).

In this paper we present the results of the first year of almost intervention-free operation of a system allowing continuous measurements of sea surface methane using a continuous equilibration technique in combination with integrated off axis cavity output spectroscopy in the southern and central parts of the Baltic Sea (*Gülzow et al.*, 2011). The system records successful methane and carbon dioxide in surface waters of the Baltic Sea since its installation in November 2009 on the cargo ship *Finnmaid*. The ferry line connects Travemünde (Germany), Helsinki (Finland) and Gdynia (Poland) and crosses the central Baltic Sea every 2 to 3 days (Fig. 3.1). The high spatiotemporal data coverage provided by the instrument allows new insights into the seasonal and spatial distribution of methane in the surface water of the Baltic Sea and the governing controls. Selected key areas are presented for detailed studies of the controlling processes and parameters, including upwelling, stratification and mixing, wind events and water level changes, seasonal temperature cycle, and the distribution of sedimentary sources.

## 3.2  Methods

### 3.2.1  Analytical setup on the cargo ship *Finnmaid*

In cooperation with the Finnish Institute of Marine Research (SYKE, ALGALINE Project), the Leibniz Institute for Baltic Sea Research Warnemünde (IOW) installed a fully automated measuring and sampling system on the cargo ship *Finnmaid*, which commutes regularly between Travemünde (Germany), Helsinki (Finland) and Gdynia (Poland) since 1993. The ALGALINE equipment on *Finnmaid* consists of a fluorometer for continuous recording of the chlorophyll a fluorescence and a sampling system for the laboratory analysis of inorganic nutrients, dissolved and particulate organic

matter, and plankton species composition. Sea surface salinity (accuracy 0.001) and temperature (accuracy 0.001° C) are recorded using a Seabird 38 thermosalinograph. The IOW installed a fully automated system for the measurement of surface $CO_2$ partial pressure in 2003 (*Schneider et al.*, 2006), later extended by optode-based recording of surface oxygen (*Schneider et al.*, 2006). An independent continuous measuring system for methane and carbon dioxide was added in 2009 (*Gülzow et al.*, 2011). The current trace gas measuring system consists of two independent established equilibrators joint with a methane/carbon dioxide analyzer (MCA; Los Gatos Research) and a LICOR gas analyzer, respectively. Details about the analytical set up, equilibration theory, essential calculations as well as temperature correction are given in *Körtzinger et al.* (1996) and *Gülzow et al.* (2011). Methane and carbon dioxide was determined with a total uncertainty of <0.8 % (*Thomas*, 2011). The response times of the system for methane and carbon dioxide were determined with $\tau = 676$ s and $\tau = 226$ s, respectively (*Gülzow et al.*, 2011). The time constant for methane implies that equilibrium between the gaseous and the water phase is reached after 35 minutes ($3\sigma$). Hence, with the average ship speed of 22 knots, the resulting methane signal is smoothed and slightly retarded in time (*Gülzow et al.*, 2011).

### 3.2.2   Air measurements and sea surface equilibrium calculations

During each transect, the measuring of the sea surface methane concentration was interrupted for 15 minutes at the position 58° N, 21° E to record the atmospheric methane concentration. The small gaps in the transects I - III (Fig. 3.1) represent the location of the air measurements. The location of the atmospheric methane sampling was chosen with the intention of minimized disturbance by coastal and urban areas. Unfortunately, for this first year of operation, a clean air line from the ship bow could not be realized, and the data showed indication for contamination. Therefore, atmospheric methane concentrations $x_{CH4atm}$ [ppm] of the NOAA station BAL (Baltic Sea, Poland) were used to calculate sea surface equilibrium concentrations. The equilibrium concentration $C_{CH4eq}$ [nM] describes the methane concentration in water at a certain salinity and temperature, which is in equilibrium with the overlaying

gaseous phase (atmosphere) and can be calculated using the Bunsen coefficient $\beta$ after *Wiesenburg and Guinasso* (1979).

$$C_{CH4eq} = \beta * x_{CH4atm} \tag{3.1}$$

The ratio of equilibrium concentration $C_{CH4eq}$ and measured seawater concentration $C_{CH4aq}$ [nM] describes the saturation state and can be distinguished in undersaturation for values below 100 % and oversaturation for values above 100 %. The difference of $C_{CH4eq}$ and $C_{CH4aq}$ is a key parameter for the calculation of sea-air methane fluxes (see section 3.3.5).

### 3.2.3   Meteorological data

To estimate the role of wind forcing on sea-air gas exchange in the selected key regions (Table 3.1) of the Baltic Sea, meteorological forcing data derived from the regional weather forecast model COSMO/EU (former DWD/LME) run by the German Weather Service (DWD) were used *Schulz and Schüttler* (2005).

The core documentation of the COSMO model is available on the web site of the international Consortium of Small-scale Modeling (COSMO). The non-hydrostatic, high-resolution model COSMO/EU covers whole Europe with a bottom grid spacing of 7 km, resolving even small scale spatial changes. The daily variation of meteorological conditions is adequately represented by prescribing a weather forecast every 3 hours and linear interpolation onto the ocean model time steps of 600 seconds. The coupling atmosphere-ocean fluxes are evaluated in the circulation model MOM-4 according to *Beljaars* (1995). Point comparisons with observations from two open sea measurement sites at DarßSill (12.7° E, 54.4° N) and in Arkona Basin (AB, 13.85° E, 54.88° N) reveal that the reliability of COSMO/EU forecasts of air pressure, air temperature, wind speed, wind direction, and relative humidity is of the same degree of accordance as shown by *Leuenberger* (2010) for ensemble forecasts in view of assimilation, e.g. bias in wind speed is well below -1 m s$^{-1}$, root mean square deviation

**Table 3.1** – For detailed contemplations of regional differences special key areas were selected to merge methane data (saturation values) with mixing depth or meteorological forcing data derived from the regional forecast model COSMO/EU. The subdivision of the area WoG and GoF reflects a better description of the field of interest than one large box respectively and improves the technical approach during modeling.

| Selected area | Latitude ° N | Longitude ° E |
|---|---|---|
| Mecklenburg Bight (MB) | 11.62 - 12.42 | 54.25 - 54.65 |
| Arkona Basin (AB) | 13.25 - 14.05 | 54.63 - 55.03 |
| Bornholm Basin (BB) | 14.55 - 15.35 | 55.29 - 55.69 |
| West of Gotland (WoG) with | | |
| West of Gotland 1 | 17.94 - 18.16 | 57.58 - 57.69 |
| West of Gotland 2 | 18.11 - 18.34 | 57.70 - 57.82 |
| West of Gotland 3 | 18.29 - 18.51 | 57.82 - 57.94 |
| East of Gotland (EoG) | 18.50 - 18.59 | 51.11 - 56.87 |
| Gotland Central Basin (GB) | 19.55 - 20.35 | 55.74 - 56.74 |
| Gulf of Finland (GoF) with | | |
| Gulf of Finland 1 | 22.65 - 24.05 | 59.35 - 59.67 |
| Gulf of Finland 2 | 21.95 - 23.35 | 59.19 - 59.51 |
| Gulf of Finland 3 | 23.35 - 24.75 | 59.51 - 59.83 |

is around 1.5 m s$^{-1}$, and linear correlation exceeds 90 % (*Seifert*, 2010). The model derived wind fields were used to derive gas exchange velocities based on the quadratic relation by *Wanninkhof et al.* (2009).

### 3.2.4   Mixed Layer depth

The COSMO/EU forecasts were used as input parameters to drive the numerical Baltic Sea model which is based on the Modular Ocean Model (MOM4, *Griffies et al.*, 2004). The model domain comprises the entire Baltic Sea with the western boundary at Skagerrak (at 8.25° E). The sea level at the open boundary and the river runoff to the Baltic Sea are prescribed from data provided by the Swedish Meteorological and Hydrological Institute (SMHI). Temperature and salinity at the open boundary are nudged to monthly mean profiles derived from climatology (*Janssen et al.* 1999). The model was started from rest with initial conditions taken from a coarser model simulation, which was corrected with measurements. The model was run for the period September 2002 to December 2010. The model bathymetry is based on a one

nautical mile grid (*Seifert et al.*, 2001). The upper water column down to 30 m depth is divided into layers of 1.5 m thickness to resolve the shallow channels and sills in the south-western Baltic. The layer thickness gradually increases to 5 m at a maximum depth of 268 m, corresponding to the deep basins in the central and northern Baltic. This vertical resolution allows the modeling of the local stratification and its evolution throughout the year in each of the respective working areas. Sub-grid scale mixing processes are modeled by the MOM-4 adaptation of the scheme (*Smagorinski*, 1963). The development of vertical stratification is simulated by the kpp scheme (*Large et al.*, 1994). Based on the analysis of the stability within the upper water column, fluxes from the sea surface are non-locally distributed to the depth which is mixed by the entrained energy. The mixing depth describes the active turbulence in the water column. The mixed layer depth is characterizes by homogeneous salinity and temperature profiles. Only stronger mixing events are able to diminish the stratification at the bottom of the mixed layer.

### 3.2.5   Sea-air methane flux calculations

The flux of methane across the sea-air interface $F$ [nmol m$^{-2}$ s$^{-1}$] can be expressed by the concentration difference of methane between the sea surface water $C_{CH4aq}$ and the atmosphere $C_{CH4atm}$, and the gas transfer velocity $k$ [cm h$^{-1}$]. The solubility of methane as a function of temperature and salinity is described with the Bunsen coefficient $\beta$ after *Wiesenburg and Guinasso* (1979),

$$F_{CH4} = k * (C_{CH4aq} - \beta * x_{CH4atm}) \tag{3.2}$$

The transfer velocity $k$ was calculated using the quadratic relation by *Wanninkhof et al.* (2009):

$$k = 0.24 * u^2 * \left(\frac{Sc_{sal}}{660}\right)^{-0.2} \tag{3.3}$$

with wind speed $u$ [m s$^{-1}$] in 10 m height as main driving kinetic parameter and the Schmidt number $Sc_{sal}$ interpolated according to the measured salinity

$$Sc_{sal} = \left[ (Sc_{35} - Sc_0) * \left( \frac{Sal}{35} \right) \right] + Sc_0 \tag{3.4}$$

with Schmidt number $Sc_{35}$ for saline water (35 psu), Schmidt number $Sc_0$ for fresh water (0 psu) after *Jähne et al.* (1987) and measured salinity $Sal$ [psu].

The parameterization of the transfer velocity $k$ as function of the wind speed $u$ is based on a conceptual model for sea-air gas transfer by relating one gas (i.e. $^{222}$Rn) to another gas (i.e. $CH_4$) on the basis of the physicochemical properties of the gases (*Wanninkhof et al.*, 2009). Although a variety of conceptual models have been introduced over the last decades, the parameterization of $k$ is still under debate (*Liss and Merlivat*, 1986; *Jähne et al.*, 1989; *Wanninkhof*, 1992; *Nightingale et al.*, 2000; *Sweeney et al.*, 2007; *Weiss et al.*, 2007; *Wanninkhof et al.*, 2009). For this study, the most recent approximation of *Wanninkhof et al.* (2009) was used. Equation 3.3 shows the influence of $u$ on the transfer velocity and methane fluxes in general. To avoid the overestimation of short time changes in wind speed in combination with the infrequently traversing (irregular intervals of transects passing or measuring gaps) by the ferry, methane fluxes were calculated based on monthly averaged parameters to achieve a general pattern of methane fluxes. The monthly flux values reported here (see also section 3.3.5) result of sea surface methane concentrations $C_{CH4aq}$ [nM] averaged for each leg crossing a selected area (Fig. 3.1, Tab. 3.1) and averaged for each month. Mean monthly atmospheric methane fractions $x_{CH4atm}$ [ppm] are derived from the NOAA Station BAL (Baltic Sea, Poland: 55.35° N, 17.22° E; *Dlugokencky et al.*, 2011). $Sc_{sal}$ was calculated based on temperature and salinity determined like $C_{CH4aq}$ (averaged for each leg crossing over the selected areas (Fig. 3.1, Tab. 3.1) and then averaged for each month). Monthly mean wind speed was calculated from the COSMO/EU wind fields averaged over the selected areas.

### 3.2.6   Bottom water temperature

The water temperature observed near the sea floor is used as a proxy for the temperature of the sediment surface. These data were derived from measurements

collected in the HELCOM data set available from the ICES (2011) Oceanographic Database. CTD (Conductivity, Temperature, Density) casts, taken at standard depth levels, supply a sufficiently dense data base with more than thousand samples at a series of stations which characterize the typical conditions in the sub-basins of the Baltic Sea since 1960. Only data registered within the lowermost 5 % of the water column have been taken into account to calculate the mean water temperature at the seafloor and its range of variation, which in this work is described by the standard deviation and the observed minimum and maximum temperatures.

### 3.2.7   Water column profiles

Vertical water profiles were taken at station TF0113 in the Arkona Basin. The dataset includes 4 profiles carried out with a 24 (12 L) Niskin-bottle rosette water sampler. For continuous CTD profiling a Seabird sbe911+ system was attached to the underwater unit. After retrieving the sampler on board, oxygen concentrations were determined using Winkler titration (*Grasshoff et al.*, 1999). Methane was extracted from the water sample using the vacuum degassing method and its mole fraction was determined with a gas chromatograph equipped with a flame ionization detector (*Keir et al.*, 2009).

### 3.2.8   Multichannel seismic profile

To observe free gas accumulations in subsurface sediments, seismo-acoustic data were collected in the Arkona Basin (student cruises of the University of Bremen) using a GI gun with a central frequency of 200 Hz and a 50 m long high resolution streamer with 48 channels. The vertical resolution in the seismic profile is approximately 1 to 5 m. Horizontal resolution is determined by the common mid-point (CMP) bin size, which was set to 1 m. Data processing followed a conventional processing flow with special emphasis on the velocity analysis.

## 3.3  Results and Discussion

The focus in the following sections will be set on the most visited transects I and II, passing West (WoG) and East (EoG) of Gotland (Fig. 3.1) in 2010. Special emphasis is given to selected key areas (Tab. 3.1) and additional to surface methane concentration measurements covering one year. Respective controlling parameters such as temperature, wind, and the mixing depth are presented. Data gaps (Fig. 3.2) due to malfunction/maintenance exist from April $9^{th}$ to $21^{th}$ 2010 and from April $26^{th}$ to May $18^{th}$ 2010. Smaller data gaps in figure 3.2 are caused by the passing of the ferry along transect III (total of 264 operational days).

First sea surface temperature anomalies were identified indicating local upwelling accompanied by elevated methane concentration. Highest methane surface values measured throughout the year in the Arkona basin are investigated in regard to the specific environmental setting of shallow gas. A potential linkage between wind and weather driven hydrostatic pressure changes and methane gas ebullition is suggested. The effects of seasonal sea surface temperature (SST) and mixing depth changes are studied in detail in regard to their control on the surface methane concentration and sea-air flux potential. Finally, a seasonal cycle of monthly averaged methane flux calculations will be presented for all key areas including the ice-influenced Gulf of Finland (GoF) area.

### 3.3.1  Overview

#### 3.3.1.1  Regionality

Surface water methane concentrations along transects I and II, passing West and East of Gotland, are shown for all lines gathered in 2010 in figure 3.2, and reveal remarkable regional differences. Strong fluctuations and increased methane concentrations in the westernmost and easternmost part of each transect have been observed. These regions are covered by both transects in a very similar way. Methane values in the Arkona Basin (Fig. 3.2, Long: 13° E - 14° E, see also Fig. 3.1 for orientation) range from 3.2 nM to 8 nM (97 - 270 % methane saturation) with exceptional high
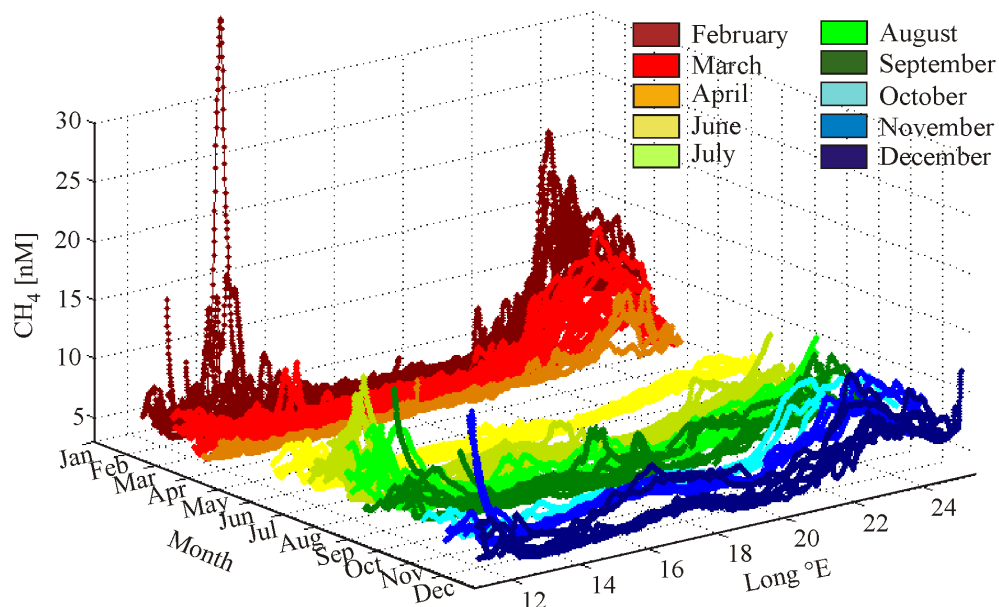
**Figure 3.2** – Methane concentrations of all lines along transect I and II in 2010 color-coded for each month. During most of April and May no data could be gathered due to maintenance. Later gaps in the continuous data set are in part due to the passage of the ferry along the transect III.

concentrations in February, which will be discussed below (section 3.3.3). The Gulf of Finland (Long: 22° E - 26° E) is characterized by elevated methane concentrations throughout the year compared to the other regions. In fact, the western part of the Gulf of Finland shows a strong variability in methane concentrations during the year, ranging from 3.4 nM (106 % methane saturation) to over 22 nM (470 % methane saturation). In the middle of each transect methane concentrations are rather uniform and in general considerably lower. In the area of the Island of Gotland (Fig. 3.2, Long: 18° E - 19° E) methane concentrations in the surface water are comparably low, ranging from 3.3 nM (95 % methane saturation) to 4.6 nM (165 % methane saturation). West (WoG) and East of Gotland (EoG; Fig. 3.2, Long: 18° E - 19° E), episodes of elevated methane concentrations lasting a couple of days were observed during the summer months June till September, when methane values increased more than 3 nM above normal.

### 3.3.1.2 Seasonality

The seasonal trend of surface water methane concentrations in the Baltic Sea is characterized by high methane concentrations during winter and lower methane values during summer, except for the very shallow areas like the Mecklenburg Bight (MB) or the Arkona Basin (see section 3.3.4). The diverse pattern illustrated in figure 3.2 shows high fluctuations of the methane concentration during the winter months compared to the rather uniform values in summer. The strongest annual fluctuations were observed in the area of the Gulf of Finland (Fig. 3.2, Long: 22° E - 26° E), where highest methane concentrations (up to 22 nM; 470 % methane saturation) were measured in February, decreasing in the time following. Lowest methane values of 3.4 nM (106 % methane saturation) were detected during the summer months June till August before concentrations rose again until the end of December.

### 3.3.2 Upwelling

Upwelling is a typical, well documented phenomenon in the Baltic Sea (*Alenius et al.*, 1998; *Vahtera et al.*, 2005; *Lehmann and Myrberg*, 2008; *Lips et al.*, 2009). The process is characterized by winds blowing predominantly parallel to the coast from a favorable direction. Together with the Coriolis effect, this results in a displacement of the upper water body leading to mixing in the water column and upwelling at the coast (*Lehmann and Myrberg*, 2008). It involves the mixing of dense, cooler and usually nutrient-rich water towards the sea surface by replacing the warmer mostly nutrient-depleted surface water (*Lehmann and Myrberg*, 2008). Depending on the strength and period of the wind forces, upwelling can range from a small scale coastal event to a large scale phenomenon influencing the open sea.

Although this mixing process occurs throughout the year, upwelling plays an essential role in the mixing of the water column during the summer season when additional thermal stratification occurs and nutrients in the surface layers are depleted by algal blooms. Sea surface temperature is a good parameter to indicate upwelling especially during the summer months, when the surface water is warmer than the
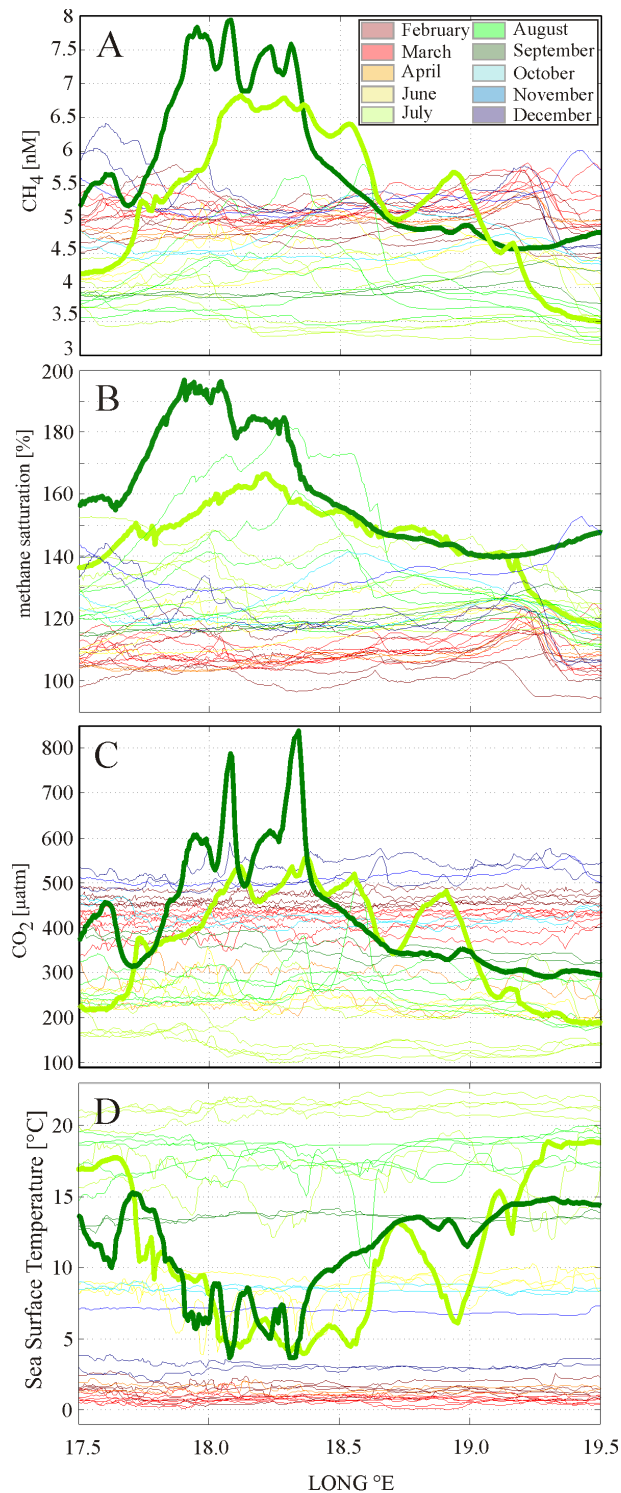
**Figure 3.3** – A: methane, B: methane saturation, C: carbon dioxide and D: sea surface temperature of the area West of Gotland for the year 2010. All data in transparent thin lines color-coded for each month. Two significant upwelling events in July and September are highlighted with outstanding light green (July $24^{th}$) and dark green (September $3^{rd}$) lines.

deeper layers. Then, upwelling can be detected by a local sharp temperature drop in the surface water, which can last a couple of days. A well developed method to observe this phenomenon, recurring in time and location, is satellite imaging of the sea surface temperature (*Siegel et al.*, 1994, 2005; *Lass et al.*, 2010).

During the measuring campaign with the ferry line Finnmaid, the effect of upwelling on the local surface methane concentrations was recorded several times at different locations of the Baltic Sea. Especially in the area around the island of Gotland various events could be observed. In figure 3.3, methane (A), methane saturation (B), partial pressure of carbon dioxide (C) and sea surface temperature (D) are shown for the area north-west of Gotland for the year 2010. Sharp drops of the sea surface temperature (Fig. 3.3 D) on July $24^{th}$ (light green line) and September $3^{rd}$ (dark green line) can be pointed out with values reaching well down below 5° C indicate the rise of deeper and colder water masses towards the sea surface and are highlighted in the following, though various weaker events were observed over the course of the year as well.

During upwelling events, strong increases in methane surface concentrations have been observed. Whereas methane concentrations in July (Fig. 3.3 A, transparent light green lines) vary in general between 3.5 nM and 4.5 nM, methane values reach up to 6.8 nM in the surface water on July $24^{th}$ (Fig. 3.3 A, light green line). On September $3^{rd}$ methane concentrations increase even up to 8 nM (Fig. 3.3 A, dark green line). Strong increases during the upwelling events could also be observed in the recorded carbon dioxide concentrations (Fig. 3.3 C) and salinity (data not shown). Usually, all parameters show elevated values for the same time and at the same locations for all recorded upwelling events. The findings reflect the transport of deeper water towards the surface, which are characterized by colder temperatures (*Umlauf et al.*, 2010), enhanced $pCO_2$ from organic matter remineralization (*Thomas and Schneider*, 1999) and often enhanced methane concentrations (*Schmale et al.*, 2010b). Methane saturation values (Fig. 3.3 B) increase during the major upwelling events in July and September, but the recorded signals vary significantly from the methane signal (Fig. 3.3 A). Although upwelled waters are enriched in methane, saturation values increase

less pronounced than the methane signal (Fig. 3.3 A) because lower temperatures imply higher solubility. During the upwelling event on September $3^{rd}$ methane values reach 8 nM and oversaturation of 194 % at water temperatures of 3.6° C (Fig. 3.3 A and B dark green line) was observed. With a water temperature of 22° C, this surface methane concentration would reach over saturation values of more than 300 %. Still, the transport of deeper water towards the surface and the increase of the sea surface methane concentration change temporally the saturation of methane in the surface water, influencing the emission of methane towards the atmosphere, which will be discussed below. Unfortunately, due to the changing frequency of transects passing the western coast of Gotland no continuous data recording could be achieved in this area. Therefore the persistence of the upwelling-induced methane (and carbon dioxide) oversaturation and the timeframe for dilution/evasion to the atmosphere could not be tracked.

The different signal widths of the corresponding curves for carbon dioxide and methane, shown in figure 3.3, need to be highlighted. The crossing of the investigated area north-west of Gotland had a duration of approximately 4h 15 min on July $24^{th}$ (Fig. 3.3, outstanding light green), and 5h 15 min on September $3^{rd}$ (Fig. 3.3, outstanding dark green line). Although both records show a similar line characteristic, the methane signal is wider than the corresponding records of carbon dioxide. To a large extend, the different shapes of the methane and carbon dioxide curves might reflect the different response times of the system for the two gases, with the time constant for $CH_4$ approximately four times longer than for $CO_2$ (for detailed discussion see *Gülzow et al.*, 2011). On the other hand, methane concentrations and carbon dioxide partial pressures do not have to be directly related. Though both properties generally increase underneath the mixed layer (*Thomas and Schneider*, 1999; *Schmale et al.*, 2010b), the $pCO_2$ increase, mostly resulting from organic matter degradation, will start immediately underneath the mixed layer, while stronger enhancement of methane is generally observed in greater depth.

### 3.3.3   Pressure induced liberation of methane from the seafloor

On February $2^{th}$, $4^{th}$ and $5^{th}$, extraordinarily high methane concentrations were measured in the surface waters of the Arkona Basin rising up to 38 nM (832 % methane saturation), 15 nM (321 % methane saturation) and 16.5 nM (360 % methane saturation), respectively (Fig 3.4). Elevated methane concentrations could be measured until 6 days after the event, with decreasing values until concentrations prior to the event were reached. These exceptional high methane concentrations in the surface water were accompanied by a longer period of strong winds, starting in the middle of January, which resulted in an oscillation of the sea level of almost 1.5 m within a day in the Arkona Basin (Fig. 3.4, grey line, station Sassnitz, Bundesanstalt für Wasserbau BAW). Further, the wind-induced mixing depth of the water column was calculated to reach down to the sediment surface at 45 m depth during this period (Fig. 3.4, blue line).

The data can be interpreted with additional data of dissolved methane measurements in the water column sampled during 4 research cruises between December 2009 and August 2010 (Fig. 3.5) in the Arkona Basin at station TF0113 (Lat: 54.92; Long: 13.50, for location see Fig. 3.1). Methane concentrations in the upper water layer were approximately 10 times higher than usual on January $28^{th}$, with concentrations around 50 nM down to 30 m depth (Fig. 3.5) and increasing towards the seafloor to a maximum concentration of 420 nM at 40 m depth.
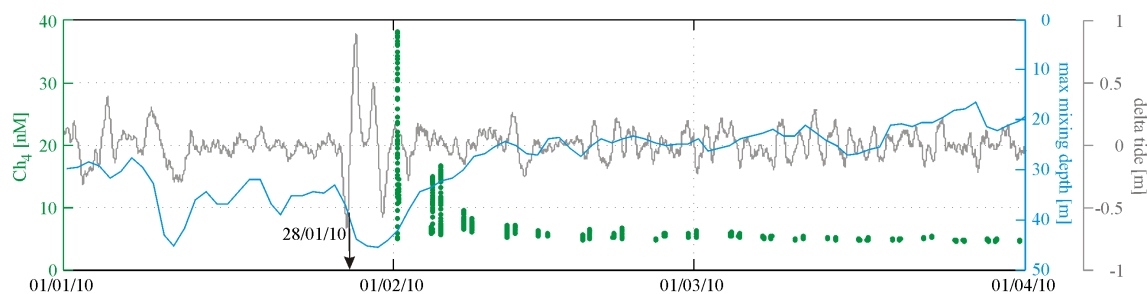


**Figure 3.4** – Data from a three month survey of the Arkona Basin. Sea surface methane concentrations (green dots, representing measured methane concentrations along each leg crossing the selected area Arkona Basin, table 3.1), daily maximum mixing depths (blue line) and sea level data (grey line, measured at station Sassnitz, Bundesanstalt für Wasserbau). Delta tide indicates the gradient of oscillation of the sea level around 0.

The parameters salinity, oxygen and temperature indicate mixing of the entire upper water column by uniform values down to nearly 40 m depth in accordance to the model-derived mixing depth (Fig. 3.4). Further towards the seafloor a gradual increase in temperature and salinity marks the existence of a narrow bottom layer.

In contrast, the average methane concentration in the water column in December 2009 at Station TF0113 (Fig. 3.5) was 7.7 nM. Methane profiles taken during cruises in July and August 2010 show similar low methane concentrations of 5.1 nM and 10.8 nM on average for the mixed layer, respectively. Turbidity signals of station TF0113 (data not shown) on January $28^{th}$ increase significantly from 0.4 NTU (Nephelometric Turbidity Unit, average of upper 40 m water column; data not shown) to 1.02 NTU in the bottom water layer, indicating enhanced shear stress at the sediment-water interface. For comparison, turbidity values this station on August $1^{st}$ show values below 0.5 NTU for the entire water column.
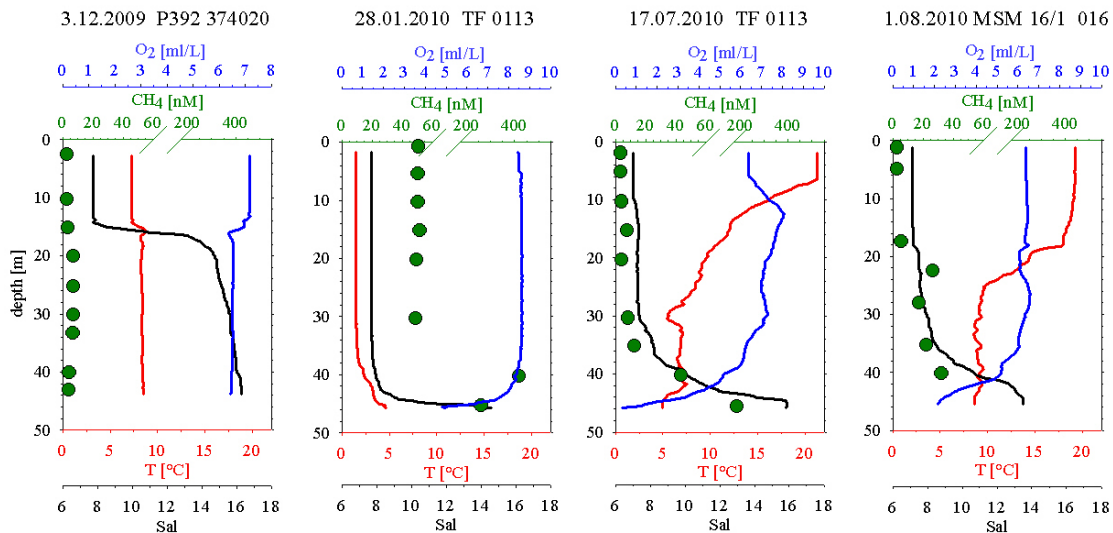


**Figure 3.5** – Data of water column properties and methane concentration of profiles at station TF0113 taken during four cruises in December 2009 (Poseidon P392), January 2010 (Heincke 06HK 1001), July 2010 (Alkor 06 AK1003) and Maria S. Merian (MSM 16/1). Methane concentration (green dots), temperature (red line), salinity (black line) and oxygen values (blue line). The sampling dates of the profiles are marked as well in time scale of the subplot AB in figure 3.7.

Based on acoustic data collected throughout the Arkona Basin, free gas accumula-

tions in the Holocene mud are known to be widespread *Mathys et al.* (2005); *Thießen et al.* (2006), but only one seabed feature has been found during the measuring campaign, which can be related to gas escape from the subsurface. The seismic section in figure 3.6 shows a subtle depression in the seafloor (Lat: 54.90° N Long: 13.61° E). The less than 1 m deep depression has a slightly elongated shape and a maximum diameter of approximately 120 m and is surrounded with high amplitude reflections on both sides forming a few hundred meter wide ring (data not shown). Distinct phase reversal and seismic blanking is interpreted as a result of gas-mediated decrease of bulk density and/or seismic velocity and bubble scattering and thus points to the existence of free gas. Given these clear indications of shallow gas together with its morphological shape we interpret this feature as a pockmark with free gas. Fig 3.6 shows a lower reflector below the seafloor, representing the top of the gas-charged layer and indicating the accumulation of vast amounts of free gas in the Holocene mud. Another strong reflector can be observed deeper in the glacial deposits indicating gas/fluid migration from deeper subsurface reservoirs.
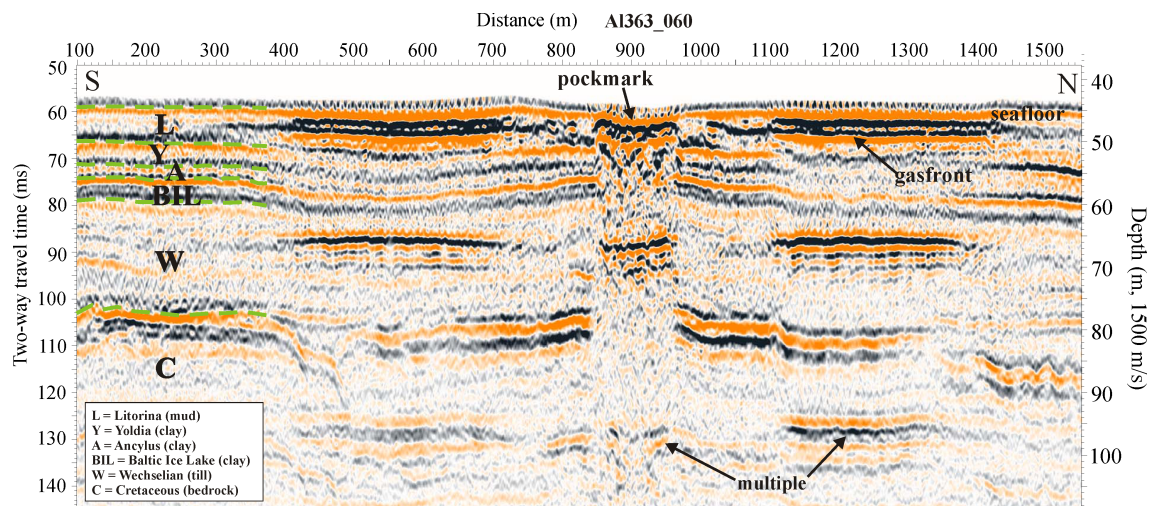


**Figure 3.6** – Multichannel seismic profile showing a pockmark and its vicinity in the Arkona Basin. The seismic section is running from south (Lat: 54.90, Long: 13.61) to north (Lat: 54.91 Long: 13.61). The presence of free gas beneath the seabed is indicated by the reversed polarity compared to the normal polarity of the seafloor outside the pockmark. The green lines indicate layer boundaries.

Highly elevated methane concentrations in the water column were detected only 6.5 nautical miles apart from this feature and in combination with the recorded sea

level fluctuation, a pressure-induced seepage event is speculated as described in *Wever et al.* (2006) for Eckernförde Bay (see also *Schneider von Deimling et al.*, 2010). Such an event could have caused extraordinary high methane values in the entire water column. It can be assumed that the oscillation of the sea level and the resulting sudden pressure drop lead to the abrupt transition of dissolved (pore water) methane into free gas followed by ebullition of free gas to the water column, or by a pressure-induced (amplified by wind and waves) pumping impulse on the pore water of the sediment and thus, seepage of methane-enriched water to the water column. For the situation at station TF0113, both mechanisms would produce the same signal with the observed enhanced but uniform distribution of methane due to the almost complete mixing of the water column (Fig. 3.5). In contrast, gas transport and advection/diffusion of dissolved methane can be clearly distinguished in waters with a density stratification, which greatly reduces diapycnal mixing of the water and thus, the vertical transport of dissolved constituents, while not hindering gas bubble mediated transport (*Schneider von Deimling et al.*, 2011). Whether methane was additionally released from gas accumulations of deeper reservoirs need to be investigated in the future, using isotope measurements.

### 3.3.4   Seasonal patterns of $CH_4$ concentration and oversaturation in the main basins of the Baltic Sea

The annual cycles of surface methane concentration and oversaturation show some distinct seasonal trends in the individual basins, which in the following are discussed in the framework of the key controlling parameters, i.e. sea surface temperature, mixing depth, sea-air exchange, and potential direct connection of the upper water body to the sediment (Fig. 3.7, Tab. 1).

#### 3.3.4.1   Sea surface temperature

The average sea surface temperature of the Baltic Sea ranged from 0° C in February to almost 23° C in July in 2010 with strong regional differences (Fig. 3.7, red lines). Strongest fluctuations of sea surface temperature were observed in the area of

the Gulf of Finland with widespread ice-coverage during the months February and March. Highest surface temperatures in the Gulf of Finland were measured in July with up to 24° C. Sea surface temperature of the Gotland Basin (GB) ranges from 4° C to 21° C in comparison. The rise in temperature mainly takes place between early April and July. During this period, a continuous increase in methane saturation was observed (Fig. 3.7, black broken line) in all basins. The temperature strongly influences the methane solubility in water and seawater, in which on average 2.4 % less methane can be dissolved for each degree of temperature rise (*Wiesenburg and Guinasso*, 1979). Thus, a water mass which is warmed will be increasingly oversaturated with respect to the atmosphere without an increase in the absolute concentration, in accordance to our observations. However, the induced oversaturation will stimulate the transfer of methane to the atmosphere (see section 3.3.5 and Fig. 3.7).

The warming of the sea surface beginning in April leads to the warming of parts of the water column below, and can also cause warming of the sediments, especially in shallow regions with a temporarily well mixed water column. The water temperature observed near the sea bottom is used as a proxy for the temperature of the sediment surface. Bottom water temperatures in the Arkona Basin e.g. show annual fluctuations between -0.32° C (minimum) and 15.6° C (maximum; ICES 2011). In deeper basins the annual fluctuation of the surface sediment temperature can be expected to be much smaller than the fluctuations at the sea surface (*Mogollon et al.*, 2011). The sediment temperature influences the solubility of methane in pore water and the depth of the shallow gas boundary layer (*Wever et al.*, 2006). With the warming of the sediment it can be expected, that less methane is solved in the pore water and saturated pore waters might get oversaturated, resulting in a lower depth of the free gas boundary layer or in an increased emission rate of sedimentary methane towards the water column. Further, temperature is a key control for the production of methane by methanogenic bacteria (*Heyer and Berger*, 2000).

### 3.3.4.2 Stratification

The Baltic Sea can be distinguished in areas with permanent (e.g. GB) and temporal stratification (e.g. AB, GoF; *Feistel et al.*, 2008). The warming of the surface water layers lead to a stratification of the water column and the formation of the temporal thermocline during the summer months. The stratification, beginning in April, separates the water column above the permanent halocline (where existent) into two sublayers with different physical properties, the lower one mostly defined by the winter surface water generated during maximum mixing depth in winter. Like the halocline, the thermocline reduces vertical mixing and the methane transport in particular between the deep water masses and sediment to the surface water. The deeper bottom layers, disconnected from the surface, start to enrich in methane due to the steady supply of methane from the seabed or the methane-enriched water below the halocline. In contrast, the surface water depletes in methane due to loss to the atmosphere by sea-air exchange, in part driven by the temperature-induced decreasing solubility.

### 3.3.4.3 Wind, mixing depth, and sea-air exchange

The sustainability of the stratification of the water column depends on the annual changing wind energy and the resulting mixing intensity and the temperature-gradient driven heat exchange. In general, wind velocities in the Baltic Sea are higher during the winter season and lower during the summer months. As a consequence, the depth of the mixed layer is shoaling until mid summer, leading to the formation of water layers with different properties (including methane concentrations). After reaching a minimum depth, the mixing depth deepens again by wind stirring and thermal convection until it reaches its maximum in winter (Fig. 3.7, blue lines). In the shallower and not permanently stratified basins, this can lead to occasional complete homogenization of the water column.

The wind speed also controls the gas transfer velocity $k$ (which in this work scales with $u^2$; Equ. 3.3; *Wanninkhof et al.*, 2009), and the air-sea exchange of methane

(see section 3.2.5). Fig. 3.9 shows $k$, which is low in the months April till July (main warming of the sea surface) and increases in mid-summer. A higher transfer velocity fosters the relaxation of the disequilibrium between surface water concentrations and atmospheric equilibrium. The mixing depth determines the thickness of the water body from which a net sea-air flux can be sustained. Thus, at a given $k$, relaxation towards methane equilibrium increases with increasing mixing depth.

### 3.3.4.4  Methane concentrations according to seasonal changes

The patterns of sea surface methane during 2010 in the different sub-basins result from the combination of the influencing parameters temperature and wind with the conveyed controls of mixing depth, stratification and change of the gas transfer velocity as described above. In spite of data gaps due to maintenance problems of the measuring system in April/May, the general trend of the surface methane distribution can be perceived and is confirmed by measurements of the year 2011 (data not shown). The combination of the controlling factors result in distinct patterns of oversaturation and methane flux into the atmosphere in different sub-regions of the Baltic, in particular contrasting areas with at least occasional interaction between the sediment, deeper water and surface water (e.g. MB, AB), and areas with a permanent decoupling of the sediment and sea surface due to a permanent halocline (e.g. GB, WoG, BB).

The winter period January till March is characterized by low sea surface temperatures and high wind velocities. Highest measured methane concentrations were recorded during this winter period especially in the regions of Arkona Basin, Bornholm Basin and Gulf of Finland (Fig. 3.7, green dots, and three day average: black solid line) with maximum values in January and declining concentrations towards March (with the exception of the GoF, see below). A high wind-induced energy input to the water column in combination with cooling from the atmosphere results in a maximum mixing depth and the mixing of the entire water column down to the sediment in some of the regions of the Baltic Sea, except for regions with a permanent halocline (e.g. GB). The intense mixing accelerates the transport of methane from

the sediment to the sea surface. Enhanced transport from the bottom layer and sediment surface into the water column can occur in completely unstratified conditions because of enhanced shear stress at the sediment-water interface. On the contrary, strong wind forces enhance the gas transfer velocity at the air-sea boundary, leading to an overall decrease of methane in the surface water later in winter (Fig. 3.7, green dots and black solid line).

During the period from early April till July/August, sea surface temperatures increase in all regions of the Baltic Sea (Fig. 3.7, red lines) and the mixing depth decreases with the development of the thermocline and summer stratification (Fig. 3.7, blue lines). In general, the stratification of the water column hampers the methane transport between deeper layers and the sea surface in the Baltic Sea (*Schmale et al.*, 2010b). The temperature-driven solubility decrease leads to an increase in methane saturation values in all regions of the Baltic Sea (Fig. 3.7, black broken lines), which could account for up to approximately 50 % additional methane saturation, assuming a temperature increase of 18° C and constant methane concentrations of the surface water during this period (2.4 % methane saturation for each degree temperature, loss to the atmosphere neglected). The emission of methane to the atmosphere is reduced due to lower wind velocities and gas transfer coefficients (Fig. 3.9) so that a slight oversaturation is sustained although the sea-air flux tends to force the surface water methane concentration towards equilibrium. During this period, the constant (though small) flux of methane to the atmosphere and the inhibited replenishment from deeper water layers due to summer stratification lead to the decrease in methane concentration in the surface layer. Deeper layers below the thermocline are characterized by steady enrichment of methane by the sediment or mixing with methane-enriched water below the halocline, forming a reservoir of methane. The reduced mixing depth and stratification of the water column allows the development of strong methane gradients within the upper 20 m (e.g.: AB, profile of August $1^{st}$, 2010, Fig. 3.5, with 3 nM methane in 2 m and 26 nM methane in 22 m depth).

After its maximum in August, sea surface temperature starts to decrease around September (Fig. 3.7, red lines), successively increasing the solubility of methane in
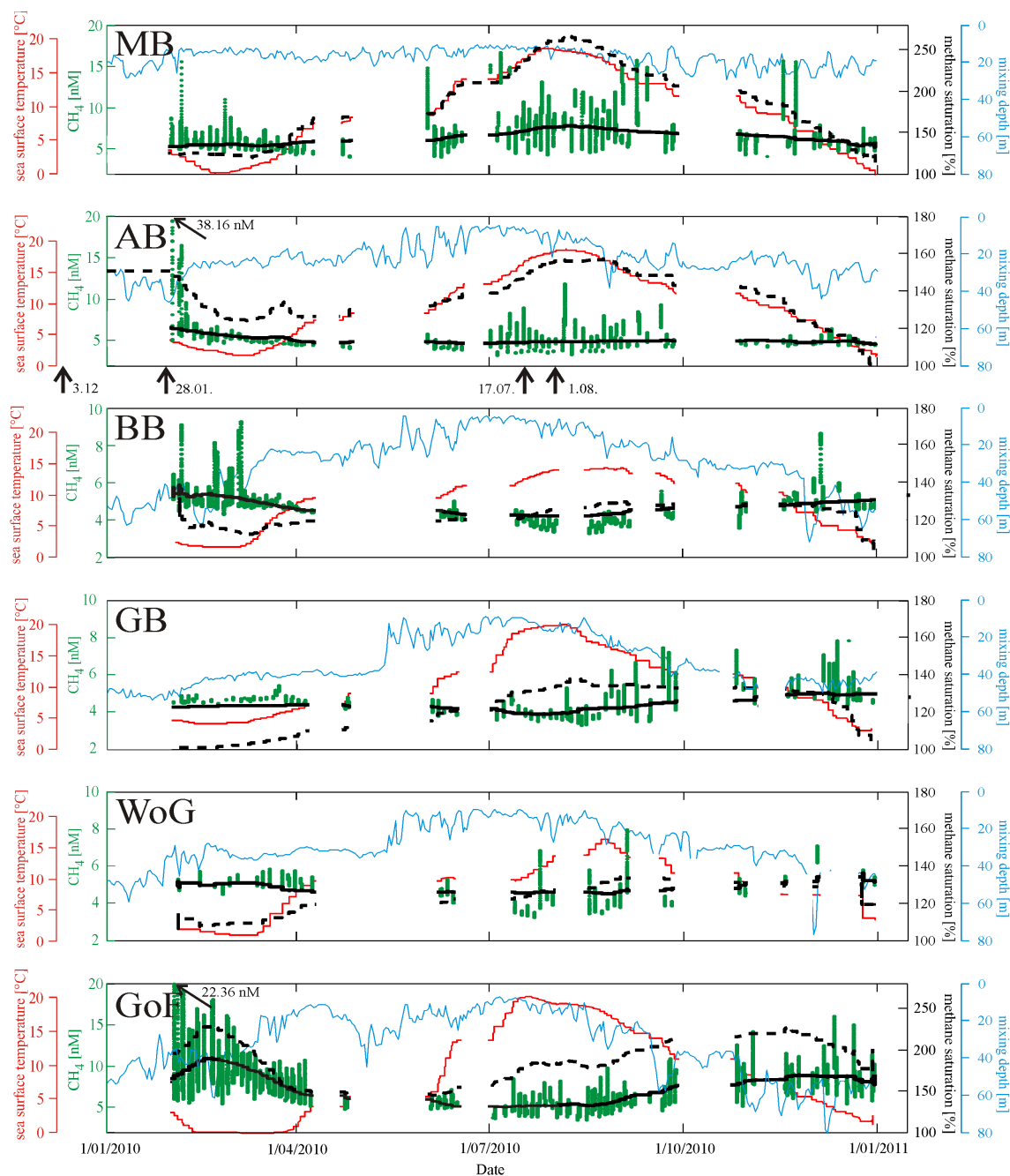
**Figure 3.7** – Compilation of various data sets for the interpretation of the seasonal methane distribution. Sub charts show measured time series of methane concentrations (green points) for each passing of the selected area (Table 3.1), its three day average (black solid line), maximum mixing depth (blue line, daily average), methane saturation (black dotted line, three day average), and sea surface temperature (red line, three day average) for Mecklenburg Bight (MB), Arkona Basin (AB), Bornholm Basin (BB), Gotland Basin (GB), West of Gotland (WoG) and Gulf of Finland (GoF). The arrows beneath subplot AB indicate the sampling date of the water column profiles shown in figure 3.5. Arrows in subplot AB and GoF show maximum values of methane concentration. Note the two different scales for methane concentration and methane saturation used for the individual subplots.

the water. Wind velocities intensify, resulting in deeper mixing of the water column. With increasing mixing depth, water layers with elevated methane content are mixed to the surface, increasing the surface methane concentrations.

For this period, strong regional differences of the methane saturation can be pointed out between the shallow regions (MB and AB) and the deeper regions of the Baltic Sea like Gotland Basin or Gulf of Finland. In the deeper basins (e.g. GB, BB, WoG, GoF), the deepening of the mixed layer leads to entrainment of methane-enriched deeper waters into the surface layer, increasing methane concentrations. Despite the deepening of the mixing depth in the Gotland Basin, the stratification of the water column sustains, and the deep water volume with high methane values as described in *Schmale et al.* (2010b) is not mixed to the surface. Cooling of the mixed layer partly dampens the effect of increasing concentrations on the oversaturation. The latter, in connection to enhanced wind speeds (and thus transfer velocities) lead to enhanced flux towards the atmosphere (see section 3.3.5). Interestingly, the net result of these co-acting processes for Bornholm Basin, West of Gotland and Gotland Basin is an increase in concentrations in connection to a relatively constant oversaturation until the end of the year.

The Gulf of Finland generally follows a similar trend, but methane concentrations increase more strongly and oversaturation increases steadily towards the end of the year with increasing mixing depth. This is consistent with the finding that the sub-thermocline waters in the Gulf of Finland are stronger enriched in methane than in the other central basins addressed above (*Schmale et al.*, 2010b). Another interesting finding is that the highest concentrations and oversaturations are found in February/March, though the maximum mixing depth has been reached before. The influence of the ice coverage on the methane distribution in this region needs to be mentioned. It is assumed that methane concentrations and saturation values of more than 200 % in this region in late winter indicate methane accumulations in the water column under the ice cover (*Berger and Heyer*, 1990) which result in elevated emission rates (discussed below) in ice free areas of the Gulf of Finland due to the main water currents along the coast (*Alenius et al.*, 1998). However, the influence of

ice coverage on sea surface methane concentrations in the Gulf of Finland needs to be investigated in more detail in the future.

An exception from these annual patterns of methane surface concentration and oversaturation is the very shallow area of the Mecklenburg Bight and, to a lesser extent, the Arkona Basin. In both basins, methane oversaturation strongly follows the trend of sea surface temperature. In the Mecklenburg Bight, methane concentrations increase during the summer, reaching a maximum in August and leading to the high saturation value of 290 % (Fig. 3.7). We suggest that wind-induced mixing remains relevant for the transport of methane from the sediment and that summer stratification is not capable nor sufficient to suppress the methane transport from the sediment to the sea surface in these shallow basins for longer timescales. The observed high fluctuations in methane concentrations throughout the year (MB, Fig. 3.7, green dots) can be related to short time wind events with enhanced mixing of the water column. Additionally, the importance of boundary mixing is enhanced and the volume of water below the thermocline will always be small in relation to the volume of the mixed surface layer in MB. As a consequence, no build up of a large methane inventory can counteract the annual variation of solubility by temperature changes, which is mirrored in the parallel trends of sea surface temperature and methane saturation. However, the amplitude of the seasonal trend is far too large to be caused by the temperature effect alone, even considering the reduced sea-air exchange from spring to summer. Apparently, the source strength for methane into the waters of the Mecklenburg Bight is modulated by sediment temperature as well. In this shallow basin, the variation of water temperature at sea bottom from 0° C to above 15° C (ICES 2011) is comparable to sea surface temperature changes (Fig. 3.7). Potential consequences are increased microbial methanogenesis due to increasing sediment temperatures as well as higher methane emissions from the sediment to the water column (*Heyer et al.*, 1990; *Heyer and Berger*, 2000) , because of the solubility effect on pore waters and shallow gas accumulations.

The Arkona Basin can be characterized as an intermediate between shallow regions like the Mecklenburg Bight and deeper regions like the Bornholm Basin or Gulf of

Finland.  The Arkona Basin is deeper than the Mecklenburg Bight and therefore the direct influence of the sediment and bottom water towards the surface layer as described above is assumed to be less dominant than in the Mecklenburg Bight, resulting in lower methane saturation values not exceeding 160 % in August (Fig. 3.7, black broken line). It is notable, that the maximum methane saturation value in the Arkona Basin is reached later than in the Mecklenburg Bight, and that the duration of this peak lasts longer (several weeks) than in the Mecklenburg Bight (couple of days).  Accordingly, the mixing depth is increasing during this period by more than 10 m (August till September) until it reaches the bottom layer and the sediment in November.  Similar to the Mecklenburg Bight but little delayed in time, saturation values start to decrease in September according to the temperature-induced solubility effect until lowest saturation values are reached by December.  This leads to the assumption, that no methane reservoir could be established in the water column of the Arkona Basin like in the Bornholm Basin or Gulf of Finland, where saturation values remain elevated until the following spring season.  Comparing the volume of water below the thermocline of shallow regions like the Mecklenburg Bight to deeper regions like the Bornholm Basin or Gulf of Finland, deeper basins contain a much larger volume of water, implying a larger methane-enriched reservoir which can be mixed to the surface. It is remarkable that the three day average of methane concentration (Fig. 3.7, black solid line) in the Arkona Basin shows almost equal methane values in the surface water from April until December, again demonstrating the characteristic between the deeper basins with methane concentration minima in summer and the Mecklenburg Bight with maximum concentrations during the same period. A basic proof of concept for our interpretation of the processes after the peak of the summer stratification based on a mass balance approach is given in section 3.3.6 for the Arkona Basin.

### 3.3.5   Flux - Methane emissions to the atmosphere

Our data show that the Baltic Sea remains a source for atmospheric methane with a positive sea-to-air methane flux throughout the year in all regions (Fig. 3.8).
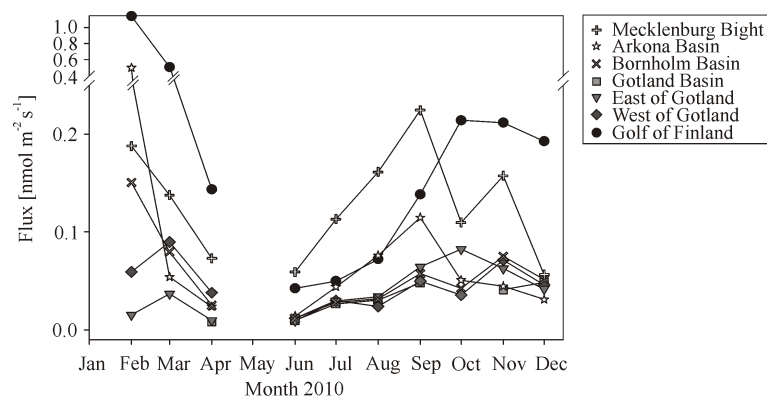
**Figure 3.8** – Methane fluxes $F$ [nmol m$^{-2}$ s$^{-1}$] calculated as monthly average for selected areas of the Baltic Sea using the equation described in *Wanninkhof et al.* (2009). Atmospheric methane data from the NOAA station in Poland were used for the calculation.

Average wind speeds and thus, transfer velocities, show a similar pattern for all areas in the Baltic Sea, with decreasing values during the spring period, very low values during the summer period, a sharp increase in August and persistent high values in fall and early winter. Figure 3.9 shows calculated transfer velocities $k$ (after *Wanninkhof et al.*, 2009) for methane in the Baltic Sea for selected areas in 2010.

Methane fluxes during the period from April to August remain in generally low, ranging from 0.008 to 0.162 nmol m$^{-2}$ s$^{-1}$ in comparison to the period September till November with fluxes ranging from 0.036 to 0.225 nmol m$^{-2}$ s$^{-1}$ (Fig. 3.8). The general increase of methane fluxes from June till August can be explained with the temperature induced solubility effect and the resulting increasing methane oversaturation in combination with a relatively low and uniform average gas transfer coefficient. All basins show a considerable increase in the calculated methane flux in August (Fig. 3.8) as a consequence of the transition to the regime of high wind velocities (see $k$, Fig. 3.9).

Beginning October, strong differences in the general flux distribution occur, with decreasing values in the Mecklenburg Bight and Arkona Basin compared to relatively stable or increasing values in deeper regions like Bornholm Basin, West of Gotland, East of Gotland, or Gulf of Finland, a consequence of the regional differences in the seasonal development of methane oversaturation as discussed in 3.3.4. Whereas

fluxes in the areas of the Bornholm Basin, Gotland Basin and around the island of Gotland show a very similar pattern, fluxes in the area of the Mecklenburg Bight and the Gulf of Finland deviate significantly. The Mecklenburg Bight shows generally elevated methane fluxes compared to the regions Arkona Basin, Bornholm Basin, Gotland Basin, West of Gotland, and East of Gotland, and significantly outstanding methane fluxes during the period of June till September. This can be explained by the mechanisms causing increasing surface water concentrations until late summer discussed in section 3.3.4.4, leading to increasing emission rates to the atmosphere. Methane fluxes in the Mecklenburg Bight drop from 0.225 nmol m$^{-2}$ s$^{-1}$ in September to 0.108 nmol m$^{-2}$ s$^{-1}$ (Fig. 3.8) in October and further on until December despite of an increase of $k$, again mirroring the (here decreasing) trend in sea surface methane concentration during this period. For the deeper basins, the constantly high average transfer velocities in combination with the relatively stable oversaturation sustained by mixed layer deepening lead to the stable enhanced methane sea-to-air fluxes from September until the end of the year (Fig. 3.8, BB, GB, WoG, EoG). The Arkona Basin is considered an intermediate between the very shallow Mecklenburg Bight and the deeper basins. Here, a methane flux of 0.497 nmol m$^{-2}$ s$^{-1}$ in February might have been caused by the described seepage event in the Arkona Basin (see also section 3.3). The Gulf of Finland shows comparable high flux values throughout the year (Fig. 3.8). Gassy sediments and temporal anoxic conditions in bottom layers of the Gulf of Finland during the summer period (*Alenius et al.*, 1998) result in high amounts of methane (dissolved in the deeper layers), which are mixed to the surface in autumn and winter. The origin of extraordinary methane fluxes of 1.145 nmol m$^{-2}$ s$^{-1}$ and 0.506 nmol m$^{-2}$ s$^{-1}$ in February and March, respectively have to be regarded with caution because of the potential role of sea ice. The ice coverage starts at the Finnish coast line of the Gulf of Finland in January and reaches its largest expansion during March (data not shown, Swedish Meteorological and Hydrological Institute, SMHI). During the period of ice coverage no or very limited sea-to-air exchange of methane can be expected. Nevertheless, the south-west part of the Gulf of Finland remained principally ice free during the winter period 2010 just as the main ship traffic route
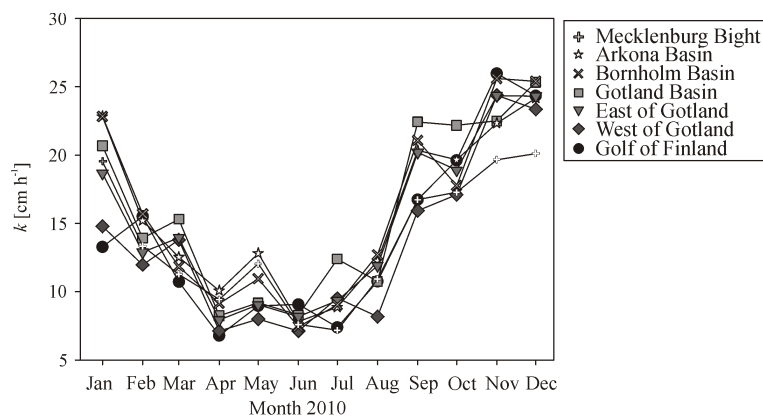
**Figure 3.9** – Transfer coefficient $k$ during 2010 for selected areas of the Baltic Sea with $k = 0.24 * u^2$ after *Wanninkhof et al.* (2009); whereas $u$ is defined as daily average wind speed [m s$^{-1}$].

of Helsinki (SMHI). Here, changing conditions of drifting ice shields with suppressed sea-air exchange and open water with high dissolved methane concentrations in the surface water (Fig. 3.2) as well as high wind speeds and transfer velocities (Fig. 3.9) can be assumed to influence methane fluxes to the atmosphere significantly but will need further investigation.

In the area of the Gotland Basin very small monthly averaged sea-air fluxes with 0.0008 nmol m$^{-2}$ s$^{-1}$ in December 2009 (data not shown) and 0.008 nmol m$^{-2}$ s$^{-1}$ in April 2010 were calculated (Fig. 3.8). Looking at averaged methane saturation values of single lines crossing the Gotland Basin in April, values of 96 % saturation with respect to the atmosphere were calculated. Findings of the year 2011 show saturation values of 94 % in February and April (data not shown), indicating that during the period December till April the direction of the net flux for methane might change frequently in the Gotland Basin. However, this occasional undersaturation of methane can be explained by the enhanced solubility of methane at lower temperatures and has only little effect on the general flux trend in this region.

*Bange et al.* (1994) calculated methane sea-air fluxes during July/August with 1.17 - 13.9 nmol m$^{-2}$ s$^{-1}$ and with 0.11 - 0.17 nmol m$^{-2}$ s$^{-1}$ during February, indicating a larger flux during summer than during winter. The flux approximations of Bange and coworkers include results of atmospheric and dissolved methane concentrations

determined using an automated gas chromatographic system during two Baltic cruises (Southern Belt Sea, AB, BB, GB) in February 1992 (63 stations) and July/August 1992 (23 stations). Flux calculations of *Bange et al.* (1994) are based on calculations after *Liss and Merlivat* (1986). The large data set underlying the flux estimations presented here provides monthly mean methane fluxes for the whole year 2010. Methane fluxes in February and July/August amounted to 0.151 - 0.080 nmol m$^{-2}$ s$^{-1}$ and 0.010 - 0.076 nmol m$^{-2}$ s$^{-1}$ for the Arkona Sea, Bornholm Sea and Gotland Sea. Results show that in this study presented summer flux values are significant lower than results presented by *Bange et al.* (1994). General seasonal changes of methane saturations with low values during winter (e.g. 107 % BB) and higher values during summer (e.g. 157 % BB) could be confirmed in this study (e.g. 116 % February - 134 % July/August, BB). Still, averaged methane supersaturation values of 3757 % based on measurements at two stations during the summer sampling campaigns by Bange and coworkers disagree with results presented in this study, showing averaged methane saturation values of 290 % for the Mecklenburg Bight for July and August. We therefore assume that estimated summer fluxes were overestimated by *Bange et al.* (1994). Further, figure 3.8 shows that the seasonality of methane fluxes is characterized by maximum values during winter and lowest values during summer for the Baltic Sea.

### 3.3.6   Methane mass balance during the period of mixed layer deepening

As proof of concept, a rough methane mass balance for the development of the methane concentration in the mixed layer, the water below and the sea-air flux for the period of mixed layer deepening has been calculated using the water column methane profiles of station TF0113 (1.08.2010, AB, Fig. 3.5) as starting condition. A scheme illustrating the approach is given in figure 3.10, showing a simplified methane concentration profile of the water column and the mixing depth for August and November. The amount of methane remaining in the upper water column $V_{rem}$ is estimated based on sea surface methane concentrations in August and November assuming a homogeneous upper water column. $V_{mix}$ illustrates the amount of methane, which is mixed

into the upper water column during the period August till November. Based on methane profile TF0113 and the model-derived mixing depth (see section 3.2.4), $V_{mix}$ is approximated with 203 $\mu$mol and can be compared to the flux during the period August till November with 303 $\mu$mol.
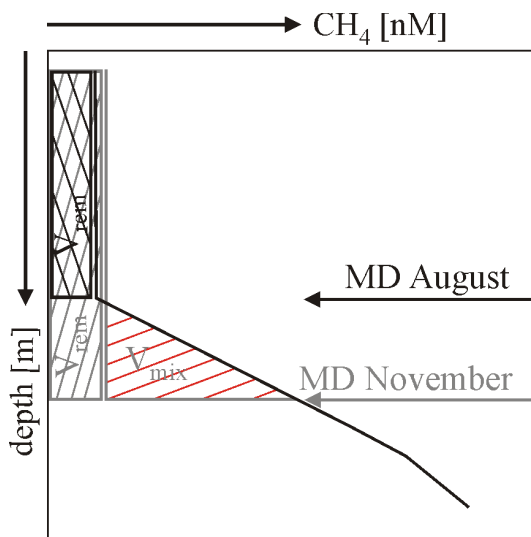


**Figure 3.10** – Diagram illustrating a methane concentration profile (black solid line) in August and the deepening of the mixing depth (MD) from August (black arrow) to November (grey arrow). The amount of dissolved methane remaining in the homogeneous mixed upper water column $V_{rem}$ is estimated according to the surface methane concentration measured in August and November, respectively. The amount of dissolved methane $V_{mix}$ is mixed into the upper water column during the period August till November.

The rough mass balance shows that the deepening of the mixing depth yields a significant amount of methane, which is mixed into the upper water column and accounts for elevated methane saturation values during the period August till September as described in section 3.3.4. A model-based estimation of sea-air exchange of methane as described in *Bange* (2006) was not attempted at this point due to the lack of available time series of water column methane concentration profiles of the Baltic Sea in the period of August to November 2010.

## 3.4 Conclusion

The first year of successful, continuous, and autonomous measurements of methane in the surface water of the Baltic Sea shows large regional and seasonal variations, influenced by a series of parameters. Processes controlling methane distributions in the surface water were identified on various temporal and spatial scales. In the area around Isle of Gotland several upwelling events could be observed, elevating the local methane distribution in the surface water. Elevated methane concentrations in the surface water and water column of the Arkona Basin in February 2010 with up to 832 % oversaturation could be related to a longer period of strong winds, resulting in a potential pressure induced gas release from the underlaying methane bearing upper sediments. Upwelling, seepage or wind events develop on a rather short temporal and spatial scale; yet influence local methane distributions significantly. Temporal stratification and low mixing depths of the water column of the Baltic Sea occurs on a longer time scale and inhibits methane transport from methane-enriched deeper water layers to the sea surface during summer. Thus, especially in deeper regions like Bornholm Basin and Gulf of Finland a methane reservoir is formed during the summer period, which is partly mixed to the surface from the beginning of autumn, leading to elevated methane concentrations for several months. Stratification in shallower regions like the Mecklenburg Bight is less dominant and no methane reservoir in deeper water persisting of longer periods of time can establish. We suggest that these regions are rather influenced by microbial methanogenesis in the sediment and emission of methane into the water column, short-time wind events and reduced solubility of methane by higher water temperatures during summer.

The Baltic Sea is a source of atmospheric methane with high emission values during the winter season (0.015 - 1.145 nmol m$^{-2}$ s$^{-1}$) and low emissions during the spring and summer season (0.008 - 0.162 nmol m$^{-2}$ s$^{-1}$). Parameters controlling the methane fluxes alternate during the seasons depending on the region. Methane fluxes in shallow regions like the Mecklenburg Bight (0.057 - 0.225 nmol m$^{-2}$ s$^{-1}$) are higher compared to deeper regions like the Gotland Basin (0.008 - 0.049 nmol m$^{-2}$ s$^{-1}$) and

show significant changes during the seasons in connection with temperature driven methane solubility changes and methanogenesis in the sediment. Methane fluxes in areas with a permanent stratification like the Gotland Basin were found to be less variable during the year and mostly influenced by temperature induced solubility and annual development of the mixed layer. Highest methane fluxes were derived for the Gulf of Finland in February 2010 with 1.145 nmol m$^{-2}$ s$^{-1}$). Here the influence of changing ice coverage needs to be investigated in more detail in the future.

The general seasonal trend of the surface water methane distribution in the Baltic Sea presented in this study could be confirmed by iterant patterns recorded in 2011. Interannual changes will be presented elsewhere once more data become available.

# Seasonal variation of methane in the water column of Arkona and Bornholm Basin in 2009 - 2011.

Gülzow, W.[1*], Rehder, G.[1], Gräwe, U.[1], Thomas, S.[1], Schmale, O.[1]

[1] Leibniz Institute for Baltic Sea Research, Seestraße 15, D-18119 Warnemünde, Germany

[*] Corresponding author: wanda.guelzow@io-warnemuende.de

## 4.1 Introduction

Various studies of the Baltic Sea concerning the greenhouse gas methane concentrate on its emission from marine environments towards the atmosphere with the aim to quantify its contribution to the global methane budget (e.g *Cicerone and Oremland*, 1988; *Bange et al.*, 1994, 1998; *Bange*, 2006; *Grunwald et al.*, 2009). Estimates of worlds ocean methane emissions range from 2 % (*Bange et al.*, 1994) to 10 % (*Grunwald et al.*, 2009) reflecting its large uncertainties due to the lack of data and the limitations of discrete data measurements.

The main source of methane in marine environments is the anoxic microbial fermentation of organic matter (methanogenesis) in marine sediments and anoxic marine basins (see also section 1.1.3; *Cicerone and Oremland*, 1988; *Heyer et al.*, 1990; *Hovland*, 1992). Emissions of methane from marine sediments into the water column are controlled by the anaerobic oxidation of methane (AOM), which converts the majority of the methane produced in marine sediments, before it enters the hydrosphere (*Treude et al.*, 2003; *Jørgensen and Kasten*, 2006). The fraction of methane entering the hydrosphere is mixed to the sea surface. During its transport through the water column, methane is further depleted by aerobic oxidation (*Whiticar et al.*, 1986; *Butler et al.*, 1989; *Berger and Heyer*, 1990; *Thießen et al.*, 2006) especially in the

oxic/anoxic transition layer, as has been shown for the Black Sea (*Schmale et al.*, 2010a).

Regarding to the strictly anaerobic microbial formation process of methane, the worldwide increasing number of areas with hypoxic and anoxic conditions in the lower water column and the sediment gives reasons of concern (*Rabalais et al.*, 2010; *Conley et al.*, 2009, 2011). Future predictions raise the question if methane concentrations in the deeper water column will increase due to the expansion of hypoxia and if this will lead to enhanced methane emissions to the atmosphere (*Bange*, 2006; *Naqvi et al.*, 2009; *Bange et al.*, 2010). So far, only few studies subject hypoxia as source of methane in the deeper water column (*Bange*, 2006; *Naqvi et al.*, 2009; *Bange et al.*, 2010; *Schmale et al.*, 2010b). Enhanced methane emissions to the atmosphere could be confirmed in late summer/autumn after increased accumulation of methane in hypoxic areas during the summer stratification (*Bange et al.*, 2010; *Gülzow et al.*, acc. for BGS:D). The correlation of seasonal hypoxic conditions and elevated methane concentrations on the contrary could not yet be observed (*Bange et al.*, 2010). Instead a bimodal seasonality of methane concentrations in the bottom layer of Boknis Eck (Eckernförder Bight, Baltic Sea) was observed, which could be triggered by sedimentary organic material after phytoplankton blooms (*Bange et al.*, 2010).

In this study we focus on dynamics and parameters, which influence the transport of methane through the water column of the Arkona and Bornholm Basin from the sediment towards the sea surface and its seasonal distribution patterns within the water column (Fig. 4.2). Vertical profiles of dissolved methane from a central station in the Arkona Basin (TF0113), sampled from January 2009 till October 2011 and the Bornholm Basin (TF0200), sampled from December 2009 till November 2011, are presented. Additional, several methane transects, taken in the Arkona and Bornholm Basin, are shown and interpreted with model derived observations of dynamics and processes along this transects. The methane distribution within the Bornholm Basin is observed in respect to seasonal appearance of hypoxic and anoxic conditions.

## 4.2   Hydrography Baltic Sea

The Baltic Sea is a rather shallow marginal brackish sea with an average depth of 52 m.  A variety of submarine sills divide the Baltic Sea in several sub basins (Fig.  4.1), which can be distinguished and characterized by different geochemical and hydrographical gradients.
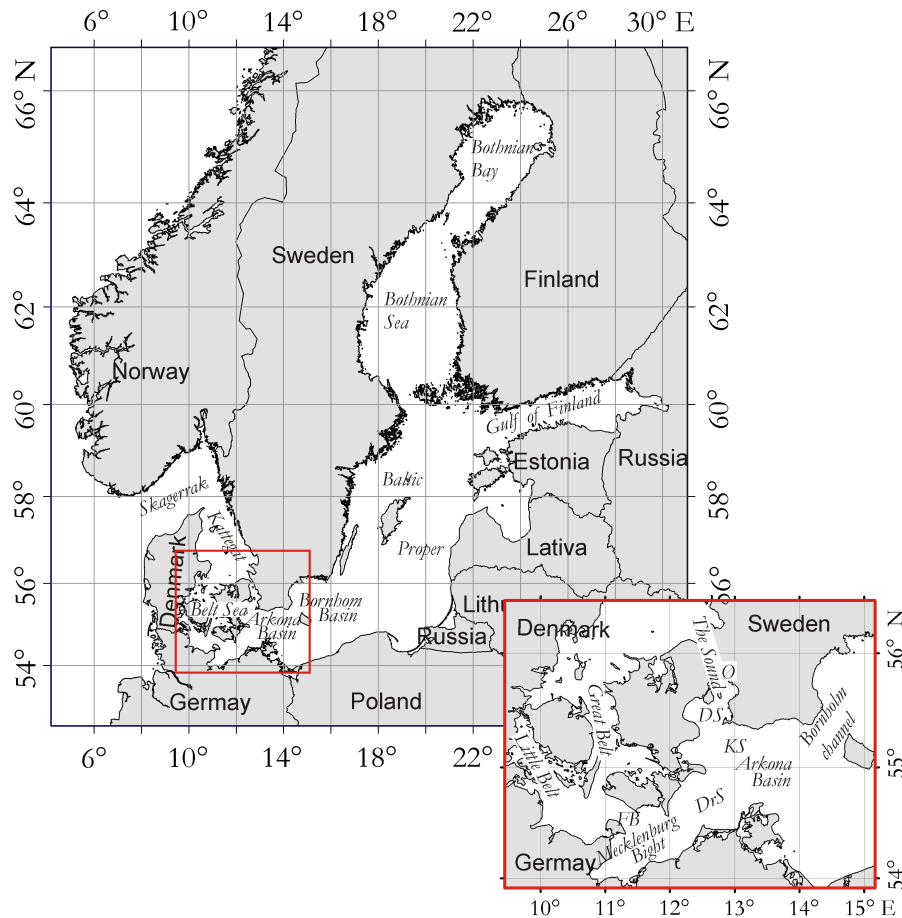


**Figure 4.1** – Overview of the Basins of the Baltic Sea with the detailed south western Belt Sea and the Arkona Basin.  The Sound can be divided in the Øresund (Ø) and Drogden Sill (DS), which is connected with the Arkona Basin via the Kriegers Shoal (KS). The Belt Sea can be divided into the Little Belt and the Great Belt and is connected with the Mecklenburg Bight via the Fehmarn Belt (FB). The Darss Sill (DrS) separates the Mecklenburg Bight and the Arkona Basin.

Today, the Skagerrak and Kattegat remain the only connection with the North Sea and the open ocean. Especially the transition zone formed by the shallow Belt Sea in the south western part of the Baltic Sea limits the water exchange with the

North Sea. The Baltic Sea is governed by a positive freshwater balance due to river runoff. Together with episodic saline inflow events a less saline or brackish out-flowing surface layer and a more saline in-flowing bottom layer is formed, separated by a permanent halocline. The water exchange between the North Sea and the Baltic Sea via the transition zone encounters effective mixing and is controlled by barotropic and baroclinic pressure gradients, local winds, bathymetry and stratification (*Schmidt et al.*, 1998).

## 4.3   Study site

The Arkona Basin is situated in the south - western part of the Baltic Proper and is characterized by a smooth morphology with a maximum water depth of 55 m. A description of the late- and postglacial sediments, which filled up the rough subsurface of the glacial morphology are specified in *Thießen et al.* (2006). Acoustic surveys detected high amounts of free gas in the uppermost Holocene sediments within 160 to 100 cm below seafloor of the Arkona Basin with decreasing values towards the centre of the Basin (*Thießen et al.*, 2006). Pore water methane concentrations were determined with approximately 4 $\mu$mol L$^{-1}$ in the central Arkona Basin, which was formed exclusively by microbial reduction of organic matter (*Thießen et al.*, 2006).

The hydrology of the Arkona Basin is dominated by frequently inflowing saline water masses from the North Sea, leading to a complex stratification of the water column (*Rheinheimer*, 1995). The salinity of the bottom water of the Arkona Basin varies between 10 and 20 psu (*Lass and Mohrholz*, 2003). During strong easterly winds the Oder river plume is guided along the German islands Usedom and Rügen into the surface water of the Arkona Basin (*Feistel et al.*, 2008). The surface water salinity of the Arkona Sea shows values with 8 psu on average. The Arkona Basin is characterized by entire mixing during the winter and autumn period and by a three-layered stratification during the summer and spring period with a colder intermediate water layer, a warm surface layer and a deeper saline bottom water layer. The water column of the Arkona Basin remains oxic throughout the year with occasional hypoxic

conditions (weeks) during strong summer stratification.
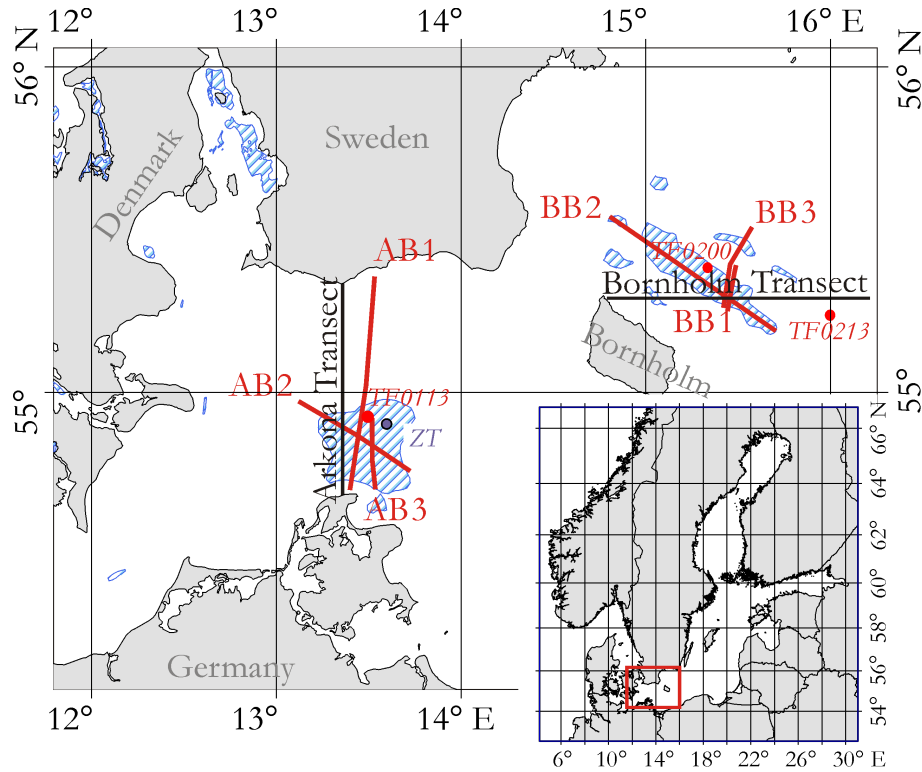


**Figure 4.2** – Sampling site Arkona Basin and Bornholm Basin. The map shows the location of the GETM model data (Arkona Transect and Bornholm Transect; black solid lines) and the transects AB1 (taken in January 2009), AB2, BB1, BB2 (taken in December 2009), AB3 and BB3 (taken in July/August 2010). The stations TF0113, TF0200 and TF0213 are monitoring stations for vertical methane profiles. ZT marks a pockmark location. The blue striped areas indicate gassy sediments after *Laier and Jensen* (2007).

The Bornholm Basin is situated in the south western part of the central Baltic Sea and is connected with the Arkona Basin in the west via the Bornholm Strait, a 30 km wide and 50 m deep channel between Sweden and Bornholm. Unlike the Arkona Basin, the Bornholm Basin can be considered as an enclosed basin, being connected with the Gotland Basin via the Słupsk Channel, 40 m shallower than the deepest part of the basin (*Feistel et al.*, 2008).

The Bornholm Basin forms one of the larger basins of the Baltic Sea with a lateral scale of 100 km and maximum depth of 105 m. During the summer period, a typical three-layered vertical stratification is formed with a thermocline in 10 - 30 m depth and a deeper halocline in 50 - 70 m depth (*van der Lee and Umlauf*, 2011).

105

The vertical mixing of the water column due to the deepening of the mixing depth during the winter period usually does not reach the sediment. After longer stagnation periods without ventilation of the deeper water layers of the Bornholm Basin oxygen is depleted via oxidation of sinking organic matter (*Reissmann et al.*, 2009). Hence, the bottom layer of the Bornholm Basin is characterized by hypoxic condition during winter and temporal anoxic conditions during summer. The occurrence of hydrogen sulfide changes the deeper water environment as well as the nutrient distribution like enhanced liberation of phosphate and iron(II)ions (*Reissmann et al.*, 2009). The ventilation of the dense bottom water pool is therefore depending on saline and oxygenated inflows from the North Sea (*Sellschopp et al.*, 2006; *Feistel et al.*, 2008).

## 4.4   Sampling and Methods

Methane profiles where taken along three transects in the Arkona Basin in January 2009 (AB1), December 2009 (AB2) and July 2010 (AB3). AB1 extends from south (54° 42.56' 13° 32.65') to north (54° 55.51' 13° 30.0') and crosses a sediment field with high amounts of trapped gas (Fig. 4.2 *Laier and Jensen*, 2007). The southern end of AB1 is situated on the shelf area with 30 m water depth and reaches to the centre of the Arkona Basin (45 m depth). AB2 crosses the area of gassy sediments from south-east (54° 56.32' 13° 41.34') to north-west (54° 58.17' 13° 9.16', Fig. 4.2) Transect AB3 extends from south (54° 42.21' 13° 23.77') to north (55° 19.46' 13° 32.02') crossing the entire Arkona Basin. Stations 14, 15 and 16 are located above the gassy sediment field (Fig. 4.5; *Laier and Jensen*, 2007).

Three methane transects were taken at the Bornholm Basin in December 2009 (BB1, BB2) and August 2010 (BB3; Fig. 4.2). BB1 extends from south (55° 14.99 15° 26.16) to north (55° 24.08 15° 28.40) and crosses a gassy sediment field (Fig. 4.2; *Laier and Jensen*, 2007). Transect BB2 is longer than BB1 and reaches from north west (55° 32.68 14° 49.96) to south east (55° 10.95 15° 45.60) alongside the gassy sediment field. Transect BB3 crosses a second smaller gassy sediment field from south

(55° 15.02 15° 26.15) to north (55° 30.02 15° 34.04; Fig. 4.2; *Laier and Jensen*, 2007).

**Table 4.1** – Overview of sampling sites, dates and methane measuring techniques

| site | date | measuring technique |
|------|------|---------------------|
| TF0113 | Jan, Dec 2009, | Purge & Trap |
|        | Jan, July 2010 | Purge & Trap |
|        | Aug 2010 | Vacuum Extraction |
|        | Mar, May, Aug, Oct 2011 | Purge & Trap |
| TF0200 | Dec 2009 | Purge & Trap |
|        | Aug 2010 | Vacuum Extraction |
|        | Mar, May, Aug 2011 | Purge & Trap |
|        | Nov 2011 | Vacuum Extraction |
| AB1 | Jan 2009 | Vacuum Extraction |
| AB2 | Dec 2009 | Vacuum Extraction |
| AB3 | Aug 2010 | Vacuum Extraction |
| BB1 | Dec 2009 | Vacuum Extraction |
| BB2 | Dec 2009 | Vacuum Extraction |
| BB3 | Aug 2010 | Vacuum Extraction |

More than 80 water column profiles were sampled during the present study using a 12 Niskin bottle (10 L) rosette sampler. For continuous CTD profiling a Seabird sbe911+ system was mounted to the sampling unit. Temperature and conductivity sensors were calibrated after each cruise. The oxygen concentrations of water samples were measured via Winkler titration to calibrate the oxygen sensors (*Grasshoff et al.*, 1999). Hydrogen sulfide in sea water was analysed spectrophotometric as methylene blue after (*Fischer*, 1883; *Fonselius*, 1969).

Water samples for methane analyses were taken instantaneously after retrieving the CTD and sampling for oxygen measurements. Methane concentration was measured using the purge and trap (section 4.4.1; analysis in the lab) or vacuum extraction method (section 4.4.2; analysis onboard) and analyzed with gas chromatography. For the purge and trap method, water samples were taken using 250 ml crimp cap glass bottles, sealed with a butyl rubber septum or 250 ml ground flasks, poisoned with 500 $\mu$l mercury chloride ($HgCl_2$) and stored at 4° C and in the dark until measuring

in the lab. Water samples using vacuum extraction were analyzed on board within 2 hours after the sampling. Table 4.1 gives an overview of all sampling sites and the applied analyzing technique.

### 4.4.1   Purge & Trap Method

The Purge and Trap method (P&T) based on *Michaelis et al.* (1990) is described in detail by *Thomas* (2011). The water sample is transferred into a purge vessel and purged with helium for 30 minutes. During this process, the total amount of dissolved gases are purged from the aqueous into the gaseous phase and methane is trapped using a HayeSep D packed column as adsorbent (25 cm 1/8" SS, 60/80 mesh), cooled down to -100° $C$. During the following heating process of the column (up to 95° $C$), methane is released from the adsorbent and transported to the gas chromatograph (Shimadzu GC-2014) equipped with a packed seperation column (3 m 1/8" SS, activated aluminium oxide, 60/80 mesh, grade F-1) and a flame ionization detector for determination. For calibration a 1 ppm and 100 ppm methane standard (Linde) was used. The methane concentration $C_{CH4}$ [mol L$^{-1}$] can be calculated:

$$C_{CH4} = \frac{V_g}{V_{mol} * V_{aq}} \qquad (4.1)$$

with the molar gas volumne $V_{mol}$ of 22.4 L mol$^{-1}$, the volume of water sample transferred into the purge valve $V_{aq}$ [L] and the purged volume of methane $V_g$ [L]. The latter can be calculated with equation 4.2 using the determined area of the measured gas $area_{sample}$, the standard gas $area_{std}$, the methane mole fraction of the standard gas $x_{std}$ [ppm] and the volume of the sample loop $V_{Loop}$ [L].

$$V_g = area_{sample} * \frac{x_{std}}{area_{std}} * V_{Loop} \qquad (4.2)$$

### 4.4.2   Vacuum Extraction Method

For methane analysis aboard a modification of vacuum extraction method (VE) described by *Lammers et al.* (1994) was used (*Rehder et al.*, 1999; *Thomas*, 2011).

700 ml of water sample was filled into pre-evacuated 1000 ml glass bottles, which were closed with valve caps to avoid any air contamination caused by leakage. A calibrated flowmeter (ENGOLIT Flow-Control 100S DMK) was used to determine the exact water volume $V_{aq}$, transferred into the glass bottles (needed for calculation purpose). The transfer of the sample water into pre-evacuated bottles leads to a degassing of $87.4 \pm 11.2$ % of the total solved gaseous volume $V_g$ (*Thomas*, 2011). The mole fraction of methane $x_{CH4}$ was subsequently determined using a gas chromatograph (Thermoscientific GC) equipped with a flame ionization detector.

The methane concentration $C_{CH4}$ can be calculated using equation 4.3 with the molar gas volume $V_{mol}$ of 22.41 L mol$^{-1}$.

$$C_{CH4} = \frac{x_{CH4} * V_g}{V_{mol} * V_{aq}} \qquad (4.3)$$

A detailed description of possible sources of errors as well as the comparability of the P&T- and VE-method is given in *Thomas* (2011). Results of duplicate field samples show that methane concentrations measured by P&T reach values on average 9 % higher than measured by VE. The disagreement of the two methods diminishes for high methane concentrations. The experimental standard deviations for laboratory conditions were determined with 5 % for the VE-method and 4 % for the P&T-method (*Thomas*, 2011).

### 4.4.3   Accompanying parameters

The three-dimensional free-surface primitive equation model GETM was used to parameterize the vertical and horizontal mixing at two transects (Arkona Transect, Bornholm Transect) of the Baltic Sea (*Gräwe et al.*, 2012, in press) for 2009. Using a grid-spacing of approximately $\Delta = 600$ meters (840x610 grid points), the important length scale of a baroclinic Rossby radius (4 - 7 km; *van der Lee and Umlauf*, 2011) can be resolved by 4 - 5 grid-points. GETM has been successfully applied to simulate inflow events into the Baltic Sea (*Burchard et al.*, 2009), and was further used for climate downscaling for the Western Baltic Sea (*Gräwe and Buchard*, 2011). Adaptive

vertical coordinates with 50 vertical layers are applied. The atmospheric forcing was derived from the operational model of the German Weather Service with a spatial resolution of 7 km and temporal resolution of 3 hours. For data analysis, 24 hourly snapshots of temperature and salinity were stored along the Arkona Transect and Bornholm Transect.

The mixed layer depths were extracted from a high-resolution circulation model of the Baltic Sea based on the Modular Ocean Model (MOM4), developed at the Geophysical Fluid Dynamics Laboratory (*Griffies et al.*, 2004). The model bathymetry is based on a one nautical mile grid (*Seifert et al.*, 2001) and described in more detail in *Gülzow et al.* (acc. for BGS:D).

## 4.5  Results & Discussion

Time series of vertical methane profiles, measured between January 2009 and November 2011, will be presented and discussed for the Arkona and Bornholm Basin in the following section. General seasonal changes of stratification and vertical mixing of the water column, influencing the vertical methane distribution will be elucidated. Water column transects from the Arkona and Bornholm Basin are shown. GETM model simulations of the vertical and horizontal mixing for 2009 will be consulted for the understanding of general seasonal flow patterns and dynamics within the water column of the Arkona and Bornholm Basin, which influence the vertical methane distribution. Due to the intensive computing time required for the model run, no model data are available for 2010 and 2011 so far. For this period, only general flow patterns can be used for interpretations.

### 4.5.1  Time series

#### 4.5.1.1  Time series at TF0113

Nine vertical methane profiles were taken at station TF0113 (station 16 at transect AB3; Fig: 4.5) from January 2009 till October 2011, showing remarkable changes in

the vertical methane distribution over time (Fig. 4.3). The profile taken on January $28^{th}$ 2009 (Fig. 4.3 A) is characterized by low methane concentrations throughout the water column (green dots). The parameters oxygen (blue solid line), temperature (red solid line) and density (black solid line) indicate the deep homogeneous mixing of the water column down to 39 m depth. A sharp density gradient (halocline) below 39 m separates the dense bottom layer from the mixed upper water column, forming the characteristic two-layered winter water column of the Arkona Basin. Similar low methane concentrations were measured on December $3^{rd}$ 2009 (Fig. 4.3 B). Profile B shows homogeneous temperature and oxygen values and a strong halocline at 12 m depth indicating a significant lower vertical mixing compared to January $28^{th}$ 2009.

Extraordinary high methane concentrations throughout the water column recorded on January $28^{th}$ 2010 (Fig. 4.3 C) result from a seepage event after a period of strong blowing winds, a significant sea-level shift and mixing of the water column down to the sediment. The event is described in detail in *Gülzow et al.* (acc. for BGS:D). The strong vertical mixing at station TF0113 results in a homogeneous methane, temperature and oxygen distribution along the profile (Fig. 4.3 C). The significant deepening of the halocline on January $28^{th}$ 2010 (Fig. 4.3 C), compared to the profile taken on December $12^{th}$ 2009 reflects the strong vertical wind-induced mixing during this period. On January $28^{th}$ 2010 methane values up to 400 nM could be measured in the bottom layer of TF0113 (Fig. 4.3 C), indicating a large amount of methane released from the sediment during the event. Elevated methane concentrations could be measured until six days after the event in the surface water of the Arkona Basin reflecting the fast exhaustion and transport of methane from the water column towards the atmosphere (*Gülzow et al.*, acc. for BGS:D).

During summer 2010, two profiles were taken within 14 days (Fig. 4.3 D, E), showing the characteristic three-layered summer stratification, with a warm surface layer, a colder intermediate layer and a thin, dense bottom layer. On July $17^{th}$ 2010, low methane concentrations were measured within the water column to 35 m depth (maximum values 12.8 nM) but significantly increasing values up to 184.7 nM, following the density gradient in the bottom layer (Fig. 4.3 D). The methane profile of
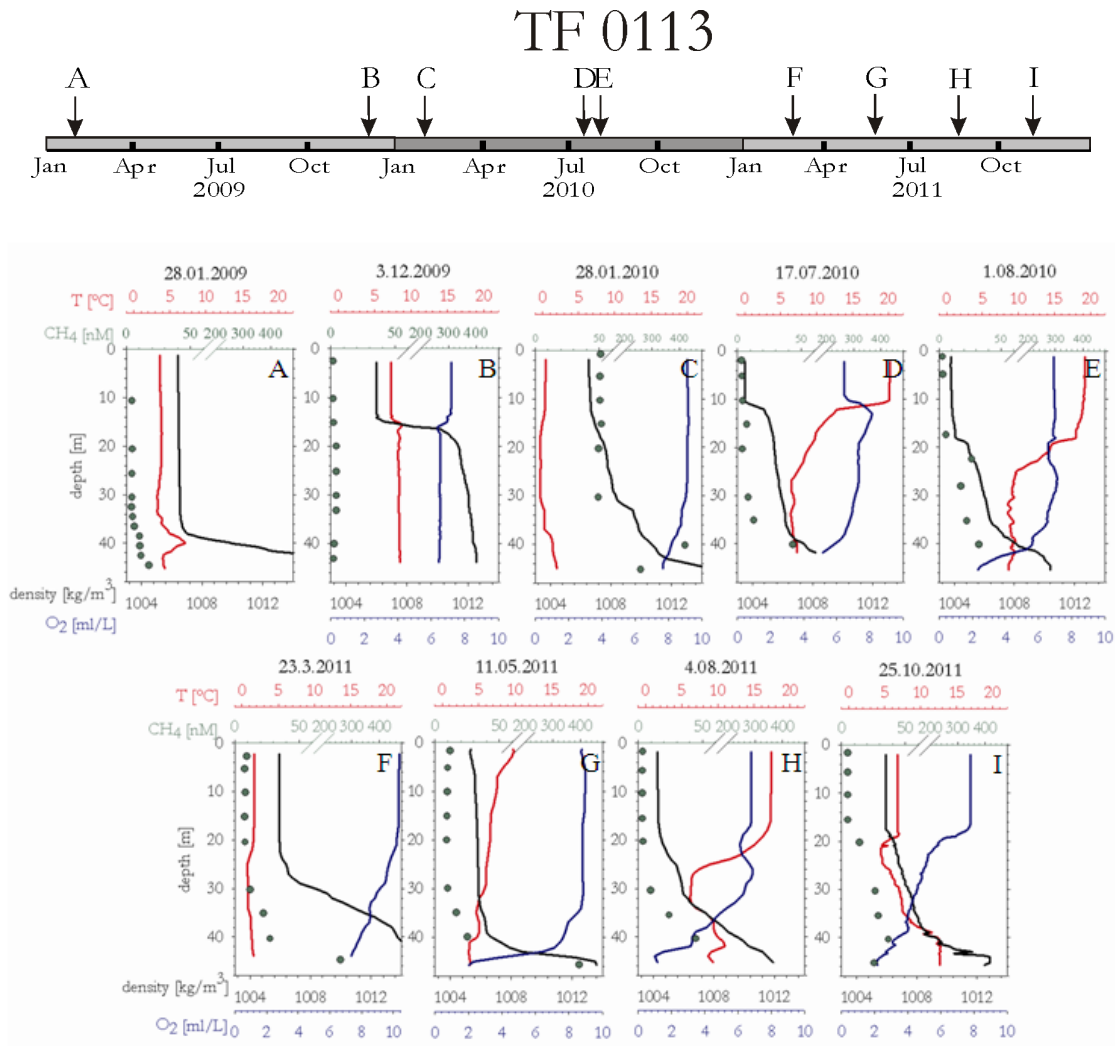
**Figure 4.3** – Vertical methane profiles at TF0113. The arrows along the time lime bar indicate when vertical water column profiles were taken. The vertical profiles A - I show the methane (green dots), temperature (red solid lines), oxygen (blue solid lines) and density distribution (black solid line) at different times at station TF0113. The black and green arrows indicate the water density and methane values outside the display range respectively. At profile A (January $28^{th}$ 2009), no oxygen concentrations were measured due to malfunction of the oxygen sensor.

August $1^{st}$ 2010 reflects the fast changes and high dynamics of the methane distribution within the water column of the Arkona Basin. Whereas methane concentrations remain low in the surface water (2.6 nM), elevated values (26.0 nM) were measured already below 22 m depth, concurrent to a deepening of the halocline and a decrease in methane concentrations in the bottom layer (125.9 nM; Fig. 4.3 E). Profile E reaches to 45 m water depth, showing a significant decrease of oxygen concentration and hypoxic conditions within the bottom layer.

Methane values of the upper water column taken on March $23^{rd}$ 2011 range from 7.8 nM - 9.2 nM (down to 40 m depth) and up to 260.0 nM in the bottom layer (43 m depth; Fig. 4.3 F). The profile shows a mixed layer to 30 m water depth with a smooth density gradient between 30 m and 40 m depth. Oxygen concentrations within the bottom layer recovered compared to August $1^{st}$ 2010, showing values of approximately 7 ml $L^{-1}$ (Fig. 4.3 F).

The profile taken on May $11^{th}$ 2011 shows a mixed upper water layer and homogeneous methane, temperature, density and oxygen values up to 41 m depth (Fig. 4.3 G). Within the dense bottom layer below 41 m on the contrary, oxygen values decrease rapidly reaching hypoxic conditions. Simultaneously, methane concentrations increase to approximately 397.3 nM (Fig. 4.3 G).

The characteristic summer stratified water column is developed again on August $4^{th}$ 2011 (Fig. 4.3 H). Methane concentrations remain low in the upper water layer and increase towards the bottom layer, following the smooth density gradient. Maximum methane values with only 90.6 nM in the bottom layer are significantly lower compared to the situation in August 2010 or May 2011 (Fig. 4.3 H, G, E). Oxygen concentrations remain low with values approximately 1.1 ml $L^{-1}$, reaching hypoxia in the bottom layer.

The vertical profile taken on October $25^{th}$ 2011 shows a similar stratified characteristic like the profile taken on August $4^{th}$ 2011. Methane concentrations decreased further within the bottom layer, reaching maximum values of 36.8 nM at 40 m depth (Fig. 4.3 I). Hypoxic condition persist with oxygen values, approximately 1.9 ml $L^{-1}$.

Following the seasonal change of the vertical temperature and density distribu-

tion at station TF0113 (Fig. 4.3), the general seasonal cycle of stratification and deep mixing can be observed. The warming of the surface layer during spring leads to the formation of a strong stratification beginning May and lasting till November and the development of a three-layered water column, forming a lighter and warmer surface water layer, a colder intermediate layer and a dense bottom layer. The deepening of the mixed layer depth, according to stronger winds during autumn, leads to the erosion of the thermocline and the formation of a two-layered water column with a homogeneous upper water body and a dense bottom layer. Accordingly, a general seasonal trend of the vertical methane distribution can be derived. Low methane values can be observed in the upper water column throughout the year. Methane concentration within the deeper water layers on the contrary vary significantly. The bottom layer remains undisturbed from vertical wave mixing and ventilation during the summer period and is constantly enriched by methane emitted from the sediment. The winter period can be characterized by homogeneous low methane values throughout the water column due to the wind induced mixing of the water column and enhanced exhaustion of methane towards the atmosphere. Decreasing methane concentrations measured in November 2011 confirm this pattern for the winter period 2011/2012 (Fig. 4.3 I). The upper water column remains oxic throughout the year with values ranging from 6.2 to 8.1 ml $L^{-1}$. The bottom layer on the contrary reaches hypoxic condition according to the development of the strong summer stratification, lasting several months.

### 4.5.1.2   Time series at TF0200

Water column profiles taken at station TF0200 in the Bornholm Basin (Fig. 4.4) differs significantly in the vertical methane distribution from December 2009 to November 2011, compared to station TF0113.

The vertical water profile of December $9^{th}$ 2009 is characterized by a well mixed upper water column with homogeneous methane, temperature, oxygen and density values down to 40 m depth (Fig. 4.4 A). The deeper, warmer water column is de-

fined by a continuously increasing density to 84 m depth, accompanied by decreasing oxygen values and hypoxic conditions with values ranging from 1.1 - 1.5 ml $L^{-1}$ between 70 and 84 m. A thin, dense bottom layer with oxygen concentrations reaching approximately 5 ml $L^{-1}$ could be observed at 86 m depth. The methane concentration below 40 m depth changes significantly towards the bottom layer (Fig. 4.4 A). Initially, methane values increase up to 25.8 nM between 40 and 70 m depth. From 70 - 84 m water depth methane concentrations decrease again, ranging from 6.2 - 7.8 nM. Within the thin bottom layer another increase in methane values con be observed reaching 22.8 nM.

Profile B (August $2^{nd}$ 2010) was taken during the characteristic three-layered summer stratification in the Bornholm Basin, forming the warm upper water layer (down to 22 m depth), a significantly colder intermediate water layer (old winter water, approximately from 23 to 76 m) and a dense bottom layer (Fig. 4.4 B). The thermocline was observed at approximately 24 m depth. Methane values at 60 m water depth remain high and increased compared to December $9^{th}$ 2009 with 50.1 nM. The bottom layer on the contrary shows significantly higher methane concentrations with maximum values of 354.6 nM. Oxygen concentrations decreased remarkably in the bottom layer, forming hypoxic conditions with only 0.1 ml $L^{-1}$ (Fig. 4.4 B).

The vertical water profile of March $31^{st}$ 2011 is characterized by a homogeneous upper water column and uniform methane, temperature, oxygen and density values down to 56 m depth, caused by strong wind-induced deep mixing (Fig. 4.4 C). A strong halocline, characterized by a sharp density gradient below 56 m depth, separates the warmer bottom layer from the upper water column. Concurrent to the halocline, elevated methane concentrations of 45.5 nM were observed. The thick homogeneous bottom layer remains undisturbed and hypoxic (approximately 0.2 ml $L^{-1}$). Methane values in the bottom layer are significantly lower with only 19.7 nM, compared to the profile taken on August $2^{nd}$ 2010 (Fig. 4.4 B, C).

The warming of the surface water (thermocline at 25 m depth) accompanied by the development of the summer stratification (and an uplift of the halocline compared to profile C), were observed on May $12^{th}$ 2011 (Fig. 4.4 D). Methane concentrations along
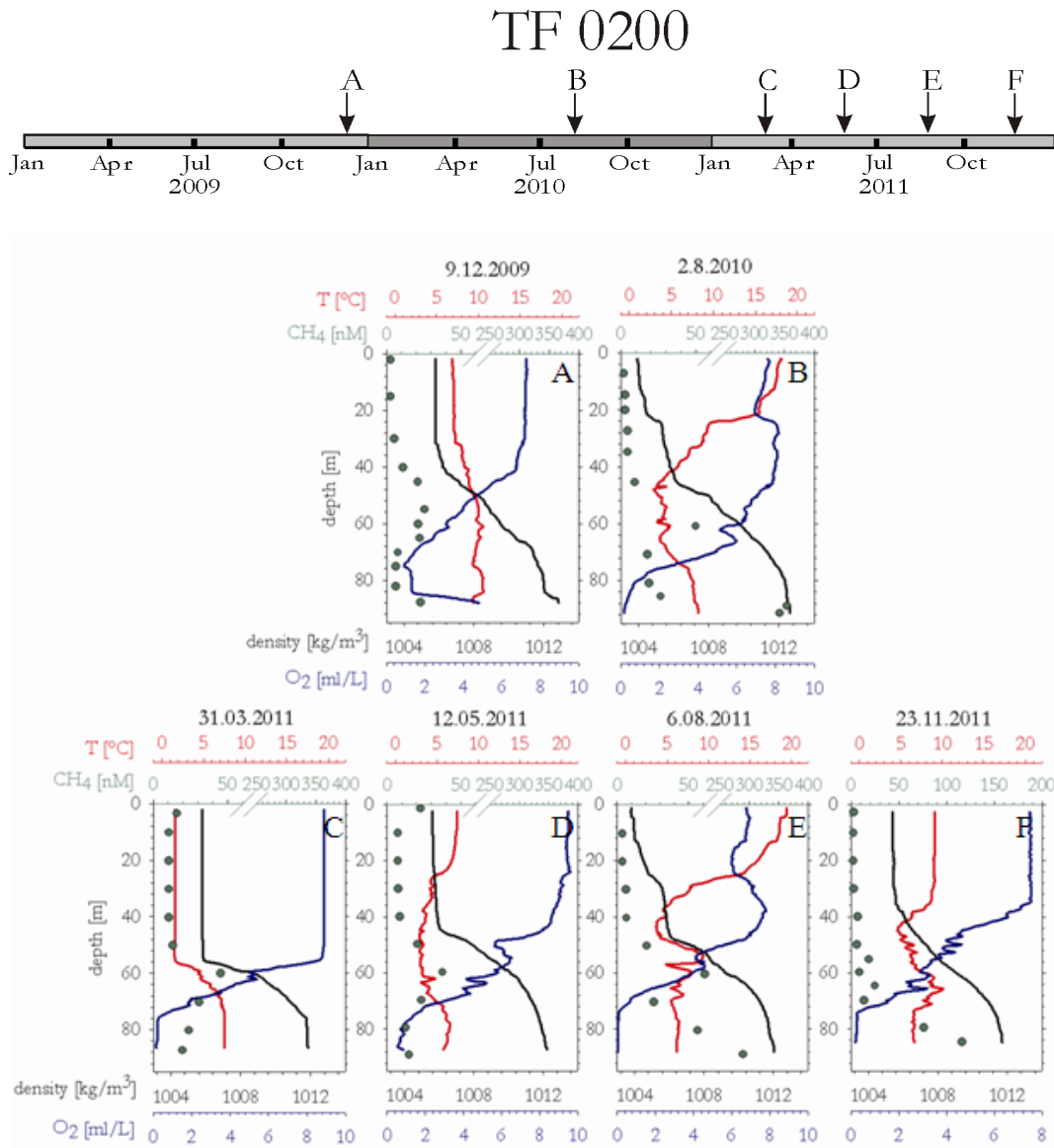
**Figure 4.4** – Vertical methane profiles at station TF0200. The arrows along the time bar indicate when vertical water column profiles were taken. The vertical profiles B - G show the methane (green dots), temperature (red solid lines), oxygen (blue solid lines) and density distribution (black solid line) at different times at station TF0200.

profile D remain almost unchanged compared to profile C . Oxygen concentrations decrease within the water column in May $12^{th}$ 2011, but slightly recovered from the strong hypoxic conditions observed in the bottom layer of August $2^{nd}$ 2010 and March $31^{st}$ 2011 (Fig. 4.4 D, C, B), indicating vertical mixing and ventilation of the bottom layer.

The profile taken on August $6^{th}$ 2011 shows the water column of the Bornholm Basin during the three-layered summer stratification (Fig 4.4 E). Similar to profile A, B, C and D (Fig. 4.4), pronounced elevated methane concentrations can be observed within the halocline at 60 m depth (61.5 nM; Fig. 4.4 E). Elevated methane concentrations within the bottom layer (290.0 nM) increased compared to May $12^{th}$ 2011, but remain lower than values observed in August $2^{nd}$ 2010 (Fig. 4.4 B). Below 74 m anoxic condition could be observed.

The profile taken on November $23^{rd}$ 2011 shows the erosion of the thermocline, compared to August $6^{th}$ 2011, and the deepening of the upper mixed layer to 40 m depth (Fig. 4.4 F). Concurring to the increasing density gradient below 40 m, oxygen values decrease reaching hypoxic conditions below 76 m depth. The bottom layer recovered from anoxia compared to August $6^{th}$ 2011, reaching oxygen values of approximately 0.2 ml $L^{-1}$, which leads continuing hypoxia. Elevated methane concentrations increased significantly in 79 - 84 m depth, compared to profile A - E, with values reaching up to 178.1 nM. Methane concentrations within the bottom layer on the contrary decreased compared to August $6^{th}$ 2011, reaching values of 34.1 nM (Fig. 4.4 F, E).

The water column at station TF0200 (Bornholm Basin) differs significantly from station TF0113 (Arkona Basin). The upper water column of the Bornholm Basin is characterized by low methane concentrations (average 5 nM) down to 40 m depth throughout the time series (Fig. 4.4). On the contrary, strong changes of the methane distribution below 45 m depth could be observed. Regarding to the general methane distribution pattern at TF0200, the water column below 45 m can be divided into an intermediate methane layer (IML; 45 - 70 m) with generally elevated methane concentrations, a deep layer (70 - 85 m) with lower methane values compared to IML and

a bottom layer with high fluctuations in methane concentrations over time (85 m - sea floor, Fig. 4.4). Further, a permanent halocline persists reaching from 50 m to 55 m depth during summer and from 55 m to 65 m depth during winter, marking the location of the IML. During the summer stratification, the halocline and the intermediate old winter water layer inhibit vertical mixing of the water column, leaving the bottom layer undisturbed. Therefore, the bottom layer is constantly enriched by methane emitted from the sediment. Additional depletion of oxygen within the water column due to decomposition of sinking organic material leads to the formation of anoxia within the bottom layer and the surface sediment. Since methanogens are strictly anaerobic organisms, the formation of anoxia within the sediment, leads to significant decline of sulfate concentrations and enhanced methane production rates within the surface sediment resulting in enhanced emission of methane towards the water column (*Piker et al.*, 1998). Whether methanogen bacteria enter the anoxic water column for methanogenesis is not known (*Jørgensen and Kasten*, 2006; *Bange et al.*, 2010).

With the deepening of the mixed layer depth at the beginning of autumn, the halocline deepens and methane-enriched water masses are mixed towards the atmosphere, leading to elevated methane fluxes (as observed in Gülzow et al. acc. for BGS:D) and to the depletion of methane within the IML during the winter period. The reason why methane concentrations in the bottom layer decrease during the winter period, remains unclear. Since the bottom layer of the Bornholm Basin remains undisturbed by wave induced vertical mixing processes, additional processes and dynamics within the water column influence the deep layer methane distribution.

### 4.5.2   Dynamics and methane distribution patterns

### 4.5.2.1   Dynamics within the Arkona Basin

To identify dynamics and processes influencing the methane distribution in the deeper water layers during summer and winter, several profiling transects were taken

in the Arkona Basin (AB1, AB2, AB3; Fig. 4.2) and Bornholm Basin (BB1, BB2, BB3; Fig. 4.2). Additional model-derived data parametrizing the vertical and horizontal mixing along the Arkona Transect and Bornholm Transect (Fig. 4.2, black solid line) are consulted.

The transect AB1 crosses an area of gassy sediments (Fig. 4.5) and was taken between January $28^{th}$ and $31^{st}$ 2009. The water column along transect AB1 can be divided into a homogeneous upper water column and a dense bottom water layer reaching to 10 m above sea floor. The strong density gradient between the upper water column and the saline bottom layer is formed at 35 m depth at the center of the Basin, fanning out towards the southern end of AB1. The methane concentrations within the upper water column range from 4.1 - 6.9 nM (except station 370260 - 370280; Fig. 4.5). A distinctive methane flare was observed within the bottom layer at station 370270, 370280 and 370290 (Fig. 4.5 AB1) with methane values between 33.4 nM - 36.7 nM forming a sharp gradient towards the surrounding water body. Methane concentrations in the bottom water of station 370280 and 370290 reach up to 44.6 nM and 61.8 nM respectivly. Elevated methane concentrations (up to the sea surface) were only measured in the southern end of the transect whereas values towards the center of the basin remain low and almost uniform throughout the water column (Fig. 4.5 AB1, black numbers). Water temperatures along the transect vary between 3 and 4° C (data not shown). No oxygen concentrations could be taken along the transect due to maintenance problems of the oxygen sensor.

The methane distribution along transect AB2, taken between December $2^{nd}$ and $5^{th}$ 2009 differs significantly from observations at transect AB1 (Fig. 4.5). The profiles at station 374100 and 374090 were taken outside the mapped gassy sediment area. The water column chemistry along transect AB2 is strongly influenced by the density gradient, which forms a wave-like structure between station 374020 and 374030 with a bulge forming bottom water layer at the same location. Temperature, oxygen and methane values follow the density gradient at approximately 30 m depth, separating the water column in a colder ($\sim 6°$ C; data not shown) and oxic ($\sim 7$ ml L$^{-1}$; data not shown) upper water layer with lower methane concentrations (2.6 - 4.9 nM) than

119
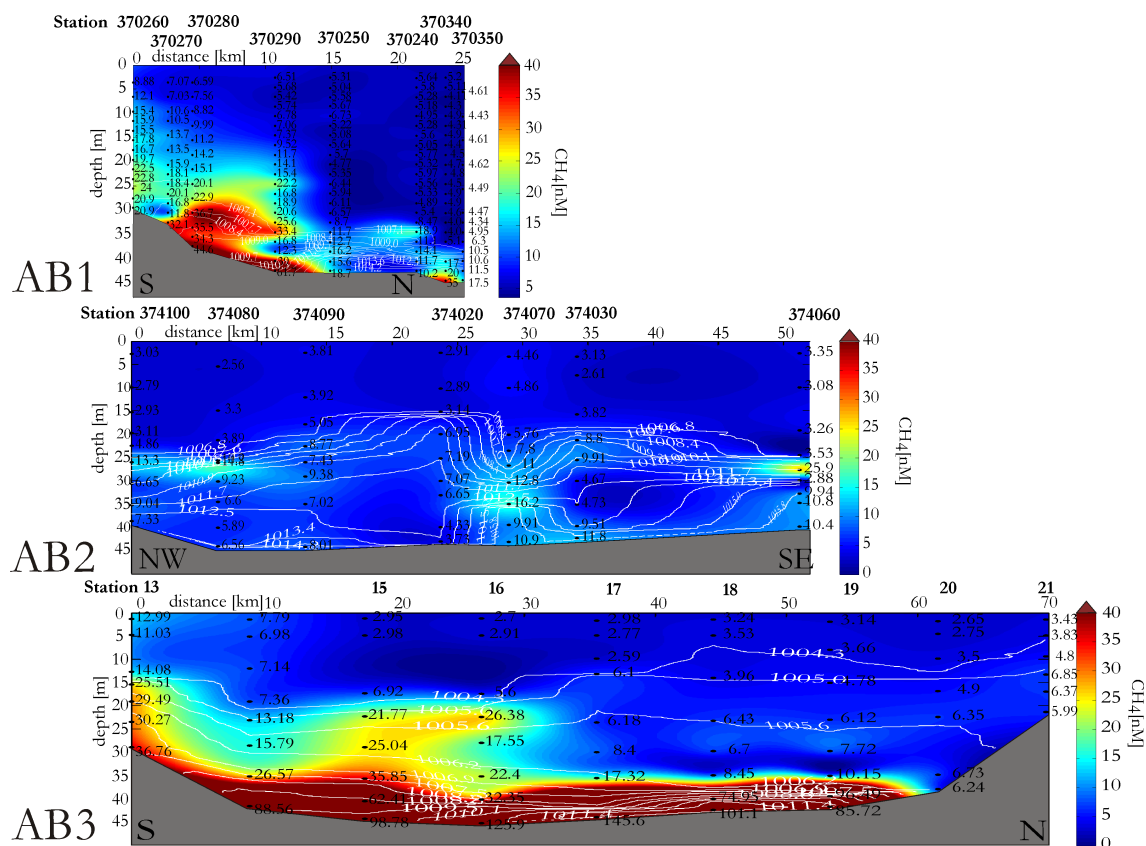
**Figure 4.5** – Illustration of methane concentrations (colour coded, nM) and density (white solid lines, kg m$^{-3}$) along transect AB1, along transect AB2 and along transect AB3. Station numbers are given above each plot. Black points illustrate the locations of discrete methane samples together with the measured methane concentrations (black numers).

observed at AB1 (Fig. 4.5). Oxygen concentrations decrease within the deeper water column (6.0 - 6.9 ml L$^{-1}$) but remain oxic throughout the transect (data not shown). The water column below the density gradient shows temperatures ranging from 8.5 to 9.5° C with several warm water lenses ($\sim$ 10.5° C; data not shown). Below the density gradient, methane concentrations are remarkable patchy with three areas of elevated values within the water column at station 374090 (14.3 nM), 374070 (16.2 nM) and 374060 (25.9 nM) and rather low methane values in the surrounding water body (3.7 - 10.8 nM). Patches of elevated methane concentrations coincide with the warm water lenses and areas with a particular sharp density gradient (e.g. bulge forming structure at station 374020 and 374060; Fig. 4.5 AB2).

Transect AB3 (Fig. 4.2), taken in August 2010, crosses the entire Arkona Basin,

showing again a significant change of the methane distribution along the transect. Methane concentrations in the upper water column of AB3 are low with values ranging from 2.7 to 7.8 nM, which reach to the bottom layer at station 20 and 21 (Fig. 4.5). On the contrary, remarkable high methane concentrations with values up to 145.6 nM were found in the bottom layer of station 13 - 19 (Fig. 4.5), forming a striking flare-like structure at station 15 and 16. Methane forms a sharp gradient at approximately 35 m in the center of the Basin and a dispersed gradient towards the southern slope of the basin. Whereas methane concentrations generally follow the density gradient along the transect AB3, the flare structure passes through all pycnoclines. Methane concentrations and density values at AB3 reveal a tilted shape within the water column towards the southern slope of the basin. Maximum methane concentrations observed at transect AB3 coincide with hypoxic conditions within the bottom layer. Oxygen concentrations in the water column of AB3 decrease from the surface layer ($\sim 7$ ml L$^{-1}$) towards the bottom layer (3 - 5 ml L$^{-1}$) reaching hypoxic conditions at station 17 and 18 ($\sim 0.9$ ml L$^{-1}$, data not shown). Similar water column profiles as shown at station 13 and 14 were taken at four stations approximately 13 nm to the east (data not shown).

The significant differences between the methane distribution along the transects AB1, AB2 and AB3 can be explained using model simulations. According to GETM derived model data, which parameterize the vertical and horizontal mixing along the Arkona transect (Fig. 4.2), AB1 and AB2 were taken during highly diverging winter situations. AB1 was taken during a comparable characteristic winter situation, showing a typical two layered water column structure. A tilted water column structure can be observed in AB1, concurring with the pycnoline (Fig. 4.5 AB1). Model data parameterize a general Coriolis induced current flow pattern within the Arkona Basin, which leads to a tilted structure of the bottom layer towards the southern slope of the basin, indicating the general pathway of inflowing saline water (Fig. 4.6; *Lass et al.*, 2005; *Burchard et al.*, 2009; *Reissmann et al.*, 2009). Out-flowing brackish water was observed, flowing along the upper water column at the northern coastline of the basin.
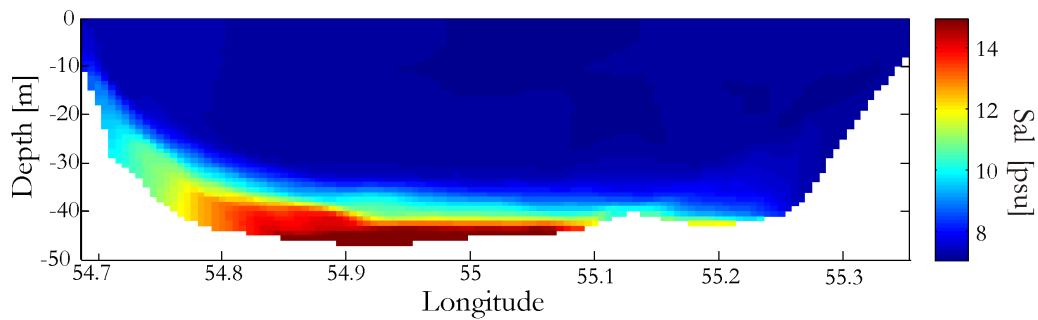
**Figure 4.6** – GETM model-derived simulation example of the tilted water column structure in July 2009 along the Arkona Transect (see Fig. 4.2, black solid line for orientation), using salinity as indicator.

The transect AB2, on the contrary was taken after two small inflow event observed in 2009. Such events occur several times a year and enter the Baltic Sea typically via the Øresund and the Drogden Sill (*Mohrholz et al.*, 2006; *Burchard et al.*, 2009). It can be distinguished between barotropic and baroclinic inflows. Barotropic inflows are driven by substantial sea level differences between the Kattegat and the southern Baltic Sea formed by persistent westerly winds during the autumn and winter season (*Burchard et al.*, 2009). They pass the Arkona Basin and usually underlay the former bottom layer of the Bornholm Basin (see also Fig. 4.9 C). Baroclinic inflows are driven by a horizontal density gradient between the Kattegat and the Baltic Sea (*Burchard et al.*, 2009) and intrude within the intermediate water layer of the Bornholm Basin (see also Fig. 4.9 B) after its passage through the Arkona Basin.

A saline and warm baroclinic inflow was observed in October 2009, which lead to an uplift of the tilted pycnocline along the Arkona Transect (data not shown). After the passing of the inflow front by November 2009, the water column along the Arkona transect is characterized by almost homogeneous temperatures and density values until 40 m depth, showing a laminar layered structure with a thin, dense bottom layer. The second, barotropic inflow was recorded in December 2009 (data not shown). During the passing of the inflow-front through the Arkona Basin, high dynamics with changing velocity fields within the water column were observed along the Arkona Transect, until a 'calmer' laminar structure develops with the beginning of January. Both inflow events show maximum velocity values at the southern rim

of the basin and the strong tilted structure of the water layers. The transect AB2 was taken after the inflow event in December 2009, showing the dynamics within the water column by means of the wave like structure of the pycnocline and the patchy distribution in temperature and methane concentrations.

Observations along TF0113 (Fig. 4.3) indicate the general formation of high amounts of methane in the bottom layer during the summer stratification. Since comparably low methane concentrations were measured directly after the observed inflow events, we conclude that large amounts of methane were transported from the Arkona Basin into the Bornholm Basin during the events.

The transect AB3 was taken during the summer stratification, showing the characteristic three-layered structure of the water column. The tilted pattern of the saline bottom layer (as described above) could be observed several times during the model run, confirming the general Coriolis induced current flow along the southern rim of the basin (*Lass et al.*, 2005; *Burchard et al.*, 2009). Model-derived vertical velocity field data confirm the distinct separation of the three-layered structure, which move with different velocities, and at times in different directions, during the summer stratification (data not shown). The separation of the bottom layer support the proposed enhanced replenishment of methane from the sediment but also the inhibited ventilation with oxygenated water masses, leading to the development of areas of hypoxia along AB3 described above. Additional elevated methane fluxes from the sediment into the water column during the summer period can be assumed, caused by higher production rates within the sediment due to higher sediment temperatures (*Iversen and Blackburn*, 1981; *Abril and Iversen*, 2002). The strong density gradient inhibits the methane transport towards the upper water column, leading to a methane distribution coinciding with the density distribution. The flare-like structure observed at station 15 and 16, on the contrary could possibly be caused by bubble mediated methane transport, which is not hindered by density stratification (*Linke et al.*, 2010; *Schneider von Deimling et al.*, 2011). A potential periodic seepage site for bubble-mediated methane transport is known in the Arkona Basin, situated 12 nm to the south east of station 16 (Fig. 4.2, ZT), and is described in detail in *Gülzow et al.*

(acc. for BGS:D). At ZT high amounts of free gas were located in the sediment using acoustic observation systems, as well as a characteristic depression indicating a pock-mark structure (*Gülzow et al.*, acc. for BGS:D). A possible explanation might be, that the flare structure of elevated methane concentrations was caused by a periodic methane escape at ZT.

### 4.5.2.2  Dynamics within the Bornholm Transect

Three transects were taken in the Bornholm Basin in December 2009 (BB1, BB2) and July 2010 (BB3). Methane concentrations along transect BB1 are characterized by low values in the upper water column and bottom layer and a prominent intermediate methane layer (IML) of remarkable high values (up to 109.3 nM) between 45 and 70 m depth (Fig. 4.7 A). Elevated methane concentrations coincide with the strong halocline between 50 and 65 m depth (Fig. 4.7 A). At station 374180 and 374170, a sharp gradient towards the IML can be observed, concurring with the sharp density gradient (Fig. 4.7 A). At station 374200 and 374190 on the contrary, the IML seams to bend towards the sea-floor, showing a slight fanning out, following the halocline and water temperature distribution (Fig. 4.7 A,B). Water temperatures along BB1 reach from 7° C in the upper water column to 11° C below the halocline, forming a homogeneous colder upper water body and a warmer bottom layer (Fig. 4.7 B). Oxygen concentrations within the upper water body range from 5.8 to 7.4 ml $L^{-1}$ to approximately 50 m depth (Fig. 4.7 B). Oxygen rapidly decreases below 55 m depth reaching hypoxic conditions to the sediment. At station 374200 and 374190 on the contrary, a thin tongue of oxic bottom water was observed with values up to 4.7 ml $L^{-1}$.

A similar methane, temperature and oxygen distribution was observed along transect BB2, which crosses transect BB1 orthogonally at station 374190. The transects BB1 and BB2 illustrate the spatial distribution of the IML within the Bornholm Basin in December 2009, which reaches methane concentrations of 67.2 nM (Fig. 4.7 a). At station 374280 a sharp front of dense, oxic (up to 5.0 ml $L^{-1}$) and methane enriched
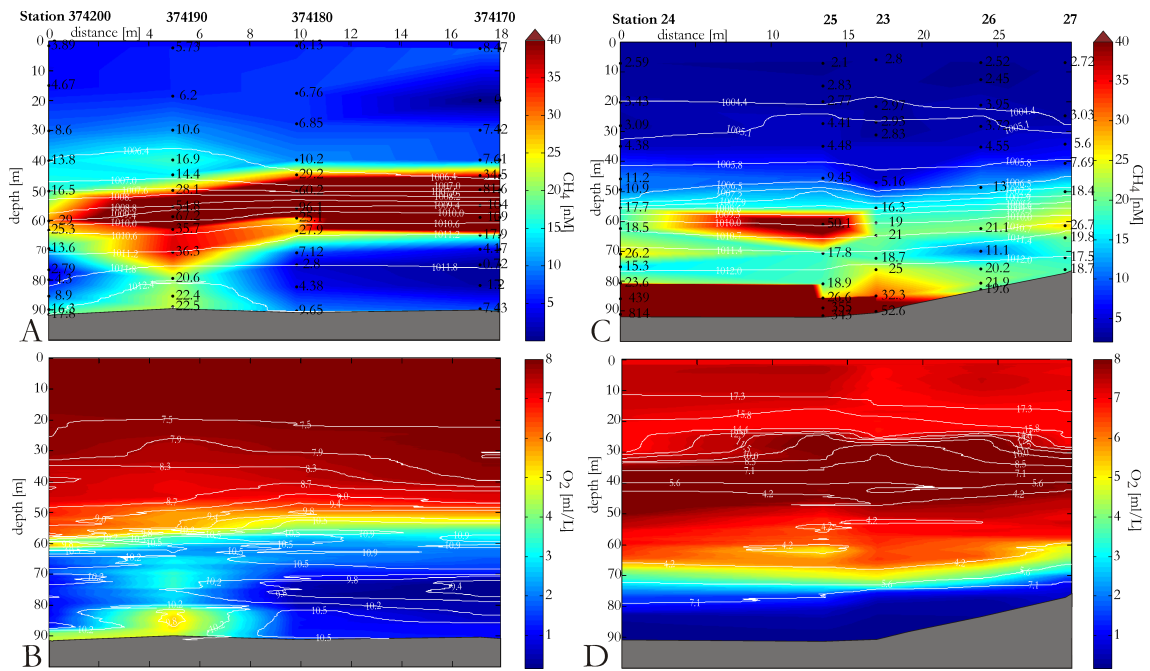
**Figure 4.7** – Illustration A and B show transect BB1, taken in December 2009. Illustration C and D show transect BB3, taken in July 2010. A and C show methane (colour coded, nM) and density (white solid lines, kg m$^{-3}$). B and D show oxygen (colour coded, ml L$^{-1}$) and temperature (white solid lines, ° C).

(up to 93.7 nM) bottom water was observed (Fig. 4.8 A). A thin oxic bottom water tongue continues along the transect, reaching until station 374270 (Fig. 4.8 B).

The water column along transect BB3 shows the characteristic three-layered summer stratification structure with a warm surface layer ($\sim 20°$ C), a colder intermediate old winter water layer with temperatures of 4 to 6° C (Fig. 4.7 D), separated by the thermocline at 25 - 30 m depth. Temperatures within the bottom layer reach 8.5° C. The methane distribution along transect BB3, taken in August 2010, changed significantly compared to BB1 and BB2, taken in December 2009, showing a distinct bottom layer with methane concentrations up to 813.7 nM (Fig. 4.7 C). Comparable high methane concentrations are only known from deeper regions of the Baltic Sea like the Gotland Basin (*Schmale et al.*, 2010b). Similar to transect BB1 and BB2 the upper water column of BB3 is characterized by low methane concentrations down to 50 m depth. The IML is less prominent along transect BB3 with significantly lower methane concentrations ($\sim 21$ nM) compared to BB1 and BB2. A spike with values

up to 50.1 nM (60 m depth) was observed at station 25 and small patches of lower methane concentrations at station 24 (26.2 nM at 75 m depth) and 27 (26.7 nM at 70 m depth). Oxygen concentrations in the surface layer are slightly lower than in the intermediate layer, with decreasing values towards the sea-floor. Below 80 m depth, oxygen values decrease rapidly, reaching hypoxic conditions in the warm bottom layer with values of 0.4 ml $L^{-1}$ (Fig. 4.7 D). High methane concentrations in the bottom layer along transect BB3 coincide with hypoxia.
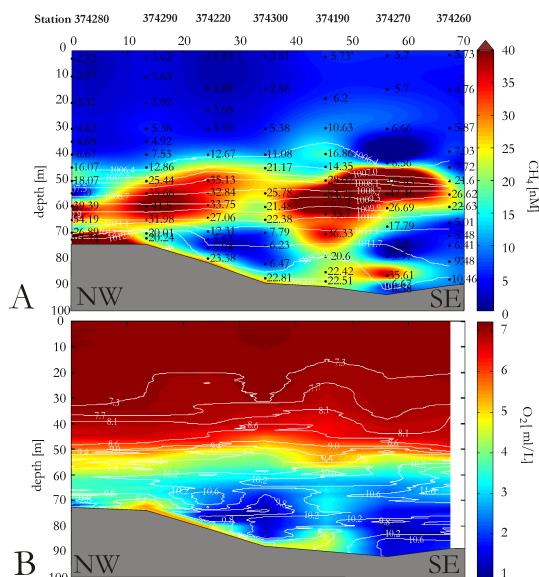


**Figure 4.8** – Methane concentrations along a transect BB2 in the Bornholm Basin, taken in December 2009 (for orientation see Fig. 4.2). A: methane (color coded, nM) and density (white solid lines, kg $m^{-3}$); B: oxygen concentrations (color coded, ml $L^{-1}$) and temperature (white solid lines, ° C).

Model simulations of vertical and horizontal mixing along the Bornholm Transect (Fig. 4.2, black solid line) reveal remarkable dynamics within the water body as well as a two-layered structure during the winter period, and a three-layered water column during summer. Data show that the strong halocline inhibits mixing of the water column to the sea floor, leaving the deeper layers unaffected from wind-driven dynamics throughout the year. During the summer stratification, model simulations reveal temporally high dynamics at the two interfaces of the colder intermediate water layer along the transect (Fig. 4.9 A).

Tongues of warmer water reach far into the intermediate water layer and connect
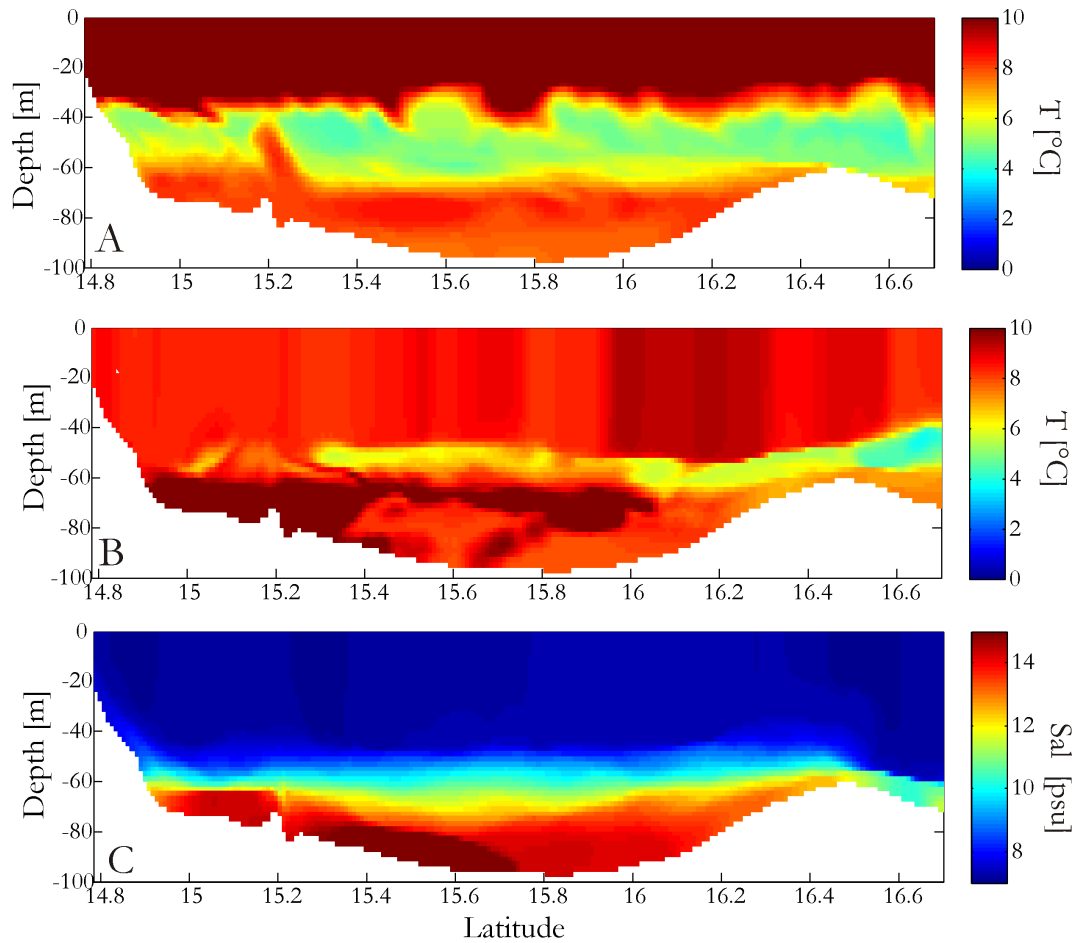
**Figure 4.9** – GETM model-derived simulation examples of different scenarios along the Bornholm Transect (for orientation see Fig. 4.2, black solid line) like A: temperature signature showing turbulences at the interface of the intermediate water layer in August 2009; B: temperature signature of a baroclinic inflow event observed in October 2009; C: Salinity signature of a barotropic inflow event in December 2009.

at times with the upper or bottom layer respectively. Further, internal waves, parameterized as described in *van der Lee and Umlauf* (2011), lead slowly to the warming of the intermediate water during summer. Especially high dynamics at the interfaces of the intermediate water layer, could be observed in October 2009 followed by the entrainment of large amounts of warm water below the halocline (Fig. 4.9 C), indicating the baroclinic inflow from the Arkona Basin. Model data reveal no intrusion of saline water into the Bornholm Basin, but the expansion of the water layer below the halocline at 65 m depth. A warm barotropic inflow event in December 2009 on the contrary transported high saline water into the bottom layer of the Bornholm Basin,

leading to intensive mixing with the ambient water body below the halocline. Further, model simulations show an inflow discharge time from the Arkona Basin into the Bornholm Basin of less than fourteen days and almost no change in the temperature or salinity signature.

We hypothize, that both inflow events significantly influenced the methane distribution within the water column of the Bornholm Basin, and that large amounts of methane were transported during this events from the Arkona Basin into the Bornholm Basin. Depending on its density signature, baroclinic inflow events (as observed in October 2009) enable the transport of methane into the Bornholm Basin, forming the characteristic IML as observed along BB1 and BB2. The entering of the barotropic inflow into the Bornholm Basin on the contrary, leads to a methane transport into the bottom layer of the Bornholm Basin. Transect BB2 shows the inflowing bottom water plume at station 374280 close to the Bornholm channel (Fig. 4.8, Fig. 4.2 and 4.1 for orientation). Elevated density, oxygen and methane values, measured at several stations along the transect, indicate that the inflowing water masses will underlay the ambient bottom water. First indications of the plume along transect BB1 can be observed in the bottom layer at station 374200 and 374190, showing increasing density values and increasing oxygen concentrations compared to the surrounding water body (Fig. 4.7 A).

The decrease of methane within the IML between December 2009 and July 2010 can be explained by strong vertical mixing during the winter period and enhanced exhaustion of methane towards the atmosphere (*Gülzow et al.*, acc. for BGS:D). For the assumption, that methane concentrations within the oxic water column are constantly depleted via oxidation, results of isotopic sample analyzes need to be awaited. As already described above, leads the stratification of the water column to the continuous replenishment of methane from the sediment within the bottom layer. The formation of anoxia within the bottom layer and the surface sediment leads additionally to enhanced methanogenesis and emission of methane towards the water column (shown above).

### 4.5.2.3   Methane versus Oxygen

The time series at station TF0113 and TF0200 as well as the transects taken in the Arkona and Bornholm Basin between January 2009 and November 2011 show the periodic formation of hypoxia during the summer stratification. Anoxic conditions were observed during summer 2010 and 2011 in the Bornholm Basin. Enhanced methane concentrations seem to coincide with hypoxic conditions within the Arkona and Bornholm Basin, but no correlation could be observed. In fact several periods of hypoxia could be observed in the deep layer of the Bornholm Basin, showing remarkable low methane concentrations (Fig. 4.4 and 4.7). On the contrary, a correlation between elevated methane values and anoxic conditions within the Bornholm Basin could be observed (Fig. 4.10), but only few data are available so far and interpretations need to be taken with caution. The correlation is described by $f(x) = -312.23\,x - 68.69$ (with x = $negO_2$), showing a correlation factor of $R^2 = 0.82$.
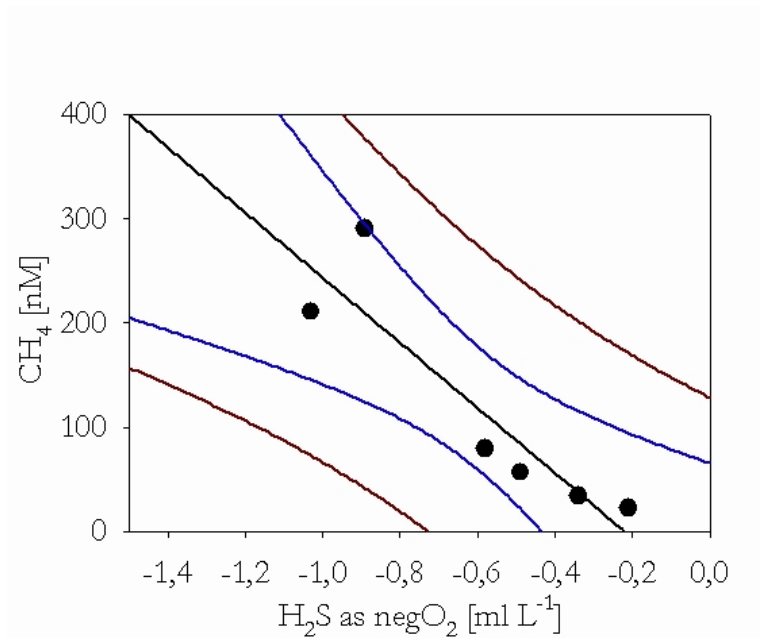


**Figure 4.10** – Correlation of $H_2S$ displayed as negative $O_2$ with methane concentrations, measured during anoxia at the summer stratification in the bottom layer of the Bornholm Basin at station TF0200 and TF0213 (Fig. 4.2), showing a correlation factor of $R^2 = 0.82$. The 95 % prediction band (red solid lines) and the 95 % confidence band (blue solid line) are displayed.

Methanogens are strictly anaerobic bacteria. Subsequently, anoxic conditions

within the bottom water layer and surface sediment support the consumption of sulfate as electron acceptor within the upper sediment via sulfate-reducing bacteria. It can be assumed, that with declining sulfate concentration, the sulfate-methane-transition-zone (*Jørgensen and Kasten*, 2006) moves upwards within the sediment and methanogenic bacteria allow methanogenesis within the surface sediment, resulting in enhanced emissions of methane towards the water column.

## 4.6  Conclusion

Between January 2009 and November 2011, time series of vertical profiles and several transects were taken within the Arkona and the Bornholm Basin, revealing recurring seasonal methane distribution patterns in both basins.

The halocline was found to be the main boundary for methane transport from the sediment towards the surface water. Especially the formation of the three-layered water column in the Arkona and Bornholm Basin during summer leads to the depletion of oxygen and subsequently to high methane concentrations in the bottom layer, caused by continuous enrichment by the sediment and inhibited methane transport towards the upper water column. The surface water on the contrary, is characterized by continuous exhaustion to the atmosphere, leading to particular low surface water methane concentrations during summer.

The formation of a flare like methane structure within the water column at transect AB3 needs to be observed in more detail in the future. The structure indicates bubble-mediated methane transport from the sediment to the water column. A potential site for bubble-mediated methane release was shown at the pockmark structure ZT (*Gülzow et al.*, acc. for BGS:D).

Model simulations showed that dynamics like deepening of the mixing depth, inflow events, internal waves and turbulence at the interfaces of the intermediate layers during summer stratification influence the seasonal methane distribution significantly. Vertical mixing within the water column influences the transport of oxygen into the bottom layer and the oxidation of methane as well as the transport of methane towards

the surface layer and enhanced exhaustion towards the atmosphere. Especially inflow events are assumed to result in the lateral transport of methane from the Arkona into the Bornholm Basin, leading to the entrainment of methane within the halocline and the formation of a intermediate methane layer of significantly elevated methane concentrations.

Anoxic conditions were observed in the Bornholm Basin bottom layer during summer 2010 and 2011. No correlation between hypoxia and elevated methane concentrations in the water column was found. A correlation between negative oxygen values and methane concentrations was observed in the Bornholm Basin. The decrease of methane concentrations in the bottom layer of the Bornholm Basin down to background concentrations during the winter period remains suspicious, considering the lack of mixing during the observation period and the missing ventilation of the bottom layer and almost persistent hypoxia. Therefore, the ventilation of the deeper water layer and bottom layer of the Bornholm Basin, as well as methane oxidation rates need to be investigated in more detail in the future. Considering that areas of hypoxic conditions will expand in the Baltic Sea (*Conley et al.*, 2011; *Meier et al.*, 2011), continuing measurements of the methane distribution will show how long term changes of oxygen will influence the methane distribution in the future.

# General Conclusions and future perspectives

The presented work investigated the methane distribution in the surface water and the water column of the Baltic Sea, based on established and new developed measuring techniques.

The new measuring system allows continuous and autonomous determination of methane and carbon dioxide in the surface water of aquatic environments and was applied at the Baltic Sea for the first time. The unrivalled spatial and temporal resolution of the system implies significant improvement especially for the determination of methane. The system allows the usage of ships of opportunity and thus amplifies the spatio-temporal range of data acquisition compared to research vessels. It is possible to observe small changes in surface water methane concentrations, achieving a new insight in processes and parameters influencing methane values in marine systems. Further, the system allows the estimation of the spatio-temporal significance of controlling processes and parameters. Thus, upwelling in the area around Gotland influences the local surface methane concentrations on a rather short (days) temporal scale. Similar classified processes of local significance and short temporal impact are wind events or seepage from the sediment. On the contrary, seasonal changes of the sea surface temperature, stratification as well as changes of the mixing depth occur on a longer time scale (weeks, month) and influence the surface water methane concentration of significant larger areas of the Baltic Sea. Additional, it was observed that the impact of processes and parameters varies significantly, depending on the water depth (shallow or deep) of a region.

The automated system reveals hot spots of extraordinary elevated or changing methane concentrations in the surface water of the Baltic Sea. For the better understanding of related dynamics in such key areas, additional surveys of the vertical methane distribution were made. Thus, elevated methane concentrations in the surface water of the Arkona Basin could be related to pressure induced gas release after

wind driven sea-level changes. A potential site for bubble mediated methane release was presented at a pockmark structure in the Arkona Basin, accompanied by a flare like methane structure within the water column, near to this site.

New insights for the comprehensive discussion of methane concentrations in the surface water and the water column of the Baltic Sea were given by the consultation of several additional parameters (e.g. oxygen) and geological (sediment properties) and mathematical (model-derived results) approaches. Thus, the results of several time series within the Arkona and the Bornholm Basin, reveal recurring hypoxic (Arkona Basin) and anoxic (Bornholm Basin) conditions during the summer stratification and imply a correlation between negative oxygen values and methane concentrations. Model simulations on the other hand, allow the parametrization of dynamics within the water column of the Baltic Sea, which influence the methane distribution, like frequent inflow events. Inflow events might lead to the lateral transport of methane from the Arkona Basin into the Bornholm Basin and to entrainment of methane within the halocline, forming the characteristic intermediate methane layer of significantly elevated methane concentrations.

The observation of methane and carbon dioxide in the surface water of the Baltic Sea will be continued (and extended) within the framework of the Integrated Carbon Observation System of Germany (ICOS-D). The integration of the setup within ICOS-D implies the development of measuring standards like additional monitoring of atmospheric methane concentrations or the acquisition of other trace gas concentrations like carbon monoxide or nitrous oxide. The monitoring of methane (besides the other trace gases) allows the investigation of long time methane changes (climate change) or frequently recurring processes (seepage, inflow events), which require long time series data (several years, decades).

Furthermore, the current set up provides data with unrivaled frequency and precision but leaves potential for technical improvement (e.g. the time constant for methane with currently 676 s). First, the Picarro G2301 sensor forms a alternative competing technology to the Los Gatos sensor used in this thesis, with reported

similar accuracy, precision, and stability but a considerably smaller inner volume. Currently, several studies subject the performance of both systems in combination with surface water measurements. Additional, the improvement of the equilibrator and the application of equilibrator systems using a permeable membrane is currently scrutinized. The application of significantly faster, continuous measuring systems accompanied by similar data precision for methane (and other trace gases) on mobile setups vantages its usage on research vessels. Mobile systems allow detailed, simplified investigations of hot spots additional to the monitoring program, compared to discrete sampling techniques. Exemplary, the influence of drifting ice coverage on methane fluxes towards the atmosphere in the Gulf of Finland, remains unclear. Current observations show elevated methane fluxes during the winter period in this region. Here, specific profiling measurements of the methane distribution in connection with observations on current flow during ice coverage as well as during drifting ice conditions are required.

# APPENDIX A

# Distribution of methane in the water column of the Baltic Sea

## A.1   Abstract

The distribution of dissolved methane in the water column of the Baltic Sea was extensively investigated. A strong correlation between the vertical density stratification, the distribution of oxygen, hydrogen sulfide, and methane has been identified. A widespread release of methane from the seafloor is indicated by increasing methane concentrations with water depth. The deep basins in the central Baltic Sea show the strongest methane enrichments in stagnant anoxic water bodies (max 1086 nM and 504 nM, respectively), with a pronounced decrease towards the pelagic redoxcline and slightly elevated surface water concentrations (saturation values of 206 % and 120 %, respectively). In general the more limnic basins in the northern part of the Baltic are characterized by lower water column methane concentrations and surface water saturation values close to the atmospheric equilibrium (between 106 % and 116 %).

In contrast, the shallow Western Baltic Sea is characterized by high saturation values up to 746 %.

## A.2   Introduction

Methane ($CH_4$) is an important atmospheric trace gas influencing directly or indirectly the global climate. Compared to carbon dioxide ($CO_2$) the global warming potential (GWP) of methane is about 25 to 40 (*Shindell et al.*, 2009) times higher on a 100 yr timescale. The atmospheric mole fraction has more than doubled since the beginning of the industrial era, but has been almost stagnant over the first 5 years of the new millennium. The reason for the observed renewed global increase of atmospheric methane since 2006 is still under debate.

Though aquatic systems constitute the largest natural source of atmospheric methane, the role of the marine environment is considered to be small (*Bange et al.*, 1994). Shelf regions comprise only 7.5 % of the ocean's surface area, but seem to be of great importance for oceanic methane emission due to high methane production rates in the sediment and a fast ventilation of the relatively shallow water column.

The Baltic Sea is a European semi-enclosed marginal sea with an average water depth of 52 m and is connected to the North Sea and the Atlantic Ocean via the Skagerrak and Kattegat (insertion in Fig. A.1). Including Belt Sea and Kattegat, the Baltic Sea covers an area of about $4.2 * 10^5$ $km^2$ with a volume of about $22 * 10^3$ $km^3$. On the basis of the hydrographic and bathymetric conditions, the Baltic Sea can be divided into a series of basins separated by submarine sills (see insertion in Fig. A.1 a). The Baltic Sea represents one of the largest brackish waters of the Earth with strong lateral variations in the salt content from near marine in the western to near limnic conditions in the northern part, i.e., the Bothnian Sea and Bothnian Bay. Water exchange with the open ocean is controlled by episodic inflow events of saline water from the North Sea. In the southern and central Baltic Sea these events, together with a positive freshwater balance, drive an estuarine circulation and result in a less saline surface layer and more saline deep and bottom water masses separated by a

permanent halocline (*Reissmann et al.*, 2009; Fig A.1 a). Especially in the central deep basins, this diapycnal feature leads to strong water column stratification, limited vertical mixing, the development of a prominent redoxcline (oxic to sub- or anoxic conditions), and the formation of biogeochemical zonations (*Nausch et al.*, 2008). The resulting periods of deep water stagnation in these basins can only be interrupted by strong inflow events of saline oxygenated water from the North Sea. Due to the strong geochemical (e.g. oxygen distribution in different basins) and hydrographical (salt) gradients, the large geographical extension of the Baltic Sea over different climatic zones, and the episodic renewal of bottom waters in some of the silled basins, the Baltic Sea represents an ideal environment to study the effects of various settings on the aquatic methane cycle. Moreover, a stronger than global effect of global warming and a strong anthropogenic influence on nutrient supply and organic matter production (i.e. eutrophication) are likely to affect the production and migration pathways of methane in the Baltic (http://www.balticgas.net/).

Only a few studies are dealing with the distribution of methane in the water column of the Baltic Sea (*Bange*, 2006, and references therein). These investigations have been conducted on a regional scale (most of them offshore Denmark and Germany) and show that the release of methane from the sediment into the water column is a widespread phenomenon. Especially in the center of the basins, geochemical pore water investigations and seismoacoustic studies of the seabed reveal large areas with high dissolved methane concentrations (*Thießen et al.*, 2006) and free gas occurring (*Laier and Jensen*, 2007) within an organicrich postglacial sediment layer known as the 'Holocene mud' of the Littorina facies. Biological investigations in the Baltic Sea could show that the microbial oxidation of methane within the sediment and water column represents an effective process which restricts the direct transfer of methane into the surface waters and the atmosphere (*Piker et al.*, 1998; *Abril and Iversen*, 2002). Nevertheless, *Bange et al.* (1994, 1998) could demonstrate that the surface waters of the Baltic Sea are considerably methane oversaturated with respect to the atmospheric equilibrium, and that the concentrations show strong seasonal and regional variations. In the present study we show a comprehensive methane con-
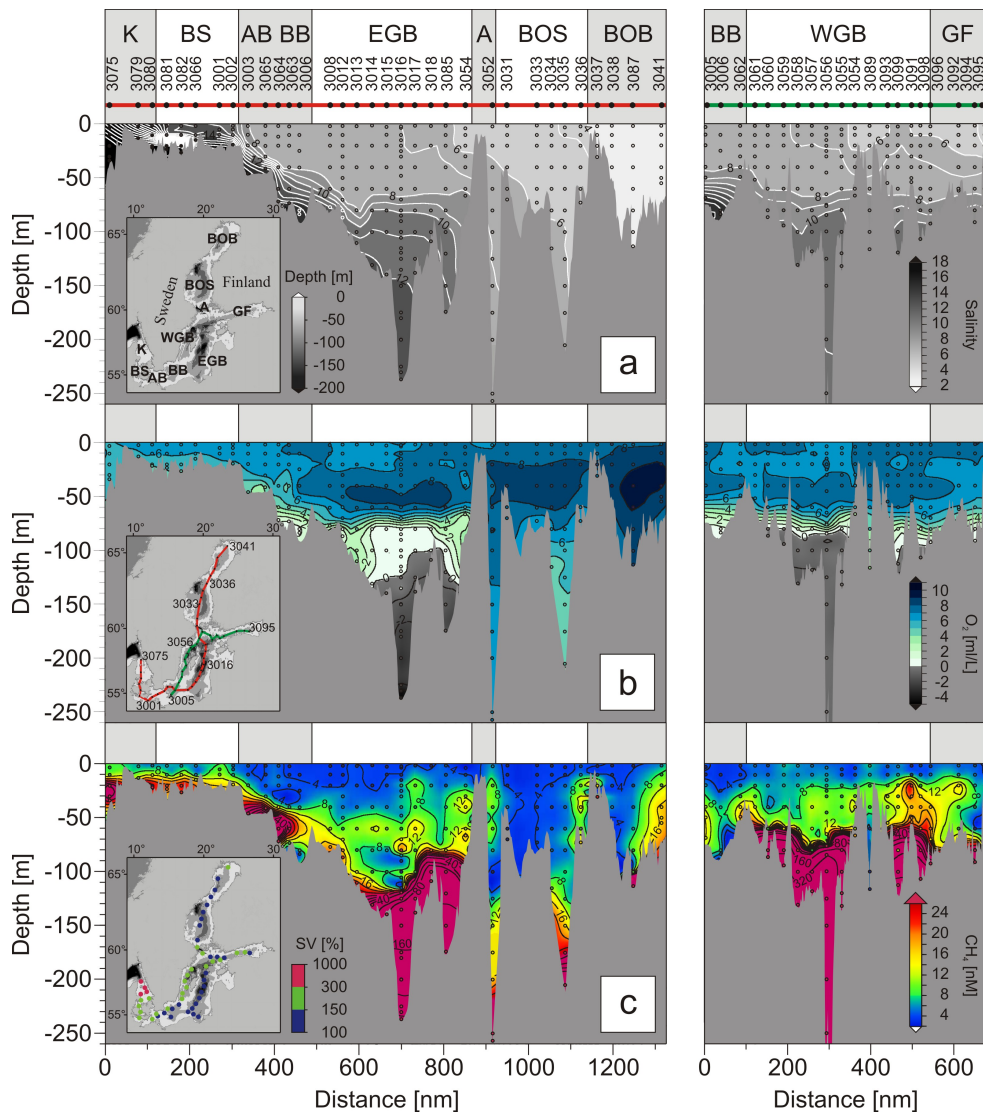
**Figure A.1** – Contour plot of (a) salinity, (b) oxygen and (c) methane concentration along two transects across the Baltic Sea. Hydrogen sulfide was converted into negative oxygen equivalents. The insertion in figure A.1 a shows the bathymetry of the Baltic Sea and the location of the main basins (K, Kattegat; BS, Belt Sea; AB, Arkona Basin; BB, Bornholm Basin; WGB, Western Gotland Basin; EGB, Eastern Gotland Basin; A, Åland Sea; BOS, Bothnian Sea; BOB, Bothnian Bay; GF, Gulf of Finland). The extension of the individual basins is also indicated at the top of the salinity section (figure A.1 a). The course of the two transects (marked with red and green lines) is displayed in the insertion in figure A.1 b together with selected station names to provide better orientation. The data obtained from the red (station 3075 to 3041) and green transect (station 3005 to 3095) are displayed on the left and right side in figure A.1, with the stations labeled at the top of figure A.1 a. The insertion in figure A.1 c shows the saturation values of surface water samples (depth interval 0 - 5 meter below sea surface).

centration dataset covering the entire Baltic Sea from the sea surface to the deepest basins.

## A.3   Sampling and Methods

Our data were gathered in summer 2008 on the German research vessel Maria S. Merian (MSM 08/3) between June $18^{th}$ and July $18^{th}$. The dataset includes 63 water stations carried out with a rosette water sampler equipped with 24 10-liter Hydrobios-Freeflow bottles. For continuous CTD profiling a Seabird sbe911+ system was attached to the underwater unit. The oxygen distribution was measured according to Winkler's method, hydrogen sulfide in the deep waters was analysed colorimetrically with the methylene blue method (*Grasshoff et al.*, 1999). Dissolved methane was extracted from the water sample by the use of a vacuum degassing method and its mole fraction was determined with a gas chromatograph equipped with a flame ionization detector (*Keir et al.*, 2009). Surface water saturation is given following the equation

$$SV[\%] = \frac{C_w}{C_{equi}} * 100 \qquad (A.1)$$

where $SV$ is the saturation value, $C_w$ is the measured concentration in seawater and $C_{equi}$ the concentration in equilibrium with the atmosphere calculated using an atmospheric mole fraction of 1.89 (annual mean 2008, available from NOAA global sampling networks, sampling station: Baltic Sea, BAL, Poland, http://www.esrl.noaa.gov/) and the solubility coefficient given by *Wiesenburg and Guinasso* (1979).

The sampling strategy for the MSM 08/3 cruise was to gather a comprehensive dataset of the entire Baltic Sea (insertion in Fig A.1 b). Sampling stations were preferentially chosen offshore in a quasi-equidistant manner to horizontally and vertically trace various geochemical parameters from all basins of the Baltic Sea.

## A.4   Results and Discussion

The vertical water column stratification was very stable during the cruise with a pronounced halocline (Fig A.1 a) and a thermocline within the upper 30 m. The prevailing wind during the sampling campaign was on average low (mean 7.2 m s$^{-1}$ $\pm$ 3.6 m s$^{-1}$) leading to a mean Ekman depth of 25 m. Overall, the distribution of oxygen, hydrogen sulfide and methane is strongly controlled by the vertical density stratification (dominated by the salt distribution; Fig A.1 a). Below the prominent halocline oxygen is decreasing with depth, whereas hydrogen sulfide and methane show enhanced concentrations in the more saline deep and bottom water (Fig A.1 a and c). The conspicuous increase of methane with increasing water depth points to a widespread release of methane from the sediment into the water column (*Thießen et al.*, 2006; *Laier and Jensen*, 2007). In this context the main basins in the southern and central Baltic Sea seem to be of great importance. These stratified basins are characterized by high transport rates of organic matter (originated from primary production and onshore erosion) into the deep water where it is partly mineralized and thus lowers the oxygen concentration in the water (*Reissmann et al.*, 2009). The sub- or anoxic conditions in the deep water support an efficient burial of organic matter and thus favor microbial methane production in the sediment. Apart from that, local input of methane by rivers and submarine groundwater discharge represent additional sources (*Bange et al.*, 1994). Subsurface production of methane in microenvironments, like fecal pellets and zooplankton guts or under phosphate limiting conditions (*Karl et al.*, 2008), is also postulated to take place in the Baltic Sea (*Bange et al.*, 1994) and may lead to an unknown source term of atmospheric methane.

In the following, the results from the main basins of the Baltic Sea (insertion in Fig A.1 a) are presented and the spatial distribution of methane is discussed for the individual regions.

### A.4.1  Kattegat

Shallow gas and gas bubble releasing seep sites were reported to occur in this region (*Dando et al.*, 1994; *Laier and Jensen*, 2007). Rapid vertical gas-bubble transport through the water column can transport a large fraction of methane from the seafloor into the atmosphere (*Schmale et al.*, 2010a). Though the Kattegat is stratified to a large extent due to the general circulation pattern, boundary and turbulent mixing can still transfer dissolved methane upwards as well. Our methane data in Figure 1c show that a plume of dissolved methane spreads unaffected from the pronounced water column stratification (Fig A.1 a) from the seafloor up to the sea surface. This results in the highest surface saturation of all regions investigated during this survey, with values between 197 % (station 3080) and 746 % (station 3075, insertion in Fig A.1 c). This is consistent with high saturation of methane in the Skagerrak and the eastern part of the North Sea at about 58° N, which have been suggested to originate from the westward transport of surface waters enriched in methane in the Kattegat and Skagerrak (*Rehder et al.*, 1998).

### A.4.2  Belt Sea

Seismo-acoustic and geochemical investigations in Århus Bay (*Jensen and Bennike*, 2009), Eckernförde- (*Wever et al.*, 2006) and Mecklenburg Bay (*Laier and Jensen*, 2007) demonstrate that free shallow gas is a frequent phenomenon. The release of methane gas bubbles and the groundwater discharge of methane-enriched fluids into the water column are known from some of these regions. Both, the depth of the free gas zone and the release of sedimentary methane into the water column were reported to depend on hydrostatic pressure (*Wever et al.*, 2006) and bottom water temperature (*Thießen et al.*, 2006) changes. Moreover, the input of fresh organic matter in surface sediments affects the microbial methane production rates (*Bange et al.*, 1998). An additional seasonal factor influencing the methane concentrations in these regions is given by varying input rates of methane-enriched river water (*Bange et al.*, 1998). Because of the shallow average water depth in this region the sedimentary

methane source strength reacts highly sensitive to seasonal or long-term air temperature changes. In addition, the transport and current regime in this bottleneck between North Sea and Baltic is highly sensitive to the meteorological conditions, leading to large variations of the water mass characteristics at individual sites. The sensitivity of this region to seasonal and meteorological fluctuations is reflected by the highest variability of surface water methane concentrations reported by *Bange et al.* (1994) for the southern Belt Sea (area weighted mean saturation values between 113 % (winter) and 395 % (summer) and maximum values in the southern Belt Sea of 15040 % during the summertime). The strong source strength of the nearshore shallow regions is characterized by high methane concentrations up to 6.71 nM (station 3081) and high saturation values at all surface water samples (saturation values between 171 % (station 3002) and 246 % (station 3081; Fig A.1 c).

### A.4.3   Arkona Sea and Bornholm Sea

Large fractions of the areas of the Arkona- and Bornholm Basin show free shallow gas within an organicrich Holocene mud (*Thießen et al.*, 2006). In the central parts of the Arkona and Bornholm Basins, a distinct plume of elevated methane arises laterally from the seabed at stations 3003, 3065, 3064, and 3063. Here, a permanent halocline at 35 40 m water depth separates the surface water from the deep water (*Reissmann et al.*, 2009). Obviously, the pronounced halocline hampers diapycnal eddy-diffusive methane transport into the well ventilated upper mixed layer (Fig A.1 a and c). Given the sharp gradient and low concentration in the upper layer, gas bubble transport as reported for the Skagerrak and Kattegat is unlikely to play an important role here in regard to vertical methane transport. The Arkona Basin and Bornholm Basin, silled to both sides, but with more frequent bottom water renewal, stronger mixing processes, and less pronounced oxygen deficiency than the Gotland Basins, provide excellent study areas for some aspects of the marine methane cycle. Over the term of stagnation periods, the water gets less oxygenated due to organic matter degradation, fresher due to vertical mixing, and presumably successively more enriched in methane.

### A.4.4   Gotland Sea and Gulf of Finland

Examinations of the methane cycle are rare for the Eastern Gotland Basin (*Bange et al.*, 1994; *Piker et al.*, 1998), and - to our knowledge - completely lacking for the Western Gotland Basin. For the Eastern Gotland Basin *Piker et al.* (1998) could demonstrate that dissolved methane diffuses from the deep sedimentary strata into the water column. Hydrographical studies show that the surface water is separated from the deep stagnant water by a permanent halocline in about 70 - 90 m depth (Fig. A.1 a; (*Reissmann et al.*, 2009)).

The deep water body of both basins is characterized by the presence of hydrogen sulfide (Fig A.1 b) and the highest concentrations of methane found in our water column studies (1086 nM) in the western basin (station 3056) and 504 nM in the eastern basin (station 3016; Fig A.1 c). These methane values are some hundred times elevated compared with the sea surface concentrations in the Gotland Sea (average Western Gotland Basin 5 nM and Eastern Gotland Basin 3 nM), which are near atmospheric equilibrium (average saturation values Western Gotland Basin 206 % and Eastern Gotland Basin 120 %, insertion in Fig A.1 c). Decreasing methane concentrations within the suboxic part (conc. $O_2 < 2$ ml l$^{-1}$) of the redoxcline (depth range between 80 and 120 m, e.g. station 3016) indicate microbial oxidation and thus transport limitation from the deep methane pool as already reported for similar oceanic settings like the Black Sea (*Schmale et al.*, 2010a). An interesting finding of our water column study in the Gotland Sea is a distinct methane elevation in about 40 - 100 m water depth in the eastern basin (methane concentrations between 8 and 12 nM; Fig A.1 c). The most likely reason for the observed feature is a baroclinic inflow entering the basin from the southwest and carrying a low methane signature (see *Reissmann et al.*, 2009 for a hydrographic overview). These inflows take place during the summer time and carrying a warm and saline hydrographic signature (indicated in our vertical CTD profiles in the central part of the basin by temperature anomalies in a depth range between 100 and 120 m water depth, data not shown). This specific process leads to an entrainment and ventilation of the affected water

body (*Reissmann et al.*, 2009). In the Western Gotland Basin a comparable feature could not be detected in our hydrochemical and hydrographical dataset (Fig A.1). This part of the Baltic Sea is characterized by a very stable chemical and physical stratification of the water column. However, elevated methane concentrations >8 nM are observed in the water column up to depth levels of 20 - 30 m in most of the Western Gotland Basin and the Gulf of Finland. This shallow methane elevation is also reflected in the surface methane concentrations in these regions (see saturation values in Fig A.1 c). The Gulf of Finland and the Western Gotland Basin appear elongated and narrow compared to the Eastern Gotland Basin. The larger importance of boundary wall shear might be the reason for a less confined salt gradient (except for the very deep part of the Western Gotland Basin), enabling better upward transport of deep methane-enriched waters. The proximity to the basin flanks allows a fast isopycnical transport of sedimentary methane into the basin interior, which is also likely to contribute to the elevated methane concentrations to these shallower depths levels. Especially high methane values in the Gulf of Finland and easternmost part of the Western Gotland Deep are again related to the stagnant (salt stratified; Fig A.1 a) deep water in the depressions (station 3094, 3096, 3098, 3099).

### A.4.5   Åland Sea, Bothnian Sea, and Bothnian Bay

The Åland Sea and the large northern basins (Bothnian Sea and Bothnian Bay) are separated from the Baltic Proper and against each other by shallow sills. Together with a pronounced positive freshwater balance, this results in fresher, not permanently stratified, and well ventilated water within these basins. Only very few methane-related studies exist (*Hutri and Kotilainen*, 2007) for the northern basins. These studies could identify seafloor structures like pockmarks and mud volcanoes that are often related to gas or groundwater seepage. However, the present activity of these structures and the corresponding methane flux remain unknown. Generally, our methane concentration dataset in the northeastern areas shows increasing concentrations towards the seafloor (e.g. station 3041, 3087, 3036 and 3035), again documenting an active emission of methane from the sediments into the water column

(Fig A.1 c).

In the Åland Sea an elevated shallow water methane signal was observed at station 3052, similar to the situation in the Gulf of Finland and Western Gotland Basin. Further north, the methane concentration significantly drops in the area of the Bothnian Sea. Except for locations very deep and close to the seafloor or land (stations 3035, 3036) the methane concentrations over large areas appear homogeneously low with surface water concentrations close to the atmospheric equilibrium (stations 3031, 3033, 3034, corresponding to saturation values between 106 % (station 3033) and 116 % (station 3034). The noticeable methane pattern in the water column reflects the sediment characteristics with spatially limited mud accumulations apparently representing the main methane source in the other basins. The stations sampled in the Bothnian Sea and Bothnian bay during the cruise were located away from these mud areas in regions characterized by hard sediments (*Al-Hamdani and Reker*, 2007). The low methane concentrations in the Bothnian Sea extend into the Bothnian Bay until the very end of the profile. Here, a pronounced methane signal throughout the water column was observed (station 3041).

## A.5   Conclusions and Outlook

The present methane dataset indicates that the sediments release methane into the water column over large areas of the Baltic Sea. Methane concentrations are highest in the central deep basins of the Gotland Sea and lowest in the Bothnian Sea and Bay, despite the higher freshwater fraction in the north. Highest concentrations are restricted to suboxic to anoxic regions. The surface water represents an atmospheric source of methane with strong oversaturations in the northwestern and southwestern regions and decreasing values towards the central and northeastern basins. In the central basins the path of methane from the deep water towards the sea surface seems to be controlled by oxidation at the redoxcline and restricted vertical transport and mixing due to density stratification.

Our dataset presents a comprehensive overview and orientation. Nevertheless, to

understand the sources and sinks of methane in the Baltic Sea, more detailed studies are needed. So far, no information of microbial mechanisms mediating the oxidation of methane at the redoxcline in the water column of the central Baltic is published. Seasonal studies could be used to evaluate the climatic influence on the methane source strength (i.e., impact on methane production rates in the sediment and water column, gas transport mechanisms between sediment and water column like gas bubble seepage, hydrographic changes like deep water ventilation). Future studies should also address the impact of eutrophication on methane production rates in the sediment and its influence on the water methane cycle (http://www.balticgas.net/). The strong salinity and redox gradients, the natural perturbatio-relaxation experiments resulting from the alteration of deep water renewal and stagnant periods on different time-scales, and the straightforward understanding of the expected response to global change in the area make the Baltic Sea a unique environment for process studies addressing the methane cycle, which could be transferred to other high productivity and silled estuary settings woldwide.

# REFERENCES

Abril, G., and N. Iversen (2002), Methane dynamics in a shallow non-tidal estuary (Randers Fjord, Denmark), *Marine Ecology Progress Series*, *230*, 171–181.

Al-Hamdani, Z., and J. Reker (2007), Towards marine landscapes in the Baltic sea, BALANCE interim rep., *BALANCE, Copenhagen (Available at http://balance-eu.org/)*, *10*.

Albert, D. B., C. S. Martens, and M. J. Alperin (1998), Biogeochemical processes controlling methane in gassy coastal sediments - Part 2: groundwater flow control of acoustic turbidity in Eckernförde Bay sediments, *Continental Shelf Research*, *18*, 1771–1793.

Alenius, P., K. Myrberg, and A. Nekrasov (1998), The physical oceanography of the Gulf of Finland: a review, *Boreal Environment Research*, *3*, 97–125.

Allan, W., D. C. Lowe, A. J. Gomez, H. Struthers, and G. W. Brailsford (2005), Interannual variation of $^1$3C in tropospheric methane: Implications for a possible atomic chlorine sink in the marine boundary layer, *Journal of Geophysical Research*, *110*(D11), pp. 8.

Amouroux, D., G. Roberts, S. Rapsomanikis, and M. O. Andreae (2002), Biogenic Gas ($CH_4$, $N_2O$, DMS) Emission to the Atmosphere from Near-shore and Shelf Waters of the North-western Black Sea, *Estuarine, Coastal and Shelf Science*, *54*(3), 575–587.

Anderson, A. L., F. Abegg, J. A. Hawkins, M. E. Duncan, and A. P. Lyons (1998), Bubble populations and acoustic interaction with the gassy floor of Eckernförde Bay, *Continental Shelf Research*, *18*(14-15), 1807–1838.

Atkins, P. W., and J. de Paula (2006), *Physikalische Chemie*, 4th ed., Wiley - VCH Verlag GmbH.

Baer, D. S., J. B. Paul, M. Gupta, and A. OKeefe (2002), Sensitive absorption measurements in the near-infrared region using off-axis integrated-cavity-output spectroscopy, *Applied Physics B: Lasers and Optics*, *75*(2-3), 261–265.

Bange, H. W. (2006), Nitrous oxide and methane in european coastal waters, *Estuarine, Coastal and Shelf Science*, *70*(3), 361–374.

References

Bange, H. W., U. H. Bartell, S. Rapsomanikis, and M. O. Andreae (1994), Methane in the Baltic and North Seas and a reassessment of the marine emissions of methane, *Global Biogeochemical Cycles*, *8*(4), 465–480.

Bange, H. W., S. Dahlke, R. Ramesh, L. A. Meyer-Reil, S. Rapsomanikis, and M. O. Andreae (1998), Seasonal Study of Methane and Nitrous Oxide in the Coastal Waters of the Southern Baltic Sea, *Estuarine, Coastal and Shelf Science*, *47*(6), 807–817.

Bange, H. W., K. Bergmann, H. P. Hansen, A. Kock, R. Koppe, F. Malien, and C. Ostrau (2010), Dissolved methane during hypoxic events at the boknis eck time series station (eckernförde bay, sw baltic sea), *Biogeosciences*, *7*(4), 1279–1284.

Beck, L., S. D. Piccot, and D. A. Kirchgessner (1993), Industrial sources, in *Atmospheric Methane: Sources, Sinks and Role in Global Change*, edited by M. A. K. Khalil, pp. 341–399, Springer-Verlag, New York, NY.

Bekki, S., and K. S. Law (1997), Sensitivity of the atmospheric ch4 growth rate to global temperature changes observed from 1980 to 1992, *Tellus B*, *49*(4), 409–416.

Beljaars, A. (1995), The parameterization of surface fluxes in large-scale models under free convection, *Quarterly Journal of the Royal Meteorological Society*, *121*(522), 255–270.

Bergamaschi, P., M. Krol, F. Dentener, A. Vermeulen, F. Meinhardt, R. Graul, M. Ramonet, W. Peters, and E. J. Dlugokencky (2005), Inverse modelling of national and european $CH_4$ emissions using the atmospheric zoom model TM5, *Atmospheric Chemistry and Physics*, *5*(9), 2431–2460.

Berger, U., and J. Heyer (1990), Distribution and Activity of Methanotrophic Bacterias in a Brackish Water Ecosystem, *Limnologica*, *20*(1), 141–144.

Björck, S. (1995), A Review of the history of the Baltic Sea, 13.00-8.0ka BP, *Quaternary International*, *27*, 19–40.

Blake, D. R., and F. S. Rowland (1988), Continuing worldwide increase in tropospheric methane, 1978 to 1987, *Science*, *239*(4844), 1129–1131.

Blunier, T., J. Chappellaz, J. Schwander, B. Stauffer, and D. Raynaud (1995), Variations in atmospheric methane concentration during the holocene epoch, *Nature*, *374*(6517), 46–49, 10.1038/374046a0.

Boetius, A. (2000), Microbial activity and particulate matter in the benthic nepheloid layer (BNL) of the deep Arabian Sea, *Deep-Sea Research II*, *47*(14), 2687–2706.

Boon, P. I., A. Mitchell, and K. Lee (1997), Effects of wetting and drying on methane emissions from ephemeral floodplain wetlands in south-eastern australia, *Hydrobiologia*, *357*(1), 73–87.

References

Boone, D. (2000), Biological formation and consumption of methane, in *Atmospheric Methane: Its Role in the Global Environment*, edited by M. A. K. Khalil, pp. 42–62, Springer-Verlag, New York, NY.

Borjesson, G., and B. H. Svensson (1997), Effects of a gas extraction interruption on emissions of methane and carbon dioxide from a landfill, and on methane oxidation in the cover soil, *Journal of Environmental Quality*, *26*(4), 1182–1190.

Born, M., H. Dörr, and I. Levin (1990), Methane consumption in aerated soils of the temperate zone, *Tellus B*, *42*(1), 2–8.

Boucher, O., P. Friedlingstein, B. Collins, and K. P. Shine (2009), The indirect global warming potential and global temperature change potential due to methane oxidation, *Environmental Research Letters*, *4*(4), pp. 5.

Bousquet, P., et al. (2006), Contribution of anthropogenic and natural sources to atmospheric methane variability, *Nature*, *443*(7110), 439–443.

Bowman, J. (2006), The Methanotrophs: The Families Methylococcaceae and Methylocystaceae: The Prokaryotes, pp. 266–289, Springer New York.

Brook, E. J., T. Sowers, and J. Orchardo (1996), Rapid variations in atmospheric methane concentration during the past 110,000 years, *Science*, *273*(5278), 1087–1091.

Brook, E. J., S. Harder, J. Severinghaus, E. J. Steig, and C. M. Sucher (2000), On the origin and timing of rapid changes in atmospheric methane during the last glacial period, *Global Biogeochemical Cycles*, *14*(2), 559–572.

Buddle, B. M., M. Denis, G. T. Attwood, E. Altermann, P. H. Janssen, R. S. Ronimus, C. S. Pinares-Patino, S. Muetzel, and D. Neil Wedlock (2010), Strategies to reduce methane emissions from farmed ruminants grazing on pasture, *The Veterinary Journal*, *188*(1), 11–17.

Burchard, H., and H. Rennau (2008), Comparative quantification of physically and numerically induced mixing in ocean models, *Ocean Modelling*, *20*, 293–311.

Burchard, H., F. Janssen, K. Bolding, L. Umlauf, and H. Rennau (2009), Model simulations of dense bottom currents in the Western Baltic Sea, *Continental Shelf Research*, *29*(1), 205–220.

Bussmann, I., and E. Süss (1998), Groundwater seepage in Eckernförde Bay (Western Baltic Sea): Effect on methane and salinity distribution of the water column, *Continental Shelf Research*, *18*(14-15), 1795–1806.

Butler, J., L. W. Elkins, C. M. Brunson, T. M. Thompson, and B. D. Hall (1988), Trace gases in and over the west pacific and east indian oceans during the el ninio southern oscillation event of 1987, *Tech. rep.*, Air Resources Laboratory.

References

Butler, J. H., J. W. Elkins, , C. M. Brunson, and B. D. Thompson, Thayne M Hall (1989), Trace gases in and over the west pacific and east indian oceans during the el nino-southern oscillation event of 1987, *Journal of Geophysical Research*, *94*, 14,865–14,877.

Cao, M., K. Gregson, and S. Marshall (1998), Global methane emission from wetlands and its sensitivity to climate change, *Atmospheric Environment*, *32*(19), 3293–3299.

Chakma, A. (1997), Co2 capture processes - opportunities for improved energy efficiencies, *Energy Conversion and Management*, *38*, S51–S56.

Chappellaz, J., J. M. Barnola, D. Raynaud, Y. S. Korotkevich, and C. Lorius (1990), Ice-core record of atmospheric methane over the past 160,000 years, *Nature*, *345*(6271), 127–131.

Chappellaz, J., I. Y. Fung, and A. M. Thompson (1993), The atmospheric CH$_4$ increase since the last glacial maximum, *Tellus B*, *45*(3), 228–241.

Chen, Y.-H., and R. G. Prinn (2006), Estimation of atmospheric methane emissions between 1996 and 2001 using a three-dimensional global chemical transport model, *Journal of Geophysical Research*, *111*(D10), pp. 25.

Christensen, T. R., T. Johansson, H. J. Akerman, M. Mastepanov, N. Malmer, T. Friborg, P. Crill, and B. H. Svensson (2004), Thawing sub-arctic permafrost: Effects on vegetation and methane emissions, *Geophysical Resarch Letters*, *31*(4), L04,501.

Cicerone, R. J., and R. S. Oremland (1988), Biogeochemical aspects of atmospheric methane, *Global Biogeochemical Cycles*, *2*(4), 299–327.

Cicerone, R. J., and J. D. Shetter (1981), Sources of atmospheric methane: Measurements in rice paddies and a discussion, *Journal of Geophysical Research*, *86*(C8), 7203–7209.

Clift, R., J. Grace, and M. Weber (1978), *Bubbles, drops and particles*, Academic Press, New York, Academic Press.

Conley, D. J., et al. (2009), Hypoxia-related processes in the baltic sea, *Environmental Science and Technology*, *43*(10), 3412–3420.

Conley, D. J., et al. (2011), Hypoxia is increasing in the coastal zone of the baltic sea, *Environmental Science and Technology*, *45*(16), 6777–6783.

Crutzen, P. (1988), Tropospheric ozone: an overview, in *Tropospheric Ozone: Regional and Global Scale Interactions*, edited by I. S. A. Isaksen, pp. 3–11, Reidel Publishing, Boston, MA.

Crutzen, P. J. (1991), Methane's sinks and sources, *Nature*, *350*(6317), 380–381.

Crutzen, P. J., and M. O. Andreae (1990), Biomass burning in the tropics: Impact on atmospheric chemistry and biogeochemical cycles, *Science*, *250*(4988), 1669–1678.

Crutzen, P. J., I. Aselmann, and W. Seiler (1986), Methane production by domestic animals, wild ruminants, other herbivorous fauna, and humans, *Tellus B*, *38*(3-4), 271–284.

Crutzen, P. J., E. Sanhueza, and C. A. M. Brenninkmeijer (2006), Methane production from mixed tropical savanna and forest vegetation in venezuela, *Atmospheric Chemistry and Physics Discussion*, *6*(2), 3093–3097.

Dahlke, S., L. A. Meyer-Reil, R. Ramesh, M. O. Andreae, C. Wolff, H. W. Bange, and S. Rapsomanikis (2000), Bodden waters (southern Baltic Sea) as a source of methane and nitrous oxide, in *Muddy coast dynamics and resources management*, vol. 1, edited by B. W. Flemming, M. T. Delafontaine, and G. Liebezeit, pp. 137–148, Elsevier, Amsterdam.

Dällenbach, A., T. Blunier, J. Flückiger, B. Stauffer, J. Chappellaz, and D. Raynaud (2000), Changes in the atmospheric $CH_4$ gradient between Greenland and Antarctica during the Last Glacial and the transition to the Holocene, *Geophysical Research Letters*, *27*(7), 1005–1008.

Dando, P. R., I. Bussmann, S. J. Niven, S. C. M. O'Hara, R. Schmaljohann, and L. J. Taylor (1994), A methane seep area in the Skagerrak, the habitat of the pogonophore Siboglinum poseidoni and the bivalve mollusc Thyasira sarsi, *Marine Ecology Progress Series*, *107*, 157–167.

DeAngelis, M. A., and C. Lee (1994), Methane production during zooplankton grazing on marine phytoplankton, *Limnology and Oceanography*, *39*(6), 1298–1308.

Diaz, R. J., and R. Rosenberg (2008), Spreading dead zones and consequences for marine ecosystems, *Science*, *321*(5891), 926–929.

Dlugokencky, E., P. Lang, and K. Masarie (2011), Atmospheric Methane Dry Air Mole Fractions from the NOAA ESRL Carbon Cycle Cooperative Global Air Sampling Network, 1983-2010, *Version: 2011-08-11*.

Dlugokencky, E. J., L. P. Steele, P. M. Lang, and K. A. Masarie (1994), The growth rate and distribution of atmospheric methane, *Journal of Geophysical Research*, *99*(D8), 17,021–17,043.

Dlugokencky, E. J., K. A. Masarie, P. P. Tans, T. J. Conway, and X. Xiong (1997), Is the amplitude of the methane seasonal cycle changing?, *Atmospheric Environment*, *31*(1), 21–26.

Dlugokencky, E. J., K. A. Masarie, P. M. Lang, and P. Tans (1998), Continuing decline in the growth rate of atmospheric methane, *Nature*, *393*, 447–450.

Dlugokencky, E. J., et al. (2009), Observational constraints on recent increases in the atmospheric CH4 burden, *Geophysical Research Letters*, *36*(18), pp. 5.

Dzyuban, A., I. Krylova, and I. Kuznetsova (1999), Properties of bacteria distribution and gas regime within the water column of the baltic sea in winter, *Oceanology*, *39*(3), 348–351.

Elken, J., and W. Matthäus (2008), Baltic Sea oceanography. , booktitle = Assessments of Climate change for the Baltic Sea Basin, pp. 379–386, Annex A.1.1, Berlin.

Etheridge, D. M., G. I. Pearman, and P. J. Fraser (1992), Changes in tropospheric methane between 1841 and 1978 from a high accumulation-rate Antarctic ice core, *Tellus B*, *44*(4), 282–294.

Etheridge, D. M., L. P. Steele, R. J. Francey, and R. L. Langenfelds (1998), Atmospheric methane between 1000 a.d. and present: Evidence of anthropogenic emissions and climatic variability, *Journal of Geophysical Research*, *103*(D13), 15,979–15,993.

Etiope, G., K. R. Lassey, R. W. Klusman, and E. Boschi (2008), Reappraisal of the fossil methane budget and related emission from geologic sources, *Geophysical Research Letters*, *35*(9), pp. 5.

Feistel, R., G. Nausch, and N. Wasmund (2008), *State and Evolution of the Baltic Sea, 1952-2005. A Detailed 50-Year Survey Of Meteorology And Climate, Physics, Chemistry, Biology, and Marine Environment*, John Wiley&Sons-Interscience, Hoboken N. J.

Fenchel, T., C. Bernard, G. Esteban, B. J. Finlay, P. J. Hansen, and N. Iversen (1995), Microbial diversity and activity in a danish fjord with anoxic deep water, *Ophelia*, *43*(1), 45–100.

Ferry, J. G., and D. J. Lessner (2008), Methanogenesis in marine sediments, *Annual Academy of Science, New York*, *1125*, 147–157.

Fischer, E. (1883), Bildung von Methylenblau als Reaktion auf Schwefelwasserstoff, *Berichte der deutschen chemischen Gesellschaft*, *16*(2), 2234–2236.

Fonselius, S. H. (1969), Hydrography of the Baltic Deep Basins III, *Fishery Board Sweden, Serie Hydrography.*, *23*, 97.

Forster, P., et al. (2007), Changes in atmospheric constituents and in radiative forcing, *Chlimate Change*, *20*, 129–234.

Fritsche, W. (1999), *Mikrobiologie*, 2nd ed., Spektrum Akademischer Verlag, Heidelberg.

Garrett, C., and W. Munk (1979), Internal waves in the ocean, *Annual Review of Fluid Mechanics*, *11*, 339–369.

References

Geodekyan, A., Y. M. Berlin, A. M. Bolshakov, and V. Y. Trotsyuk (1991), Distribution of methane in sediments and bottom water of the southern Baltic Sea, *Oceanology*, *31*(1), 54–59.

Grasshoff, K., K. Kremling, and M. Ehrhardt (1999), *Methods of seawater analysis*, 3rd ed., Verlag Chemie, Gulf Publishing, Houston.

Gräwe, U., and H. Buchard (2011), Storm surges in the western baltic sea: the present and a possible future, *Climate Dynamics*, pp. 1–19.

Griffies, S., M. Harrison, R. Pacanowski, and A. Rosati (2004), A technical guide to MOM4, *Tech. rep.*, Geophysical Fluid Dynamics Laboratory.

Groszko, W., and R. M. Moore (1998), A semipermeable membrane equilibrator for halomethanes in seawater, *Chemosphere*, *36*(15), 3083–3092.

Grunwald, M., O. Dellwig, M. Beck, J. W. Dippner, J. A. Freund, C. Kohlmeier, B. Schnetger, and H.-J. Brumsack (2009), Methane in the southern North Sea: Sources, spatial distribution and budgets, *Estuarine, Coastal and Shelf Science*, *81*(4), 445–456.

Gülzow, W., G. Rehder, B. Schneider, J. Schneider von Deimling, and B. Sadkowiak (2011), A new method for continuous measurement of methane and carbon dioxide in surface waters using off-axis integrated cavity output spectroscopy (ICOS): An example from the Baltic Sea, *Limnology and Oceanography-Methods*, *9*, 176–184.

Gülzow, W., G. Rehder, J. Schneider von Deimling, T. Seifert, and Z. Tóth (acc. for BGS:D), One year of continuous measurements constraining methane emissions from the Baltic Sea to the atmosphere using a ship of opportunity, *Biogeoscience*, *accepted for Biogeoscience: Discussion.*

Hendriks, D., A. Dolman, M. van der Molen, and J. van Huissteden (2008), A compact and stable eddy covariance set-up for methane measurements using off-axis integrated cavity output spectroscopy, *Atmospheric Chemistry and Physics Discussion*, *8*(2), 431–443.

Heyer, J., and U. Berger (2000), Methane Emission from the Coastal Area in the Southern Baltic Sea, *Estuarine, Coastal and Shelf Science*, *51*(1), 13–30.

Heyer, J., U. Berger, and R. Suckow (1990), Methanogenesis in different parts of a brackish water ecosystem, *Limnologica*, *20*(1), 135–139.

Heyer, J., U. Berger, I. L. Kuzin, and O. N. Yakovlev (2002), Methane emissions from different ecosystem structures of the subarctic tundra in Western Siberia during midsummer and during the thawing period, *Tellus Series B-Chemical and Physical Meteorology*, *54*(3), 231–249.

Hinrichs, K.-U., J. M. Hayes, S. P. Sylva, P. G. Brewer, and E. F. DeLong (1999), Methane-consuming archaebacteria in marine sediments, *Nature*, *398*(6730), 802–805.

Houweling, S., T. Kaminski, F. Dentener, J. Lelieveld, and M. Heimann (1999), Inverse modeling of methane sources and sinks using the adjoint of a global transport model, *Journal of Geophysical Research*, *104*(D21), 26,137–26,160.

Hovland, M. (1992), Hydrocarbon Seeps in Northern Marine Waters - Their Occurence and Effects, *Palaios*, *7*(4), 376–382.

Hübschmann, H.-J. (2009), Handbuch der GC/MS: Grundlagen und Anwendungen, *Weinheim*, p. 586.

Hutri, K.-L., and A. Kotilainen (2007), An acoustic view into holocene palaeoseismicity offshore southwestern finland, baltic sea., *Marine Geology*, *238*, 45–59.

IPCC (2007), Intergovernmental panel on climate change: Report.

Iversen, n., and T. H. Blackburn (1981), Seasonal rates of methane oxidation in anoxic marine sediments, *Applied and Environmental microbiology*, *41*(6), 1295–1300.

Iversen, N., and B. B. Jørgensen (1985), Anaerobic methane oxidation rates at the sulfate-methane transition in marine sediments from Kattegat and Skagerrak (Denmark), *Limnology and Oceanography*, *30*(5), 944–955.

Jackson, D. R., K. L. Williams, T. F. Wever, C. T. Friedrichs, and L. D. Wright (1998), Sonar evidence for methane ebullition in Eckernförde Bay, *Continental Shelf Research*, *18*(14-15), 1893–1915.

Jähne, B., G. Heinz, and W. Dietrich (1987), Measurement of the diffusion coefficients of sparingly soluble gases in water, *Journal of Geophysical Research*, *92*(C10), 10,767–10,776.

Jähne, B., P. Libner, R. Fischer, T. Billen, and E. J. Plate (1989), Investigating the transfer processes across the free aqueous viscous boundary layer by the controlled flux method, *Tellus Series B-Chemical and Physical Meteorology*, *41*(2), 177–195.

Jahnke, R. A. (1996), The global ocean flux of particulate organic carbon: Areal distribution and magnitude, *Global Biogeochemical Cycles*, *10*(1), 71–88.

Jensen, J. B., and O. Bennike (2009), Geological setting as background for methane distribution in Holocene mud deposits, Aarhus Bay, Denmark, *Continental Shelf Research*, *29*(5-6), 775–784.

Jensen, P., I. Aagaard, R. A. Burke Jr., P. R. Dando, N. O. Jørgensen, A. Kuijpers, T. Laier, S. C. M. O'Hara, and R. Schmaljohann (1992), Bubbling reefs in the Kattegat: submarine landscapes of carbonate-cemented rocks support a diverse ecosystem at methane seeps, *Marine Ecology Progress Series*, *83*(2-3), 103–112.

Jørgensen, B. (1982), Mineralization of organic matter in the sea bed - the role of sulphate reduction, *Nature*, *296*, 643–645.

Jørgensen, B. B., and S. Kasten (2006), Sulfur Cycling and Methane Oxidation, in *Marine Geochemistry*, edited by H. D. Schulz and M. Zabel, 2nd ed., pp. 271–309, Springer Verlag, Berlin.

Jørgensen, B. B., M. Bang, and T. H. Blackburn (1990), Anaerobic mineralization in marine sediments from the Baltic Sea - North Sea transition, *Marine Ecology Progress Series*, *59*, 39–54.

Judd, A. G. (2003), The global importance and context of methane escape from the seabed, *Geo-Marine Letters*, *23*(3), 147–154.

Judd, A. G. (2004), Natural seabed gas seeps as source of atmospheric methane, *Environmental Geology*, *46*, 988–996.

Judd, A. G., M. Hovland, L. I. Dimitrov, S. Garcia Gil, and V. Jukes (2002), The geological methane budget at continental margins and its influence on climate change, *Geofluids*, *2*(2), 109–126.

Kamykowski, D. (1974), Possible interactions between phytoplankton and semidiurnal internal tides, *Journal Marine Research*, *32*, 67–89.

Karl, D. M., and B. D. Tilbrook (1994), Production and transport of methane in oceanic particulate organic matter, *Nature*, *368*(6473), 732–734.

Karl, D. M., L. Beversdorf, K. M. Björkman, M. J. Church, A. Martinez, and E. F. DeLong (2008), Aerobic production of methane in the sea, *Nature Geocience*, *1*, 473–478.

Keir, R., J. Greinert, M. Rhein, G. Petrick, J. Sültenfuß, and K. Fürhaupter (2005), Methane and methane carbon isotope ratios in theNortheast Altantic including in the Mid-Atlantic Ridge 50N, *Deep Sea Research Part I: Oceanographic Research Papers*, *52*(6), 1043–1070.

Keir, R., O. Schmale, R. Seifert, and J. Sültenfuß(2009), Isotope fractionation and mixing in methane plumes from the logatchev hydrothermal field., *Geochemistry Geophysics Geosystems*, *10*.

Keppler, F., J. T. G. Hamilton, M. Bra, and T. Rockmann (2006), Methane emissions from terrestrial plants under aerobic conditions, *Nature*, *439*(7073), 187–191.

Khalil, M. A. K., and R. A. Rasmussen (1993), Decreasing trend of methane: Unpredictability of future concentrations, *Chemosphere*, *26*(1-4), 803–814.

Khalil, M. A. K., and R. A. Rasmussen (1994a), Global emissions of methane during the last several centuries, *Chemosphere*, *29*(5), 833–842.

Khalil, M. A. K., and R. A. Rasmussen (1994b), Trends in atmospheric methane, *Pure and Applied Chemistry*, *66*(1), 137–200.

Khalil, M. A. K., and M. J. Shearer (2000), Sources of methane: an overview, in *Atmospheric Methane: Its Role in the Global Environment*, edited by M. A. K. Khalil, pp. 98–111, Springer-Verlag, New York, NY.

Khalil, M. A. K., and M. J. Shearer (2006), Decreasing emissions of methane from rice agriculture, *International Congress Series*, *1293*, 33–41.

Konovalov, S. K., et al. (2003), Lateral injection of oxygen with the Bosporus plume: Fingers of oxidizing potential in the Black Sea, *Limnology and Oceanography*, *48*(6), 2369–2376.

Kopf, A. J. (2003), Global methane emission through mud volcanoes and its past and present impact on the earth's climate, *International Journal of Earth Sciences*, *92*(5), 806–816.

Körtzinger, A., H. Thomas, B. Schneider, N. Gronau, L. Mintrop, and J. C. Duinker (1996), At-sea intercomparison of two newly designed underway $pCO_2$ systems - Encouraging results, *Marine Chemistry*, *52*(2), 133–145.

Kreuzer, M., and I. K. Hindrichsen (2006), Methane mitigation in ruminants by dietary means: The role of their methane emission from manure, *International Congress Series*, *1293*, 199–208.

Kundu, P. K., and I. M. Cohen (2008), Fluid Mechanics, *Academic London*, *4th ed.*, 872.

Laier, T., and J. Jensen (2007), Shallow gas depth - contour map of the Skagerrak - western Baltic Sea region, *Geo-Marine Letters*, *27*(2), 127–141.

Laier, T., N. O. Jørgensen, B. Buchardt, T. Cederberg, and A. Kuijpers (1992), Accumulation and seepages of biogenic gas in northern Denmark, *Continental Shelf Research*, *12*(10), 1173–1186.

Lammers, S., and E. Süss (1994), An improved head-space analysis method for methane in seawater, *Marine Chemistry*, *47*(2), 115–125.

Large, W., J. McWilliams, and S. Doney (1994), Oceanic vertical mixing: A review and a model with a nonlocal boundary layer parameterization, *Reviews of Geophysics*, *32*(4), 363–403.

Lass, H., V. Mohrholz, G. Nausch, and H. Siegel (2010), On phosphate pumping into the surface layer of the eastern Gotland Basin by upwelling, *Journal of Marine Systems*, *80*(1-2), 71–89.

Lass, H. U., and W. Matthus (1996), On temporal wind variations forcing salt water inflows into the Baltic Sea, *Tellus A*, *48*(5), 663–671.

## References

Lass, H. U., and V. Mohrholz (2003), On dynamics and mixing of inflowing saltwater in the Arkona Sea, *Journal of Geophysical Research*, *108*(C2), 3042–3057.

Lass, H. U., V. Mohrholz, and T. Seifert (2005), On pathways and residence time of saltwater plumes in the Arkona Sea, *Journal of Geophysical Research*, *110*(C11), pp. 24.

Lassey, K. R. (2007), Livestock methane emission: From the individual grazing animal through national inventories to the global methane cycle, *Agricultural and Forest Meteorology*, *142*(2-4), 120–132.

Lehmann, A., and K. Myrberg (2008), Upwelling in the Baltic Sea - a review, *Journal of Marine Systems*, *74*(1), S3–S12.

Lelieveld, J. (2006), Climate change - a nasty surprise in the greenhouse, *Nature*, *443*(7110), 405–406.

Lelieveld, J., and P. J. Crutzen (1992), Indirect chemical effects of methane on climate warming, *Nature*, *355*(6358), 339–342.

Lelieveld, J., P. J. Crutzen, and F. J. Dentener (1998), Changing concentration, lifetime and climate forcing of atmospheric methane, *Tellus B*, *50*(2), 128–150.

Leuenberger, D. (2010), Statistical analysis of high-resolution cosmo ensemble forecasts in view of data assimilation, *Tech. rep.*, Deutscher Wetterdienst.

Levine, J. S., W. R. Cofer III, and J. P. Pinto (2000), Biomass burning, in *Atmospheric Methane: Its Role in the Global Environment*, edited by M. A. K. Khalil, pp. 190–201, Springer-Verlag, New York, NY.

Linke, P., S. Sommer, L. Rovelli, and D. F. McGinnis (2010), Physical limitations of dissolved methane fluxes: The role of bottom-boundary layer processes, *Marine Geology*, *272*(1-4), 209–222.

Lips, I., U. Lips, and T. Liblik (2009), Consequences of coastal upwelling events on physical and chemical patterns in the central Gulf of Finland (Baltic Sea), *Continental Shelf Research*, *29*(15), 1836–1847.

Liss, P., and L. Merlivat (1986), Air-Sea exchange rates: introduction and synthesis, in *The Role of Air-Sea Exchange in geochemical Cycling*, edited by P. Buat-Menard, pp. 113–127, Springer, New York.

Liss, P. S., and P. G. Slater (1974), Flux of gases across the air-sea interface, *Nature*, *247*, 181–184.

Mathys, M., O. Thießen, F. Theilen, and M. Schmidt (2005), Seismic characterization of gas-rich near surface sediments in the Arkona Basin, Baltic Sea, *Marine Geophysical Researches*, *26*, 207–224.

# References

Matthäus, W., and H. Franck (1992), Characteristics of major Baltic inflows - a statistical analysis, *Continental Shelf Research*, *12*(12), 1375–1400.

Matthäus, W., and H. U. Lass (1995), The recent salt water inflow into the Baltic Sea, *Journal of Physical Oceanography*, *25*(2), 280–288.

McDermitt, D., et al. (2011), A new low-power, open-path instrument for measuring methane flux by eddy covariance, *Applied Physics B: Lasers and Optics*, *102*, 391–405.

McGinnis, D. F., J. Greinert, Y. Artemov, S. E. Beaubien, and A. Wuest (2006), Fate of rising methane bubbles in stratified waters: How much methane reaches the atmosphere?, *Journal of Geophysical Research*, *111*(C9), pp. 15.

Meier, H. E. M., H. C. Andersson, K. Eilola, B. G. Gustafsson, I. Kuznetsov, B. Müller-Karulis, T. Neumann, and O. P. Savchuk (2011), Hypoxia in future climates: A model ensemble study for the Baltic Sea, *Geophysical Research Letters*, *38*(24), L24,608.

Michaelis, W., G. Bönisch, A. Jenisch, S. Ladage, H. H. Richnow, R. Seifert, and P. Stoffers (1990), Methane and $^3$He anomalies related to submarine intraplate volcanic activities, *Mitteilungen aus dem Geologisch-Palontologischen Institut der Universität Hamburg*, *69*, 117–127.

Middelburg, J. J., and J. Nieuwenhuize (2000), Nitrogen uptake by heterotrophic bacteria and phytoplankton in the nitrate - rich Thames estuary, *Marine Ecology Progress Series*, *203*, 13–21.

Milkov, A. V., R. Sassen, T. V. Apanasovich, and F. G. Dadashev (2003), Global gas flux from mud volcanoes: A significant source of fossil methane in the atmosphere and the ocean, *Geophysical Research Letters*, *30*(2), pp. 4.

Miller, J. B., L. V. Gatti, M. T. S. d'Amelio, A. M. Crotwell, E. J. Dlugokencky, P. Bakwin, P. Artaxo, and P. P. Tans (2007), Airborne measurements indicate large methane emissions from the eastern Amazon Basin, *Geophysical Research Letters*, *34*(10), pp. 5.

Mitchell, C. (1993), Methane emissions from the coal and natural gas industries in the UK, *Chemosphere*, *26*, 441–446.

Mogollon, J. M., A. W. Dale, H. Fossing, and P. Regnier (2011), Timescales for the development of methanogenesis and free gas layers in recently-deposited sediments of Arkona Basin (Baltic Sea), *Biogeosciences Discussion*, *8*, 7623–7669.

Mohrholz, V., J. Dutz, and G. Kraus (2006), The impact of exceptionally warm summer inflow events on the environmental conditions in the Bornholm Basin, *Journal of Marine Systems*, *60*(3-4), 285–301.

Morimoto, S., S. Aoki, T. Nakazawa, and T. Yamanouchi (2006), Temporal variations of the carbon isotopic ratio of atmospheric methane observed at Ny Alesund, Svalbard from 1996 to 2004, *Geophysical Research Letters*, *33*(1), pp. 4.

Moros, M., W. Lemke, A. Kuijpers, R. Endler, J. B. Jensen, O. Bennike, and F. Gingele (2002), Regressions and transgressions of the Baltic Basin reflected by a new high-resolution deglacial and postglacial lithostratigraphy for Arkona Basin sediments (western Baltic Sea), *Boreas*, *31*(2), 151–162.

Moss, A. R., J.-P. Jouany, and J. Newbold (2000), Methane production by ruminants: its contribution to global warming, *Annales de Zootechnie*, *49*(3), 231–253.

Munk, W. (1981), Internal waves and small-scale processes, in *Evolution of Physical Oceanography*, edited by B. A. Warren and C. Wunsch, pp. 264–291, The MIT Press, Cambridge, Mass.

Munk, W. (2001), Internal tidal mixing, *Encyclopedia of Ocean Sciences*, *3*, 1323–1327.

Murray, C., J.W.and Fuchsman, J. Kirkpatrick, B. Paul, and K. Konovalov (2005), Species and d15N signatures of nitrogen transformations in the suboxic zone of the Black Sea., *ceanography*, *18*, 36–47.

Murray, J., K. Konovalov, and A. Callaham (2003), Nitrogen reactions in the suboxic zone of the black sea: new data and models, in *Oeanography of the Eastern Mediterranean and Black Sea: Similarities and Differences of Two Interconnected Basin*, edited by B. A. Warren and C. Wunsch, pp. 591–602, Tubitak Publishers.

Naqvi, S. W. A., H. W. Bange, L. Farías, P. M. S. Monteiro, M. I. Scranton, and J. Zhang (2009), Coastal hypoxia/anoxia as a source of $CH_4$ and $N_2O$, *Biogeosciences Discussions*, *6*, 9455–9523.

Nauhaus, K., T. Treude, A. Boetius, and M. Krüger (2005), Environmental regulation of the anaerobic oxidation of methane: a comparison of ANME-I and ANME-II communities, *Environmental Microbiology*, *7*(1), 98–1006.

Nausch, G., D. Nehring, and K. Nagel (2008), Nutrient concentrations, trends and their relation to eutrophication, in *State and Evolution of the Baltic Sea, 1952-2005*, pp. 337–366, John Wiley, Hoboken, N. J.

Nightingale, P. D., G. Malin, C. S. Law, A. J. Watson, P. S. Liss, M. I. Liddicoat, J. Boutin, and R. C. Upstill-Goddard (2000), In situ evaluation of air-sea gas exchange parameterizations using novel conservative and volatile tracers, *Global Biogeochemical Cycles*, *14*(1), 373–387.

Parkes, R. J., et al. (2007), Biogeochemistry and biodiversity of methane cycling in subsurface marine sediments (Skagerrak, Denmark), *Environmental Microbiology*, *9*(5), 1146–1161.

Petit, J. R., et al. (1999), Climate and atmospheric history of the past 420,000 years from the Vostok ice core, Antarctica, *Nature*, *399*(6735), 429–436.

Piker, L., R. Schmaljohann, and J. F. Imhoff (1998), Dissimilatory sulfate reduction and methane production in Gotland Deep sediments (Baltic Sea) during a transition period from oxic to anoxic bottom water (1993-1996), *Aquatic Microbial Ecology*, *14*(2), 183–193.

Pimenov, N., M. Ulyanova, T. Kanapatsky, E. Veslopolova, P. Sigalevich, and V. Sivkov (2010), Microbially mediated methane and sulfur cycling in pockmark sediments of the Gdansk Basin, Baltic Sea, *Geo-Marine Letters*, *30*(3), 439–448.

Platt, U., W. Allan, and D. Lowe (2004), Hemispheric average Cl atom concentration from $^{13}C/^{12}C$ ratios in atmospheric methane, *Atmospheric Chemistry and Physics*, *4*, 2393–2399.

Plattner, G., T. F. Stocker, P. Midgley, and M. Tignor (2009), Meeting report of the expert meeting on the science of alternative metrics, *IPCC Working Group I Technical Support Unit, University of Bern, Bern, Switzerland,*.

Prather, M., et al. (2001), Atmospheric chemistry and greenhouse gases, in *Climate change 2001: the scientific basis. Third Assessment Report of the Intergovernmental Panel on Climate Change*, edited by J. T. Houghton, Y. Ding, D. J. Griggs, M. Noguer, P. J. van der Linden, X. Dai, K. Maskell, and C. A. Johnson, Cambridge University Press, Cambridge, NY.

Prinn, R. G., R. F. Weiss, B. R. Miller, J. Huang, F. N. Alyea, D. M. Cunnold, P. J. Fraser, D. E. Hartley, and P. G. Simmonds (1995), Atmospheric trends and lifetime of ch3ccl3 and global oh concentrations, *Science*, *269*(5221), 187–192.

Rabalais, N. N., R. J. Diaz, L. A. Levin, R. E. Turner, D. Gilbert, and J. Zhang (2010), Dynamics and distribution of natural and human-caused hypoxia, *Biogeosciences*, *7*, 585–619.

Rao, A. B., and E. S. Rubin (2002), A technical, economic, and environmental assessment of amine-based $CO_2$ capture technology for power plant greenhouse gas control, *Environmental Science & Technology*, *36*(20), 4467–4475.

Reeburgh, W. S. (2007), Oceanic methane biogeochemistry, *Chemical Reviews*, *107*(2), 486–513.

Reeburgh, W. S., S. C. Whalen, and M. J. Alperin (1993), The role of methylotrophy in the global methane budget, in *Microbial Growth on C-1 Compounds*, edited by J. C. Murrell and D. S. Kelley, pp. 1–14, Intercept, Andover, UK.

Rehder, G. (1996), Quellen und Senken marinen Methans zwischen Schelf und offenem Ozean.

## References

Rehder, G., and E. Süß(2001), Methane and pCO$_2$ in the Kuroshio and the South China Sea during maximum summer surface temperatures, *Marine Chemistry*, *75*(1-2), 89–108.

Rehder, G., R. S. Keir, E. Süß, and T. Pohlmann (1998), The multiple sources and patterns of methane in North Sea waters, *Aquatic Geochemistry*, *4*(3), 403–427.

Rehder, G., R. S. Keir, E. Süß, and M. Rhein (1999), Methane in the Northern Atlantic controlled by microbial oxidation and atmospheric history, *Geophysical Research Letters*, *26*(5), 587–590.

Rehder, G., S. Grandel, S. Mau, and K. Stange (2002), Water column and upper sediment investigations, *IFM-GEOMAR*.

Reissmann, J. H., H. Burchard, R. Feistel, E. Hagen, H. U. Lass, V. Mohrholz, G. Nausch, L. Umlauf, and G. Wieczorek (2009), Vertical mixing in the baltic sea and consequences for eutrophication - a review, *Progress in oceanography*, *82*(1), 47–80.

Rella, C. (2010), Accurate greenhouse gas measurements in humid gas streams using the picarro G1301 CO$_2$, CH$_4$ and H$_2$O gas analyzer, *White paper, Picarro Inc*, pp. 1–18.

Rheinheimer, G. (1995), *Die Meereskunde der Ostsee*, 2nd ed., 338 pp., Springer Verlag, Heidelberg, Berlin.

Saito, H., N. Tamura, H. Kitano, A. Mito, C. Takahashi, A. Suzuki, and H. Kayanne (1995), A compact seawater pCO$_2$ measurement system with membrane equilibrator and nondispersive infrared gas analyzer, *Deep Sea Research Part I: Oceanographic Research Papers*, *42*(11-12), 2025–2029, 2031–2033.

Sass, R. L., F. M. Fisher, P. A. Harcombe, and F. T. Turner (1990), Methane production and emission in a Texas rice field, *Global Biogeochemical Cycles*, *4*(1), 47–68.

Sauter, E. J., S. I. Muyakshin, J.-L. Charlou, M. Schlüter, A. Boetius, K. Jerosch, E. Damm, J.-P. Foucher, and M. Klages (2006), Methane discharge from a deep-sea submarine mud volcano into the upper water column by gas hydrate-coated methane bubbles, *Earth and Planetary Science Letters*, *243*(3-4), 354–365.

Schlüter, M., E. J. Sauter, C. E. Anderson, H. Dahlgaard, and P. R. Dando (2004), Spatial distribution and budget for submarine groundwater discharge in Eckernförde Bay (Western Baltic Sea), *Limnology and Oceanography*, *49*(1), 157–167.

Schmale, O., J. Greinert, and G. Rehder (2005), Methane emission from high-intensity marine gas seeps in the Black Sea into the atmosphere, *Geophysical Research Letters*, *32*, pp. 4.

Schmale, O., S. E. Beaubien, G. Rehder, J. Greinert, and S. Lombardi (2010a), Gas seepage in the Dnepr paleo-delta area (NW-Black Sea) and its regional impact on the water column methane cycle, *Journal of Marine Systems*, *80*(1-2), 90–100.

Schmale, O., J. Schneider v. Deimling, W. Gülzow, G. Nausch, J. Waniek, and G. Rehder (2010b), The distribution of methane in the water column of the Baltic Sea, *Geophysical Research Letters*, *37*, pp. 5.

Schmale, O., M. Häckel, and D. F. McGinnis (2011), Response of the Black Sea methane budget to massive short-term submarine inputs of methane, *Biogeosciences*, *8*(4), 911–918.

Schmaljohann, R. (1996), Methane dynamics in the sediment and water column of Kiel Harbour (Baltic Sea), *Marine Ecology Progress Series*, *131*, 263–273.

Schmidt, M., T. Seifert, H. U. Lass, and W. Fennel (1998), Patterns of salt propagation in the Southwestern Baltic Sea, *Deutsche Hydrographische Zeitschrift*, *50*(4), 345–364.

Schmitt, M., E. Faber, R. Botz, and P. Stoffers (1991), Extraction of methane from seawater using ultrasonic vacuum degassing, *Analytical Chemistry*, *63*(5), 529–532.

Schneider, B., K. Kremling, and J. Duinker (1992), Co2 partial pressure in northeast atlantic and adjacent shelf waters: Processes and seasonal variability, *Journal of Marine Systems*, *3*(6), 453–463.

Schneider, B., S. Kaitala, and P. Maunula (2006), Identification and quantification of plankton bloom events in the Baltic Sea by continuous pCO$_2$ and chlorophyll a measurements on a cargo ship, *Journal of Marine Systems*, *59*(3-4), 238–248.

Schneider, B., B. Sadkowiak, and F. Wachholz (2007), A new method for continuous measurements of O$_2$ in surface water in combination with pCO$_2$ measurements: Implications for gas phase equilibration, *Marine Chemistry*, *103*(1-2), 163–171.

Schneider von Deimling, J. (2009), Hydroacoustic and geochemical traces of marine gas seepage in the North Sea, Dissertation, *Universität Kiel*.

Schneider von Deimling, J., J. Greinert, N. R. Chapman, W. Rabbel, and L. P. (2010), Acoustic imaging of natural gas seepage in the North Sea: Sensing bubbles under control of variable currents., *Limnology and Oceanography: Methods*, *8*, 155–171.

Schneider von Deimling, J., G. Rehder, J. Greinert, D. F. McGinnnis, A. Boetius, and P. Linke (2011), Quantification of seep-related methane gas emissions at Tommeliten, North Sea, *Continental Shelf Research*, *31*(7-8), 867–878.

Schulz, J.-P., and U. Schüttler (2005), Kurze Beschreibung des Lokal-Modells LME und seiner Datenbanken auf dem Datenserver des DWD, *Tech. rep.*, Deutscher Wetterdienst.

Seifert, T. (2010), Comparison of weather model data with station measurements, *Tech. rep.*, Institute for Baltic Sea Research.

Seifert, T., F. Tauber, and B. Kayser (2001), A high resolution spherical grid topography of the Baltic Sea - revised edition., *Baltic Marine Environment Bibliography 1970- (Finland)*, *Nov.*(147), 25–29.

Sellschopp, J., L. Arneborg, M. Knoll, V. Fiekas, F. Gerdes, H. Burchard, H. U. Lass, V. Mohrholz, and L. Umlauf (2006), Direct observations of a medium-intensity inflow into the Baltic Sea, *Continental Shelf Research*, *26*(19), 2393–2414.

Shindell, D. T., G. Faluvegi, D. M. Koch, G. A. Schmidt, N. Unger, and S. E. Bauer (2009), Improved attribution of climate forcing to emissions, *Science*, *326*(5953), 716–718.

Siegel, H. (2000), Satellite-based studies of the 1997 oder flood event in the southern Baltic Sea., *Remote sens. environ.*, *73*, 207–217.

Siegel, H., and M. Gerth (2000), Remote-sensing studies of the exceptional summer of 1997 in the Baltic Sea: the warmest August of the century, the Oder flood, and phytoplankton blooms., in *Satellites, oceanography and society*, edited by D. Halpern, pp. 239–255, Elsevier oceanography series.

Siegel, H., M. Gerth, R. Rudloff, and G. Tschersich (1994), Dynamical features in the western baltic sea investigated by noaa- avhrr- data, *Deutsche Hydrographische Zeitschrift*, *46*(3), 191–209.

Siegel, H., R. Seifert, G. Schernewski, M. Gerth, J. Reimann, T. Ohde, and V. Podsetchine (2005), Discharge and transport processes along the German Baltic Sea Coast, *Ocean Dynamics*, *55*(1), 47–66.

Skoog, L. (1996), *Instrumentelle Analytik: Grundlagen - Geräte - Anwendungen*, Springer Verlag.

Smagorinski, J. (1963), General circulation experiments with the primitive equations: I. the basic experiment, *Monthly Weather Review*, *91*(3), 99–164.

Söderberg, P., and T. Flodén (1992), Gas seepages, gas eruptions and degassing structures in the seafloor along the stromma tectonic lineament in the crystalline stockholm archipelago, east sweden, *Continental Shelf Research*, *12*(10), 1157–1171.

Solomon, E. A., M. Kastner, I. R. MacDonald, and I. Leifer (2009), Considerable methane fluxes to the atmosphere from hydrocarbon seeps in the Gulf of Mexico, *Nature Geoscience*, *2*(8), 561–565.

Spahni, R., et al. (2005), Atmospheric methane and nitrous oxide of the late pleistocene from Antarctic ice cores, *Science*, *310*(5752), 1317–1321.

## References

Sweeney, C., E. Gloor, A. R. Jacobson, R. M. Key, G. McKinley, J. L. Sarmiento, and R. Wanninkhof (2007), Constraining global air-sea gas exchange for $CO_2$ with recent bomb $^{14}C$ measurements., *Global Biogeochemistry Cycles*, *21*(GB-2015).

Swinnerton, J. W., and V. J. Linnenbom (1967), Gaseous hydrocarbons in sea water: Determination, *Science*, *156*(3778), 1119–1120.

Swinnerton, J. W., V. J. Linnenbom, and C. H. Cheek (1962), Determination of dissolved gases in aqueous solutions by gas chromatography, *Analytical Chemistry*, *34*(4), 483–485.

Takahashi, T., J. Olafsson, J. G. Goddard, D. W. Chipman, and S. C. Sutherland (1993), Seasonal variation of $CO_2$ and nutrient salts in the high-latitude surface oceans: a comparative study, *Global Biogeochemical Cycles*, *7*, 843–848.

Takahashi, T., et al. (2009), Climatological mean and decadal change in surface ocean $pCO_2$, and net sea-air $CO_2$ flux over the global oceans, *Deep Sea Research Part II: Topical Studies in Oceanography*, *56*(8-10), 554–577.

Thießen, O., M. Schmidt, F. Theilen, M. Schmitt, and G. Klein (2006), Methane formation and distribution of acoustic turbidity in organic-rich surface sediments in the Arkona Basin, Baltic Sea, *Continental Shelf Research*, *26*(19), 2469–2483.

Thomas, H., and B. Schneider (1999), The seasonal cycle of carbon dioxide in Baltic Sea surface waters, *Journal of Marine Systems*, *22*(1), 53–67.

Thomas, S. (2011), Vergleich und Optimierung analytischer Methoden zur Bestimmung des Methangehaltes in Seewasser, *Diplomarbeit; Universität Rostock*.

Thompson, A. M. (1992), The oxidizing capacity of the earth's atmosphere: Probable past and future changes, *Science*, *256*(5060), 1157–1165.

Thompson, A. M., R. W. Stewart, M. A. Owens, and J. A. Herwehe (1989), Sensitivity of tropospheric oxidants to global chemical and climate change, *Atmospheric Environment*, *23*(3), 519–532.

Thompson, A. M., J. A. Chappellaz, I. Y. Fung, and T. L. Kucsera (1993), The atmospheric $CH_4$ increase since the last glacial maximum, *Tellus B*, *45*(3), 242–257.

Tilbrook, B. D., and D. M. Karl (1995), Methane sources, distributions and sinks from california coastal waters to the oligotrophic north pacific gyre, *Marine Chemistry*, *49*(1), 51–64.

Tomczak, M., and J. S. Godfrey (1994), *Regional Oceanography: an Introduction*, Pergamon Press, New York.

Treude, T., A. Boetius, K. Knittel, K. Wallmann, and B. Jørgensen (2003), Anaerobic oxidation of methane above gas hydrates at Hydrate Ridge, NE Pacific Ocean, *Marine Ecology Progress Series*, *264*, 1–14.

Treude, T., J. Niggemann, J. Kallmeyer, P. Wintersteller, C. J. Schubert, A. Boetius, and B. B. Jørgensen (2005), Anaerobic oxidation of methane and sulfate reduction along the Chilean continental margin, *Geochimica et Cosmochimica Acta*, *69*(11), 2767–2779.

Umlauf, L., and L. Arneborg (2009), Dynamics of rotating shallow gravity currents passing through a channel. Part II: Analysis, *Journal of Physical Oceanography*, *39*(10), 2402–2416.

Umlauf, L., L. Arneborg, H. Burchard, V. Fiekas, H.-U. Lass, V. Mohrholz, and H. Prandke (2007), The transverse structure of turbulence in a rotating gravity current, *Geophysical Research Letters*, *34*.

Umlauf, L., L. Arneborg, R. Hofmeister, and H. Burchard (2010), Entrainment in shallow rotating gravity currents: A modeling study, *Journal of Physical Oceanography*, *40*(8), 1819–1834.

Vahtera, E., J. Laanemets, J. Pavelson, M. Huttunen, and K. Kononen (2005), Effect of upwelling on the pelagic environment and bloom-forming cyanobacteria in the western Gulf of Finland, Baltic Sea, *Journal of Marine Systems*, *58*(1-2), 67–82.

Valentine, D. L., D. C. Blanton, W. S. Reeburgh, and M. Kastner (2001), Water column methane oxidation adjacent to an area of active hydrate dissociation, Eel River Basin, *Geochimica et Cosmochimica Acta*, *65*(16), 2633–2640.

van Bodegom, P. M., and C. M. Scholten (2001), Microbial processes of $CH_4$ production in a rice paddy soil: Model and experimental validation, *Geochimica et Cosmochimica Acta*, *65*(13), 2055–2066.

van der Lee, E. M., and L. Umlauf (2011), Internal wave mixing in the Baltic Sea: Near-inertial waves in the absence of tides, *Journal of Geophysical Research*, *116*, pp. 16.

van Loon, G. W., and S. J. Duffy (2005), *Environmental Chemistry, A Global Perspective*, 515 pp., Oxford University Press, Oxford.

Velichko, A. A., C. V. Kremenetski, O. K. Borisova, E. M. Zelikson, V. P. Nechaev, and H. Faure (1998), Estimates of methane emission during the last 125,000 years in Northern Eurasia, *Global and Planetary Change*, *16-17*, 159–180.

Voipio, A. (1981), The Baltic Sea, *Elsevier oceanography series*, *30*(1), 418.

Wahlen, M. (1993), The global methane cycle, *Annual Review of Earth and Planetary Sciences*, *21*(1), 407–426.

Walter, K. M., S. A. Zimov, J. P. Chanton, D. Verbyla, and F. S. Chapin (2006), Methane bubbling from Siberian thaw lakes as a positive feedback to climate warming, *Nature*, *443*(7107), 71–75, 10.1038/nature05040.

Wanninkhof, R. (1992), Relationship between wind speed and gas exchange over the ocean, *Journal of Geophysical Research*, *97*(C5), 7373–7382.

Wanninkhof, R., W. E. Asher, D. T. Ho, C. Sweeney, and W. R. McGillis (2009), Advances in quantifying air-sea gas exchange and environmental forcing, *Annual Review of Marine Science*, *1*(1), 213–244.

Weiss, A., J. Kuss, G. Peters, and B. Schneider (2007), Evaluating transfer velocity-wind speed relationship using a long-term series of direct eddy correlation $CO_2$ flux measurements., *Journal of Marine Systems*, *66*, 130–139.

Weiss, R. F. (1970), The solubility of nitrogen, oxygen and argon in water and seawater, *Deep Sea Research and Oceanographic Abstracts*, *17*(4), 721–735.

Weiss, R. F. (1981), Determinations of carbon dioxide and methane by dual catalyst flame ionization chromatography and nitrous oxide by electron capture chromatography, *Journal of Chromatographic Science*, *19*, 611–616.

Weiss, R. F., and B. A. Price (1980), Nitrous oxide solubility in water and seawater, *Marine Chemistry*, *8*(4), 347–359.

Wever, T. F., R. Lühder, H. Vo, and U. Knispel (2006), Potential environmental control of free shallow gas in the seafloor of Eckernförde Bay, Germany, *Marine Geology*, *225*(1-4), 1–4.

Whiticar, M. (2002), Diagentic relationship of methanogenesis, nutrients, acoustic turbidity, pockmarks and freshwater seepages in Eckernförde Bay, *Marine Geology*, *182*, 29–53.

Whiticar, M. J. (1978), Relationships of interstitial gases and fluids during early diagennesis in some marine sediments, *Tech. rep.*, Universität Kiel.

Whiticar, M. J. (1996), Isotope tracking of microbial methane formation and oxidation, *Mitteilungen Internationale Vereinigung für Theoretische und Angewandte Limnologie*, *25*, 39–54.

Whiticar, M. J., E. Faber, and M. Schoell (1986), Biogenic methane formation in marine and freshwater environments: Co2 reduction vs. acetate fermentation–isotope evidence, *Geochimica et Cosmochimica Acta*, *50*(5), 693–709.

Wiesenburg, D. A., and J. N. L. Guinasso (1979), Equilibrium solubilities of methane, carbon monoxide, and hydrogen in water and sea water, *Journal of Chemical and Engineering Data*, *24*(4), 356–360.

Wuebbles, D. J., and K. Hayhoe (2002), Atmospheric methane and global change, *Earth-Science Reviews*, *57*(3-4), 177–210.

Wyrtki, K. (1954), Der grosse Salzeinbruch in die Ostsee im November und Dezember 1951, *Kieler Meeresforschung*, *10*(3), 19–25.

Xu, S., P. R. Jaff, and D. L. Mauzerall (2007), A process-based model for methane emission from flooded rice paddy systems, *Ecological Modelling*, *205*(3-4), 475–491.

Zahniser, M. S., D. D. Nelson, J. B. McManus, P. L. Kebabian, and D. Lloyd (1995), Measurement of trace gas fluxes using tunable diode laser spectroscopy, *Philosophical Transactions of the Royal Society A: Mathematical, Physical and Engineering Sciences*, *351*(1696), 371–382.

# CONTRIBUTION TO MANUSCRIPTS

The contributions of the authors to the manuscripts are indicated in the following:

Gülzow, W., Rehder, G., Schneider, B., Schneider von Deimling, J. and Sadkowiak, B.: (2011) A new method for continuous measurement of methane and carbon dioxide in surface waters using off-axis integrated cavity output spectroscopy (ICOS): An example from the Baltic Sea. *Limnology and Oceanography-Methods*, 9, 176-184.

Specific contribution: Experiments, concept and manuscript writing by W. Gülzow. Technical support by B. Sadowiak. Revision of manuscript by G. Rehder, B. Schneider and J. Schneider von Deimling. Project holder: G. Rehder.

Gülzow, W., Rehder, G., Schneider von Deimling, J., Seifert, T. and Tóth, Zs.: One year of continuous measurements constraining methane emissions from the Baltic Sea to the atmosphere using a ship of opportunity. (accepted at Biogeoscience: Discussion).

Specific contribution: Data analysis, concept and manuscript writing by W. Gülzow. Additional data were provided by T. Seifert. Contributions to the manuscript and additional data by Zs. Tóth. Revision of manuscript by G. Rehder and J. Schneider von Deimling. Project holder: G. Rehder.

Gülzow, W., Rehder, G., Gräwe, U., Thomas, S., Schmale, O.; (in prep.) Seasonal variation of methane in the water column of Arkona and Bornholm Basin in 2009 - 2011.

Specific contribution: Data analysis, concept and manuscript writing by W. Gülzow. Sample measurements by W. Gülzow and S. Thomas. Establishment VE-Method by O. Schmale. GETM-model simulations data by U. Gräwe. Revision of manuscript by G. Rehder. Project holder: G. Rehder.

Schmale, O., Schneider v. Deimling, J. Gülzow, W., Nausch, G., Waniek, J. J. and Rehder, G.: (2010) The distribution of methane in the water column of the Baltic Sea. *Geophysical Research Letters*, 37, L12604.

Specific contribution: Sample measurements, concept and manuscript writing by O. Schmale. Data analysis by W. Gülzow. Revision of manuscript by W. Gülzow, J. Schneider v. Deimling, G. Rehder and G. Nausch. Initiator and project holder: O. Schmale.

# ACKNOWLEDGEMENTS

## EIDESSTATTLICHE ERKLÄRUNG

Ich versichere hiermit, dass ich die vorliegende Arbeit selbstständig angefertigt und ohne fremde Hilfe verfasst habe. Es wurden keine, außer den von mir angegebenen Hilfsmitteln und Quellen dazu verwendet. Die den benutzten Werken inhaltlich und wörtlich entnommenen Stellen wurden als solche kenntlich gemacht.

Rostock, den